Dissection of Signaling Pathways Regulating TrkB-Dependent Gephyrin Clustering

Dissertation

zur Erlangung des Grades eines

Doktors der Naturwissenschaften

der Mathematisch-Naturwissenschaftlichen Fakultät

und

der Medizinischen Fakultät

der Eberhard-Karls-Universität Tübingen

vorgelegt

von

Lisa-Sophie Wüstner

aus Reutlingen, Deutschland

2025

Tag der mündlichen Prüfung: 09.04.2025

Dekan der Math.-Nat. Fakultät: Prof. Dr. Thilo Stehle

Dekan der Medizinischen Fakultät: Prof. Dr. Bernd Pichler

1. Berichterstatter: Prof. Dr. Hansjürgen Volkmer

2. Berichterstatter: Prof. Dr. Andrea Burgalossi

Prüfungskommission: Prof. Dr. Hansjürgen Volkmer

Prof. Dr. Andrea Burgalossi

Prof. Dr. Jan Benda

Prof. Dr. Simone Mayer

Erklärung / Declaration:

Ich erkläre, dass ich die zur Promotion eingereichte Arbeit mit dem Titel:

„Dissection of Signaling Pathways Regulating TrkB-Dependent Gephyrin Clustering”

selbständig verfasst, nur die angegebenen Quellen und Hilfsmittel benutzt und wörtlich oder inhaltlich übernommene Stellen als solche gekennzeichnet habe. Ich versichere an Eides statt, dass diese Angaben wahr sind und dass ich nichts verschwiegen habe. Mir ist bekannt, dass die falsche Abgabe einer Versicherung an Eides statt mit Freiheitsstrafe bis zu drei Jahren oder mit Geldstrafe bestraft wird.

I hereby declare that I have produced the work entitled

“Dissection of Signaling Pathways Regulating TrkB-Dependent Gephyrin Clustering”,

submitted for the award of a doctorate, on my own (without external help), have used only the sources and aids indicated and have marked passages included from other works, whether verbatim or in content, as such. I swear upon oath that these statements are true and that I have not concealed anything. I am aware that making a false declaration under oath is punishable by a term of imprisonment of up to three years or by a fine.

Tübingen, den 07.05.2025 .....

Lisa-Sophie Wüstner

für Wilhelm.

Table of Contents

List of Figures

List of Tables

Abbreviations

°C	Degree Celsius
µg, µl, µM	Micrograms, -liters, -molar
A.U.	Arbitrary unit
aa	Amino acid
AAV	Adeno-associated virus
AB	Antibody
AIS	Axon initial segment
Akt	Protein kinase B
AMP	Amplitude
AMPA; AMPAR	α-amino-3-hydroxy-5-methyl-4-isoxazolepropionic acid; -receptor
ANOVA	Analysis of variance
ASD	Autism spectrum disorder
ATP	Adenosine triphosphate
Bdnf	Brain-derived neurotrophic factor
BLA	Basolateral amygdala
BMB	Blocking reagent
bp	Base pair
BSA	Bovine serum albumin
ca	Constitutively active
Ca^{2+}	Calcium (cation)
CaMKII/; CaMKIV	Calmodulin-dependent protein kinase II; IV
Cb	Collybistin
cDNA	Complementary desoxyribonucleic acid
cds	Coding sequence
CKK	Cholecystokinin
Cl^-	Chloride (anion)
CMV	Cytomegalovirus
CNQX	Cyanquixaline
CNS	Central nervous system
CTR	Control
CREB	cAMP response element-binding protein
cAMP	Cyclic adenosine monophosphate
Cy3; Cy5	Cyanine3; Cyanine5
DAG	Diacylglycerol
DG	Dentate gyrus
DIV	Days in vitro
DMEM	Dulbecco's Modified Eagle Medium
DN	Dominant negative

DNA	Deoxyribonucleic acid
DPBS	Dulbecco's Phosphate-Buffered Saline
e.g.	*exempli gratia* – for example
E/I	Excitatory/inhibitory
E18	18th day of gestation/embryonic day 18
EDTA	Ethylenediaminetetraacetic acid.
EGFP	Enhanced green fluorescence protein
eLTD, iLTD, LTD	Excitatory, inhibitory, long-term depression
eLTP, iLTP, LTP	Long-term potentiation
EphA7	Ephrin type-A receptor 7
EPSP, IPSP	Excitatory/Inhibitory postsynaptic potential
Erk1/2 (MAPK1/3)	Extracellular signal-regulated kinases 1/2; Mitogen-activated protein kinase 1/3
FBS	Fetal bovine serum
Fgs2	Fibroblast growth factor receptor substrate 2
FGF; FGFR	Fibroblast growth factor; -receptor
FWHM	Full-width-half-maximum
g	Gram
Gab1	Grb2-associated-binding protein 1
GABA	Gamma(γ)-aminobutyric acid
$GABA_AR$; $GABA_BR$	Gamma(γ)-aminobutyric acid receptor type A; B
GAD	Glutamate decarboxylase
GDP; GTP	Guanosine diphosphate; Guanosine triphosphate;
Gef	Guanine nucleotide exchange factor
GlyR	Glycine receptor
Gphn; *Gphn*	Gephyrin
Grb2	Growth factor receptor-bound protein 2
Gsk3ß	Glycogen synthase kinase 3 beta
h	Hour
HC	Hippocampus
HCl	Hydrochloric acid
HEK	Human embryonic kidney cells
HRP	Horseradish peroxidase
K^+	Potassium (cation)
kb	Kilobase (1000 bases)
KD	TrkB K571A mutant (kinase-dead)
kg	Kilogram
KO	Knock out
l	Liter
IP_3	inositol-1,4,5-trisphosphate

M	Molar
MAP2	Microtubules associated protein 2
MAPK	Mitogen-activated protein kinase
MDD	Major depression disorder
MEK1 (MAP2K2)	Dual specificity mitogen-activated protein kinase kinase 1
MEM	Minimal Essential Medium
mg, ml, mM, ms, mV	Milligrams, -liters, -molar, -seconds, -volt
min	Minute
miRNA	Micro ribonucleic acid
mPFC	Medial prefrontal cortex
mRNA	Messenger ribonucleic acid
mTOR (here synonym for mTORC1)	Mechanistic Target of Rapamycin
Na^{2+}	Sodium (cation)
NaCl	Sodium chloride
NaOH	Sodium hydroxide
NCAM	Neural Cell Adhesion Molecule
NEAA	Non-essential amino acids
ng, nl, nM	Nanograms, -liters, -molar
NL2	Neuroligin 2
NMDA/NMDAR	*N*-Nitrosodimethylamine/-receptor
***Ntrk2* (TrkB gene)**	Neurotrophic receptor tyrosine kinase 2
o.n.	Overnight
P/S	Penicillin/Streptomycin
PBS	Phosphate-buffered saline
PCR	Polymerase chain reaction
Pdk1	Pyruvate dehydrogenase kinase isoform 1
PFA	Paraformaldehyde
Pi3K	Phosphoinositide 3-kinase
PIP2	Phosphatidylinositol 4,5-bisphosphate
PIP3	Phosphatidylinositol (3,4,5)-triphosphate
PKA	Protein kinase A
PLC-	TrkB Y816F mutant
PSD95	Postsynaptic density protein 95
PTB	Phosphotyrosine-binding domain
PV	Parvalbumin
Rab (GTPase)	Ras-associated binding protein
Raf (kinase)	Rapidly accelerated fibrosarcoma kinase
Ras (GTPase)	Rat sarcoma GTPase
Rheb (GTPase)	Ras homolog enriched in brain GTPase

RNA	Ribonucleic acid
RNAi	RNA interference
ROI	Region of interest
rpm	Rotations per minute
RT	Room temperature
RTK	Receptor tyrosine kinase
RT-PCR	Reverse transcription polymerase chain reaction
s	Seconds
S6K (p70S6K)	Ribosomal protein S6 kinase
SDS	Sodium dodecyl sulfate
SEM	Standard error of the mean
SFCA	Surfactant-Free Cellulose Acetate
SHC-	TrkB Y515F mutant
SHC, Shc	SHC-transforming protein
shRNA	Short hairpin RNA
siRNA	Small interfering RNA
Sos (GTPase)	Son of sevenless GTPase
TBS; TBST	Tris-buffered saline; containing Tween-20
TMD	Transmembrane domain
TrkA; TrkC	Tropomyosin receptor kinase A/C
TrkB	Tropomyosin receptor kinase B or tyrosine receptor kinase B or BDNF/NT3 growth factor receptor
TSC1/2	Tuberous sclerosis protein 1/2
U	Units
V	Volt
vGAT	Vesicular GABA transporter
vGLUT1	Vesicular glutamate transporter 1
W/O (WO)	Without
WT	Wild type
xg	Times gravity (g = 9.81 m/s^2)

Abstract

Bdnf/TrkB signaling plays an essential role in excitatory and inhibitory synapse stabilization and plasticity, and its disruption is closely linked to the pathophysiology of various neuropsychiatric and neurodevelopmental disorders. Further understanding these mechanisms may provide novel insights into therapeutic strategies for treating synaptic dysfunctions in these conditions. Over the past decade, TrkB has emerged in its role in inhibitory synapse regulation through its impact on gephyrin (Gphn), the key scaffolding protein at the inhibitory postsynapse. Clustering of gephyrin is a direct correlate for inhibitory transmission, and aberrations in TrkB function are associated with decreased Gphn clusters. This study aimed to elucidate how TrkB exerts its control over gephyrin, particularly dissecting the individual contributions of cognate Shc- and PLCγ-dependent pathways to provide a more profound knowledge of the molecular mechanisms underlying TrkB-dependent regulation of GABAergic synaptic plasticity.

To dissect the individual contribution of TrkB signaling pathways in neurons, mutants of the rat TrkB receptor-deficient in autophosphorylation or the induction of PLCγ- or Shc-dependent signaling pathways were developed. By lentiviral overexpression in primary hippocampal neurons, their contribution to the regulation of inhibitory synaptic protein accumulation was assessed by immunocytochemistry and confocal laser scan microscopy with a specific focus on gephyrin clustering. Furthermore, the functional consequences of aberrant synaptic connectivity were evaluated by analyzing patterns of intracellular calcium transients of neurons with aberrant TrkB signaling. The results revealed that TrkB cognate signaling pathways specifically account for the regulation of Gphn by limiting its clustering in size and density (Shc-dependent pathways) and the localization of Gphn at synaptic sites (PLCγ-dependent pathways) at the somata of primary hippocampal neurons, therefore maintaining the E/I balance in neurons. To further address the contribution of TrkB to inhibitory synaptic plasticity, inhibitory long-term potentiation was chemically induced through a moderate increase in intracellular calcium concentration. This revealed a novel role for TrkB in the calcium-dependent potentiation of inhibitory synapses since the catalytic activity of TrkB was a prerequisite for the associated increase in Gphn accumulation and density of inhibitory synapses. This potentiation was exerted by both signaling pathway strands, including MAPK/Erk1/2 and CaMKII signaling.

The findings presented in this study support the notion of TrkB as a crucial regulator of GABAergic synapses through its modulation of Gphn clustering. Furthermore, by extending the role of TrkB in calcium-dependent synaptic plasticity by iLTP, they suggest TrkB as an upstream cross-talking mediator of activity-dependent homeostatic heterosynaptic plasticity, crucial for maintaining and adjusting E/I balance.

Zusammenfassung

Die Bdnf/TrkB-Signalübertragung spielt eine zentrale Rolle bei der Stabilisierung und Plastizität exzitatorischer und inhibitorischer Synapsen. Eine Fehlfunktion dieser Signalübertragung steht in engem Zusammenhang mit der Pathophysiologie zahlreicher neuropsychiatrischer und neurologischer Erkrankungen. Ein besseres Verständnis der Mechanismen, welche Synapsen stabilisieren und formen, könnte Erkenntnisse für die Behandlung neuer therapeutische Ansätze bei diesen Erkrankungen liefern.

In den letzten Jahren rückte insbesondere die Rolle von TrkB bei der Regulierung inhibitorischen Synapsen in den Fokus, vor allem durch seinen Einfluss auf Gephyrin (Gphn), das zentrale Gerüstprotein inhibitorischer Postsynapsen. Die Ansammlung von Gephyrin an der postsynaptischen Membran ist ein direktes Korrelat für die hemmende Signalübertragung, und eine beeinträchtigte Funktion von TrkB steht im Zusammenhang mit einer verminderten Anzahl von Gphn-Clustern. Ziel dieser Studie war es, die Mechanismen hinter der TrkB-vermittelnden Regulation von Gephyrin zu verstehen, wobei insbesondere die jeweiligen Beiträge der zugehörigen Shc- und PLCγ-abhängigen Signalwege aufgeschlüsselt werden sollten. Dadurch sollten die molekularen Grundlagen der TrkB-abhängigen Regulierung der GABAergen synaptischen Plastizität offengelegt werden.

Um die spezifische Rolle der TrkB-Signalwege in Neuronen zu untersuchen, wurden gezielt Mutanten des TrkB-Rezeptors entwickelt, die entweder die katalytische Aktivität des Rezeptors oder die Aktivierung von PLCγ- oder Shc-abhängigen Signalwegen verhinderten. Durch lentivirale Überexpression in primären hippokampalen Neuronen wurde ihr Beitrag zur Regulierung der Proteinakkumulation in inhibitorischen Synapsen mittels Immunozytochemie und konfokale Laserscan-Mikroskopie untersucht und dabei ein besonderes Augenmerk auf die Gephyrin-Anhäufung gelegt. Darüber hinaus wurden die funktionellen Auswirkungen veränderter synaptischen Konnektivität durch die Analyse intrazellulärer Kalziumtransienten von Neuronen mit abweichender TrkB-Signalisierung erfasst.

Die Ergebnisse zeigen, dass die einzelnen TrkB-Signalwege spezifische Funktionen in der Regulierung von Gphn übernehmen, indem sie seine Clusterbildung in Größe und Dichte beeinflussen (Shc-abhängige Signalwege) und die Lokalisierung von Gphn an synaptischen Arealen steuern (PLCγ-abhängige Wege) und somit das E/I-Gleichgewicht in Neuronen aufrechterhalten. Um die Rolle von TrkB in der Plastizität inhibitorischer Synapsen zu untersuchen, wurde eine chemisch induzierte Langzeitpotenzierung inhibitorischer Synapsen durch einen moderaten Anstieg der intrazellulären Kalziumkonzentration ausgelöst.

Dabei konnte eine neue Funktion für TrkB nachgewiesen bei der kalziumabhängigen Potenzierung inhibitorischer Synapsen nachgewiesen werden, da die katalytische Aktivität von

TrkB eine Voraussetzung für die damit verbundene Zunahme der Gphn-Akkumulation und der Dichte inhibitorischer Synapsen war. Diese Potenzierung wurde sowohl durch Shc- als auch PLCγ- abhänge Signalwege bewirkt.

Zusammenfassend unterstützen die Ergebnisse dieser Studie die Hypothese, dass TrkB durch Modulation der Gphn-Clusterung ein entscheidender Regulator GABAergen Synapsen ist. Zudem erweitern sie das Verständnis von TrkB bei der kalziumabhängigen synaptischen Plastizität durch seine Rolle bei iLTP und deuten darauf hin, dass TrkB ein vorgeschalteter Vermittler der aktivitätsabhängigen homöostatischen, heterosynaptischen Plastizität ist, der für die Aufrechterhaltung und Anpassung des E/I-Gleichgewichts entscheidend ist.

1. Introduction

1.1. The Balanced Brain: The Crucial Role of Synapses

The human brain contains about 86 billion neurons, accompanied by a nearly equal number of glial cells (1). Together, they create a vast network of interconnected neurons that enables the incredible complexity of human thought, memory, and learning and even allows us to read this dissertation. To support these remarkable abilities, neurons are constantly receiving, processing, and integrating signals and are capable of creating numerous unique pathways and patterns essential for efficient information transfer.

To enable communication across neurons and brain areas, the central nervous system (CNS) contains several hundred trillion synapses, connection points of neurons, which serve as the foundational units of neuronal signaling that wire circuits (2, 3). Synapses can be classified by their mode of transmission: some transmit their information via electrical signals, whereas others make use of chemical substances, such as neurotransmitters, and are therefore referred to as chemical synapses (4, 5). Chemical synapses all share core structural features, including the presynaptic bouton of a transmitting neuron and the postsynaptic compartment of a receiving neuron, separated by a 20 nm gap known as the synaptic cleft (5). Both terminals contain specialized, protein-rich structures that anchor signaling molecules near the membrane: the presynaptic active zone and the postsynaptic density (PSD), which bothsupport efficient signal transmission. Alongside the fine processes of astrocytes that extend to surround both pre- and postsynaptic compartments, these structures form the tripartite synapse (6). However, the following sections will focus exclusively on the neuronal components of synapses.

Given the diversity of neurons in the brain, several types of synaptic connections can be formed. The two major neuronal types in the CNS are excitatory and inhibitory neurons, classified according to their effects on the target neuron. The molecular composition of pre- and postsynaptic regions varies according to the types of neurons forming the synapses.

1.1.1. The Excitatory Synapse

Excitatory synapses play a crucial role in activating the postsynaptic neuron by increasing the likelihood of depolarization and the initiation of an action potential, which is essential for the onward transmission of neuronal signals. To induce excitation, the presynaptic neuron releases excitatory neurotransmitters, such as glutamate. Glutamate is the principal neurotransmitter of the mammalian brain, and neurons utilizing glutamate as a neurotransmitter are referred to as glutamatergic neurons. These neurons store glutamate in vesicles within the presynaptic

terminal through vesicular glutamate transporters (VGluts, see Figure 1). Upon an incoming action potential, these vesicles fuse with the membrane at the presynaptic active zone, thereby releasing the neurotransmitters.

Glutamate navigates across the synaptic cleft and binds to receptors densely packed within the excitatory PSD of the receiving neuron, which is mainly located on dendritic protrusions, so-called spines (7). The PSD of excitatory synapses contains several receptors ionotropic glutamate receptors, including N-methyl-D-aspartate- (NMDA), α-amino-3-hydroxy-5-methyl-4-isoxazolepropionic acid- (AMPA) and kainate receptors, which mediate excitatory signaling. Receptors for NMDA and AMPA form tetramers composed of four types of subunits: For AMPA receptors (AMPARs), this involves GluA1 to GluA4 subunits, forming either homo- or hetero-tetrameric receptors, with their subunit composition determining the calcium permeability of AMPARs (8, 9). Functional NMDA receptors (NMDARs) comprise two GluN1 subunits combined with either two GluN2 subunits or a combination of GluN2 and GluN3 subunits (9, 10). Upon glutamate binding, the calcium-permeable receptors undergo conformational changes that permit the influx of sodium and calcium ions. This results in an increase in intracellular cation concentration, which raises the membrane potential increasing the likelihood of depolarization and action potential initiation.

To anchor receptors at the synaptic site, a network of scaffolding proteins is responsible for tethering these receptors to the PSD (11). The major scaffolding protein at excitatory synapses is the post-synaptic density protein 95 (Psd95), which contains three PDZ domains that play a key role in linking receptor proteins located within the membrane to cytoskeletal components (12). Psd95 also interacts with various components of excitatory synapses, connecting receptors, ion channels, and signaling proteins at the postsynaptic membrane (11). Additionally, Psd95 is essential for synaptic plasticity, which will be discussed in detail in section 1.1.3.

1.1.2. The Inhibitory Synapse

In contrast to excitatory synapses, mature inhibitory synaptic connections inhibit the receiving neurons by reducing the likelihood of depolarization in postsynaptic neurons, thereby decreasing the probability of an action potential initiation. Inhibitory neurons release neurotransmitters such as gamma-aminobutyric acid (GABA), for inhibition. Next to glycine, GABA is the primary inhibitory neurotransmitter in the mature CNS and is synthesized from glutamate through glutamate decarboxylase (GAD, see Figure 1) (13). Neurons that release GABA are termed GABAergic neurons. Similar to glutamate, GABA is stored in vesicles within

the presynaptic terminal via the vesicular GABA transporter (VGat) and is released upon an arriving action potential.

As with excitatory synapses, the PSD of inhibitory synapses contains receptors that mediate the inhibitory signal to the receiving cell. For GABA, two main classes of receptors are present: ionotropic $GABA_A$ receptors ($GABA_A$Rs) and metabotropic $GABA_B$ receptors. Typically, functional ionotropic pentameric $GABA_A$Rs consist of two α subunits, two β subunits, and a single γ or δ subunit, with different subunit combinations giving rise to various structurally and functionally distinct $GABA_A$R subtypes (14, 15). Upon ligand binding, ionotropic $GABA_A$Rs undergo a conformational change that facilitates the influx of chloride ions into the postsynaptic neuron, leading to hyperpolarization and thus reducing the likelihood of action potential initiation shape signal transduction.

Like AMPARs and NMDARs, $GABA_A$Rs also require to be anchored within the postsynaptic membrane. At inhibitory synapses, the major protein responsible for tethering receptors at synaptic sites is gephyrin (Gphn). Gphn forms multimeric complexes by auto-aggregation and by interaction with other postsynaptic proteins, such as cell adhesion molecule Neuroligin-2 (NL2), GTP/GDP exchange factor collybistin (Cb), and the actin cytoskeleton, which cluster $GABA_A$Rs at the postsynapse (16, 17). Like Psd95, Gphn also plays a potential part in the ability of inhibitory synapses to adapt to changes in activity by modulating the clustering of $GABA_A$Rs at the postsynapse (18). Given the central role of Gphn in this study, it will be discussed in detail in a separate chapter (see 1.2), including its functions during inhibitory synaptic plasticity. Beforehand, however, it is essential to understand the underlying mechanisms that enable synapses to adapt.

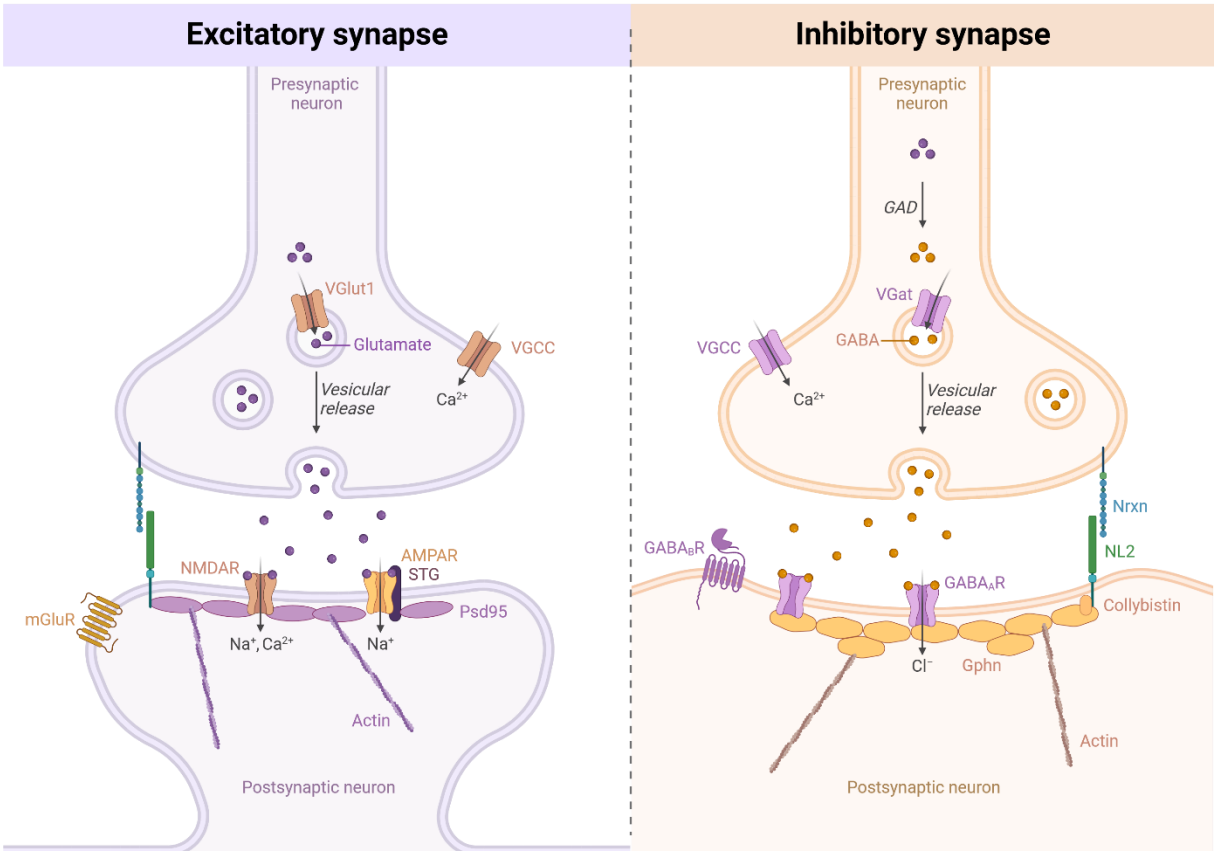

Figure 1: Molecular architecture of inhibitory and excitatory synapses. The left and right panels illustrate the simplified microanatomy of inhibitory and excitatory synapses, respectively, highlighting their unique assemblies of neurotransmitter receptors, ion channels, scaffolding proteins, and other critical pre- and postsynaptic molecules. *AMPAR: AMPA receptor, GAD: Glutamate decarboxylase, GABA: Gamma(γ)-aminobutyric acid, $GABA_AR$: ionotropic GABA receptor (type A), $GABA_BR$: metabotropic GABA receptor (type B), Gphn: gephyrin, mGluR: metabotropic glutamate receptor, NL2: Neuroligin-2, Nrx: Neurexin, NMDAR: NMDA receptor, Psd95: postsynaptic density protein 95, STG: Stargazin, VGat: vesicular GABA transporter, VGCC: voltage-gated calcium channel, VGlut1: vesicular glutamate transporter 1.* Created in BioRender.com.

1.1.3. Molecular Mechanisms of Synaptic Plasticity and Balance in Neuronal Networks

Synaptic plasticity refers to a process by which synapses adjust their relative strength in response to the intensity and spatio-temporal timing of specific activity patterns (19). This process is fundamental to learning, memory, and the brain's adaptive capacity (20, 21). Several forms of synaptic plasticity exist, producing adaptations that may last from milliseconds to minutes (short-term synaptic plasticity) or from hours to days (long-term synaptic plasticity) (22). It is widely believed that experience modifies subsequent behavior, at least in part through activity-dependent, long-lasting changes in synaptic strength (20, 22).

Homeostatic and Hebbian plasticity constitute two primary forms of activity-dependent regulation of synaptic transmission (23). During Hebbian plasticity, synapses rapidly adjust to their strength in the same direction as the applied stimulus, typically resulting in a persistent

strengthening or weakening of neurotransmission, known as long-term potentiation (LTP) and long-term depression (LTD), respectively (24). LTP and LTD include processes that have been described in detail for both pre- and postsynaptic sites (23). At the postsynaptic site, for example, receptor trafficking, particularly lateral diffusion between synaptic and extrasynaptic sites, allows for rapid adjustment of excitatory or inhibitory synaptic strength. Postsynaptic scaffolds help to tether ionotropic receptors at the postsynaptic site, whereas diffusion to extrasynaptic regions facilitates receptor internalization (25, 26). In contrast, during homeostatic plasticity, synapses respond slower and in the opposite direction of the applied stimulus, compensating for the shift in activity, which maintains the balance between excitation and inhibition and further shapes the output of excitatory neurons (27, 28).

LTP, as well as LTD, can occur on both excitatory (eLTP, eLTD) and inhibitory synapses (iLTP, iLTD) (29, 30). Increasing evidence suggests a coordinated interplay between GABAergic and glutamatergic synapses to maintain the optimal balance of neuronal activity (31). Further supporting this interplay, a study showed that iLTP induced by low-frequency stimulation caused eLTD, reducing the amplitudes of excitatory postsynaptic potentials (32). The same study additionally demonstrated differential plasticity of $GABA_AR$ synapses based on their relative spatial localization to the potentiating spine, such that inhibitory synapses within three µm of the potentiating spine underwent iLTD, whereas synapses beyond three µm away underwent iLTP. Another example of heterosynaptic plasticity, where unstimulated synapses undergo plastic changes in response to stimulation of a different synapse, demonstrated that spines close to the potentiated synapses undergo eLTD and that this is mediated by calcium-dependent proteins such as the Ca^{2+}/calmodulin-dependent protein kinase (CaMKII) and calcineurin (33).

Calcium as a Mediator of Homeostatic Plasticity

Calcium-dependent signaling pathways represent a major mechanism for synaptic crosstalk during plasticity, with important examples including voltage-gated calcium channels (VGCCs); CaMKII and protein kinase C (PKC); the phosphatase calcineurin and the protease calpain (24, 34, 35). Synaptic activity triggers Ca^{2+} influx through ionotropic NMDARs, inducing calcium-dependent processes such as the activation of the CaMKIIα and its autophosphorylation at Thr286, which prolongs its activity in a calcium-independent manner (36-38). CaMKIIα translocates to excitatory synapses, where it facilitates the insertion of AMPARs at synapses and stabilizes them via phosphorylation, therefore inducing eLTP (39, 40).

Notably, it has been shown that iLTP similarly relies on glutamatergic NMDAR or metabotropic glutamate receptor (mGluR) signaling and the associated increase in intracellular calcium (32,

41). Unlike eLTP, which requires a high calcium influx, iLTP occurs at low to moderate levels of NMDAR activation (42, 43). Under these conditions, CaMKIIα is translocated to inhibitory synapses, facilitating iLTP through the recruitment of gephyrin and enhanced $GABA_AR$ insertion (44-48). Additionally, mGluR-dependent, moderate calcium release from internal stores, such as the endoplasmic reticulum (ER), can prompt PKC-mediated $GABA_AR$ stabilization, contributing to the strengthening of inhibitory synapses (43).

Collectively, several studies point to converging glutamatergic and GABAergic signaling pathways that allow activity-dependent receptor coordination for regulation and tuning of excitation/inhibition (E/I) balance through calcium/CaMKII-dependent mechanisms (24, 49). Therefore, identifying cross-talking proteins and pathways that coordinate these processes is an important current and future area of investigation.

1.2. The Organizer of GABAergic Synapses: Gephyrin

Highly condensed and dynamically regulated receptor and ion channel clustering at postsynaptic sites is crucial for efficient and precise neuronal signal transmissions. Specialized structures of postsynaptic synapses provide spatial constraints to facilitate condensed localization of molecular components, including scaffold proteins and neurotransmitter receptors in these micron-sized compartments (50).

As one of the most extensively studied proteins at inhibitory synapses, gephyrin (Gphn) is a master organizer that links transmembrane receptors to downstream signaling proteins for inhibitory synaptic transmission (50-52). Emerging as a central regulator of inhibitory synaptic function, neuronal Gphn controls synaptic structure, postsynaptic receptor retention, density, and trafficking of glycine receptors (GlyR) and $GABA_A$Rs (14). Its function is finely controlled by excitatory activity, depolarization, and calcium signals upstream of numerous activity-regulated kinases that target different residues in the gephyrin molecule (48, 51, 53, 54).

Initially identified as a 93-kDa GlyR-associated protein purified with tubulin (55, 56), it is highly conserved in vertebrates and contains two structured domains: an N-terminal trimerization G-domain and a C-terminal dimerization E-domain linked by a flexible C-domain (14). The E-domain mediates binding with the intracellular loops of GlyR and $GABA_A$Rs of gephyrin (57). Through this binding capacity, gephyrin establishes a scaffold at inhibitory synapses that organizes receptor clustering, essential for effective inhibitory signal transmission.

When establishing a complex with either GlyR or $GABA_A$R, Gphn spontaneously forms highly condensed molecular assemblies of an estimated size of ~0.04 - 0.05 mm^2 containing approximately 200-300 gephyrin molecules at synapses of hippocampal neurons and the cluster of $GABA_A$Rs are spatially correlated with those of Gphn (18, 50, 58, 59). Importantly, gephyrin's affinity for $GABA_A$Rs subunits is approximately ten times weaker than that for the GlyRs β3. Therefore, in contrast to glycinergic synapses, gephyrin is believed to require additional proteins or cofactors for the formation of postsynaptic $GABA_A$R clusters, such as inhibitory proteins 1 and 2 (ISyns), Cb or NL-2 (see Figure 1) (14, 52, 60, 61).

The importance of gephyrin regarding the anchoring of receptors at synaptic sites becomes evident with knocking down Gphn, which resulted in the disruption of $GABA_A$R α1, α2, α3 subunits (62, 63). Gphn tethers freely diffusing receptors at synaptic sites by binding $GABA_A$R subunits (64). The $GABA_A$Rs containing α and β subunits (α1, α2, α3, and β2, β3) of those that are known to preferentially localize at postsynaptic membrane specializations have all been shown to covalently bind gephyrin, whereas subunits of extrasynaptic $GABA_A$Rs did not (62, 65-67).

In conclusion, modular scaffold proteins like Gphn are crucial for the internal organization of synapses, acting as pivotal modulators of receptor diffusion dynamics at inhibitory synapses (68). By providing binding sites for the transient immobilization of neurotransmitter receptors at the postsynaptic membrane, Gphn effectively sets the gain on synaptic transmission and ensures precise control over inhibitory signaling.

1.2.1. Phosphorylation-Driven Regulation of Gephyrin Cluster Dynamics

The size and molecular density of gephyrin clusters vary considerably between individual inhibitory synapses (51, 59). This variability correlates strongly with the density of $GABA_A$Rs or GlyRs and, consequently, with synaptic strength, suggesting that alterations in gephyrin clustering will also alter the strength of inhibition (51, 53, 59). A primary mechanism for dynamically regulating the clustering properties of Gphn is through posttranslational modifications (PTMs). Several PTMs, including acetylation, SUMOylation, and phosphorylation, have been identified as acting in concert to regulate Gphn scaffolding and, thus, GABAergic transmission (18, 69).

Protein kinases selectively modify other proteins through phosphorylation. This involves removing a phosphate group from ATP and covalently attaching it to amino acids that contain a free hydroxyl group, which includes serine, threonine, and tyrosine (70). Phosphorylation typically occurs on unstructured protein modules; for gephyrin, this predominantly includes its C-domain, which harbors approximately 40 potential phosphorylation sites (14). In the past decade, several protein kinases and their corresponding phosphorylation sites on gephyrin have been identified (46, 53, 71-73). Collectively, these studies demonstrated how various protein kinases orchestrate the complex fine-tuning of Gphn clustering, including crosstalk between phosphorylation sites.

For example, phosphorylation of Ser268 by extracellular-signal regulated kinases 1/2 (Erk1/2) has been shown to negatively affect both Gphn and $GABA_A$R clustering (53). However, the effect of phosphorylation of gephyrin can have opposing effects depending on the targeting protein kinase: whereas phosphorylation of Ser270 through glycogen synthase kinase-3 ß (Gsk3ß) decreases Gphn and $GABA_A$R cluster densities, phosphorylation of the same tyrosine residue by cyclin-dependent kinase 5 (Cdk5) increases cluster density (72, 74, 75). Adding further complexity, there is a context-dependent crosstalk between the phosphorylation states of Ser268 and Ser270 that modifies how the negative effect on gephyrin is exerted (53).

In addition to Ser 286 and Ser270, Ser305 has been identified as the phosphorylation site targeted by CaMKII and plays an important role in the activity-dependent regulation of gephyrin and, consequently, inhibitory synaptic plasticity (46).

Activity-Dependent Regulation of Gephyrin Clustering and Inhibitory Synaptic Plasticity

Studies have demonstrated that NMDAR-dependent neuronal depolarization not only impacts excitatory synaptic plasticity but also modulates Gphn clustering and the recruitment of $GABA_A$Rs in a CaMKII-dependent mechanism, enhancing perisomatic inhibition in an activity-dependent manner and facilitating neuronal homeostasis (46, 71). This process is likely induced by local calcium signaling from excitatory synapses, which results in the activation of kinases such as CaMKII at nearby inhibitory sites (51) (as described in section 1.1.3). This calcium-dependent regulation of inhibitory synapse plasticity is also observed on the level of Gphn clustering: on the one hand, strong pharmacological activity results in a calcium-dependent reduction in Gphn clustering, mediated by calcineurin, resulting in reduced retention of receptors and diminished inhibitory synaptic currents (76). On the other hand, moderate increases in intracellular calcium accumulate Gphn and $GABA_A$Rs at synapses through direct phosphorylation and translation-dependent processes (43, 48, 77).

Furthermore, following the induction of plasticity, such as iLTP, some but not all synapses undergo accumulation and rearrangement of gephyrin clusters, which stabilize the amplitude of inhibitory postsynaptic responses (78). This implies that inhibitory synaptic plasticity is selectively enabled at synapses where specific mechanisms permit it. A profound understanding of how signaling pathways contribute to plasticity requires the identification of both upstream signaling effectors as well as downstream signaling targets within this regulatory network. Thus, characterizing additional signal transduction pathways that converge on gephyrin will likely provide valuable insights into the adaptive mechanism underlying GABAergic inhibition in response to dynamic fluctuations within neuronal networks.

1.2.2. The Role of Receptor Tyrosine Kinases in Modulating Gephyrin

Receptor tyrosine kinases have emerged as promising upstream regulators of gephyrin clustering since their signaling pathways involve several protein kinases previously implicated in Gphn regulation (73). Thus positioning them as potential critical modulators of GABAergic synaptic transmission.

Receptor tyrosine kinases (RTKs) are cell surface receptors that bind various growth factors, cytokines, and hormones, enabling cells to communicate with their environment effectively. Therefore, RTKs are essential in numerous critical cellular processes, including cell proliferation, differentiation, migration, survival, and synaptic plasticity (79-81). They consist of 19 different subfamilies, each specialized in different functions but similar in architecture: they all contain an N-terminal extracellular domain (ECD), which binds the ligand, a single transmembrane domain (TMD), and an intracellular kinase domain followed by a largely

unstructured C-terminal tail region (81). The kinase domains of most RTKs share a conserved architecture, while ECDs are highly divergent among receptor subfamilies. This diversity allows for the recognition of structurally distinct protein ligands, each uniquely modulating kinase domain activation (81).

A comprehensive kinome-wide small-interference ribonucleic acid (siRNA) screen in a human HeLa cell-based model for Gphn clustering identified candidate protein kinases implicated in the stabilization of gephyrin clusters (73). Among these were several RTKs, including fibroblast growth factor receptor 1 (FGFR1), ephrin-like receptors, including ephrin-like receptor A7 (EphA7), hepatocyte growth factor receptor Met and tropomyosin receptor kinases B (TrkB) and C (TrkC). This study further evaluated the involvement of protein kinases in gephyrin regulation by identifying critical components of the Ras/MAPK, Pi3K/Akt/mTOR, and PLCγ signaling pathways, all of which are integral pathways through which RTKs exert their intracellular functions (54).

Consecutive to this work, several studies investigated the specific mechanisms by which these RTKs regulate gephyrin clustering and contribute to stabilizing inhibitory synapses (82-84). EphA7, as well as Met were found to be crucial for stabilizing Gphn and inhibitory synapses *in vitro* and *in vivo* (82, 84). Furthermore, behavioral studies showed the far-reaching impact of RTKs through the reduction of EphA7 in the basolateral amygdala (BLA), which resulted in decreased Gphn expression and increased symptoms of stress-induced anxiety (83). These studies collectively highlight the relevance of RTK-dependent Gphn regulation and, consequently, the impact on GABAergic network functionality in neuronal circuits and behavior.

1.3. The TrkB Receptor

Another RTK identified in the foundational siRNA screen and discussed in the context of Gphn regulation and GABAergic synaptic stability is the tropomyosin-related kinase B (TrkB), which belongs to the neurotrophic tropomyosin receptor kinases (TRKs), a subclass of RTKs that play an important role in neural development and function (73, 85). Within the TRK family, TrkA, TrkB, and TrkC are encoded by the *Ntrk1*, *Ntrk2*, and *Ntrk3* genes, respectively (86). These TRKs share a structural architecture that includes an extracellular ligand-binding domain, a TMD, and an intracellular domain with kinase activity and high sequence homology (87). The main differences among these TRKs are their binding ligands: while TrkA binds with high affinity to the nerve growth factor (NGF) (88), TrkB preferentially binds to the brain-derived neurotrophic factor (Bdnf) and neurotrophin -4/5, and although with a lower affinity, to neurotrophin-3, which has its major affinity for TrkC (89-91).

Of these receptors, TrkB is prominently expressed in tissues derived from the neural epithelium and neural crest cells and is, therefore, widely present in the CNS, as well as in neuronal subpopulations of the peripheral nervous system (PNS) (86).

Structure

The human *NTRK2* gene, located on chromosome 9q22, spans over 590 kbp and contains 24 exons (92). Four major protein isoforms of the TrkB receptor are derived from translation start sites at the exon 5 start codon: the full-length tyrosine kinase receptor (TrkB), a C-terminal truncated receptor (TrkB.T1), a C-terminal truncated Shc^+ receptor (TrkB.Shc), and a C-terminal truncated receptor which retains tyrosine kinase activity (TrkB.T.TK) (92, 93). The ECD of TrkB includes five extracellular binding domains comprising two cysteine-rich regions (C1/2), a leucine-rich region (LRR), and 2 IgG-like domains (Ig1/2) that confer ligand-binding specificity, whereas a signaling sequence directs receptor localization to the plasma membrane (92, 94-96). Neurotrophins bind to the near-membrane Ig1/2 domains of the monomeric TrkB, triggering oligomerization of TrkB monomers and promoting the formation of homologous TrkB dimers. Dimerization enables trans-autophosphorylation of tyrosine residues within the intracellular tyrosine kinase domain (97). This domain comprises three tyrosine residues (Y701, Y705 and Y706), which are evolutionarily conserved tyrosine residues in vertebrate cytoplasmic domains, forming an autoregulatory loop within the tyrosine kinase domain (86, 97, 98). Together with the ATP binding site at K571, the tyrosine kinase domain provides phosphorylation sites required for its catalytic and signaling activities (99, 100). Autophosphorylation induces structural changes, revealing further phosphorylation sites allowing the recruitment of signaling adapter proteins, including Src homology 2-containing protein (Shc), fibroblast growth factor receptor substrate 2 (Frs2), and phospholipase Cγ

(PLCγ), which consequently result in the induction of cognate signaling pathways that will be discussed in detail in section 1.3.1 (95, 98, 101-103).

Brain-Derived Neurotrophic Factor Bdnf

Bdnf, as a major TrkB ligand, is synthesized in cell bodies of neurons and glia and is most abundantly expressed in the hippocampus (104-106). Transcription of Bdnf is tightly regulated by multiple activity-dependent and -independent promotors (106-108). The corresponding mRNA is translated into a precursor protein, pre-pro-Bdnf, sequentially processed to mature Bdnf. Released in an activity-dependent manner as a mixture of pro- and mature Bdnf, each form binds to distinct receptors (TrkB for mature Bdnf and p75 neurotrophic factor receptor (p75Ntr) for pro-Bdnf) that influence neuronal survival and neuroplasticity in opposite ways (109, 110). During development, Bdnf plays an essential role in neuronal survival and differentiation, while in the adult brain, it modulates both excitatory and inhibitory synaptic transmission and activity-dependent plasticity (85, 111, 112).

Ligand-Independent Modulation of TrkB Activation

In addition to ligand-dependent activation, TrkB signaling can be modulated through ligand-independent mechanisms (111). For example, low-affinity p75Ntr preferentially binds to phosphorylated TrkB, promoting the ability of TrkB to activate and maintain Akt signaling without altering Erk1/2 phosphorylation (see 1.3.1) (104, 113, 114). Furthermore, interactions with synaptic proteins, such as Psd95, can facilitate TrkB signaling (115). Additionally, both TrkB.T1 and TrkB.Shc isoforms can inhibit TrkB activity by blocking TrkB to inhibit its activity, potentially by competing for ligand binding or by forming inactive heterodimers with the full-length TrkB, which consequently prevents autophosphorylation (94, 116). These ligand-independent interactions broaden the scope of TrkB's functional signaling modulation beyond neurotrophic factor dependence, adding complexity to its functional regulation.

1.3.1. TrkB Functions and its Major Signaling Pathways

As the receptor for Bdnf, TrkB mediates pleiotropic cellular effects, playing an essential role in neuronal survival, proliferation, development, and synaptic plasticity, and is further found to be essential in memory and cognition (80, 117-119). In particular, TrkB contributes to the formation and maturation of glutamatergic and GABAergic synapses and, therefore, plays a pivotal role in the establishment of precisely connected networks (120-122). TrkB mediates the diverse effects of Bdnf by activating cognate signaling pathways, of which the three major cascades are the Pi3K/Akt, the Ras/MAPK/Erk1/2, and the PLCγ signaling pathway.

The Pi3K/Akt pathway

The Pi3K/Akt signaling pathway is primarily involved in neuronal dendritic and axonal growth and is the major pathway of TrkB, promoting neuronal survival and protecting against apoptosis (85, 95, 123). Upon autophosphorylation of rat TrkB, tyrosine residue 515 (Y515) in the intracellular juxtamembrane region is phosphorylated, recruiting the Shc-transforming protein (Shc) adaptor protein through phosphotyrosine-binding domains (see Figure 2) (80, 124). Shc forms a protein complex with growth factor receptor-bound protein 2 (Grb2), the Grb2-associated-binding protein 1 (Gab1), and son of sevenless (Sos) to stimulate G-proteins such as the Rat sarcoma GTPase (Ras) (125). Subsequently, Ras activates phosphatidylinositol 3-kinase (Pi3K), which generates 3-phosphoinositides that activate 3-phosphoinositide-dependent protein kinase 1 (Pdk1). Alongside 3-phosphoinositides, Pdk1 activates the protein kinase Akt. Involved in various processes, Akt signaling promotes neuronal survival by interfering with pro-apoptotic signaling pathways, which include the cleavage of Caspase 3, a key zymogen in cell apoptosis (80, 126-129). Additionally, Pi3K/Akt pathway activates protein translation via the mammalian target of rapamycin (mTOR), a major regulator of protein synthesis, which will be further discussed below (130). Ras can also signal through Pi3K to induce axonal growth together with Gsk3β, which is inhibited by Akt (73, 95, 131, 132). Gsk3ß has additionally emerged as a key regulator of inhibitory synapse formation. As discussed in section 1.2.1, Gsk3ß reduces Gphn and $GABA_AR$ clusters, consequently decreasing inhibitory transmission in primary hippocampal neurons and *in vivo* (71, 73, 75). Therefore, this pathway plays a pivotal role in the long-term maintenance of synaptic plasticity through translation and regulation of synaptic proteins (133).

The Ras/MAPK/Erk pathway

The recruitment of Shc at Y515 and the consecutive complex formation with Grb2 and Sos additionally results in the induction of the mitogen-activated protein kinase (MAPK) signaling cascade (see Figure 2) (95, 125). Alongside Pi3K/Akt signaling, this pathway is involved in the regulation of cell survival but is mainly known for its role in regulating cellular growth, differentiation, neuronal activity, and synaptic plasticity partially by activating transcription factors through cAMP response element-binding protein (CREB) (95, 134-136). Upon activation, Ras induces a phosphorylation cascade involving the rapidly accelerated fibrosarcoma kinase (Raf), the MAPK kinases 1/2 (Mek1/2), and the Erk1/2 (137). Transient and long-term activation of the MAPK/Erk1/2 pathway induce differentiation and proliferation, respectively (95). Ras/MAPK/Erk signaling is also involved in regulating synapse formation and plasticity by enhancing protein synthesis and directly phosphorylating synaptic proteins such as Psd95 and synapsin (133, 138-140). Erk1/2 has also been described as being involved

in the regulation of inhibitory synapses, although the exact mechanisms are still under debate. As already indicated in section 1.2.1, Erk1/2, together with Gsk3ß, has been described to reduce Gphn cluster size and density in a calpain-1-dependent manner (53). Additionally, it was demonstrated to decrease synaptic $GABA_AR$ clustering by facilitating receptor diffusion away from synapses (141). In contrast, the downregulation of MAPK signaling has been described to decrease gephyrin cluster density, suggesting that MAPK signaling is facilitating Gphn clustering (73).

The mTOR pathway

Pi3K/Akt, as well as MAPK/Erk signaling, achieve mTOR activation by downregulating the tuberous sclerosis complex protein 1/2 complex (Tsc1/2) (see Figure 2) (142, 143). In turn, Tsc1/2 inhibits the ras homolog enriched in brain GTPase (Rheb), which is an activator of mTOR. mTOR has been reported to generate two functional different multi-protein complexes named mTORC1 and mTORC2. It is important to note that mTOR hereafter refers specifically to mTORC1. Active mTOR is a major regulator of mRNA translation, mainly via the phosphorylation of p70S6kinase (S6K) and eukaryotic translation initiation factor 4E-BP1, and is further known to be involved in autophagy and induction of lipid biogenesis, therefore considered a master regulator of protein homeostasis (144). It also plays a major role in myelination and regulation of synapses in neurons (145, 146). Literature suggests that the response to neuronal activity critically engages mTOR signaling to produce long-lasting changes to neural circuits by regulating the local protein synthesis of synapsin or potassium channels in dendrites (147, 148). This highlights the role of mTOR in the context of synaptic LTP. Additionally, mTOR was linked to the regulation of Gphn availability for clustering at inhibitory synapses. It has been demonstrated that inactive mTOR binds Gphn, which becomes released upon mTOR activation (73). This suggests that mTOR regulates the availability of Gphn for synaptic clustering, thereby influencing inhibitory transmission (73, 149). However, the precise molecular mechanisms underlying mTOR-dependent regulation of Gphn clustering remain to be elucidated.

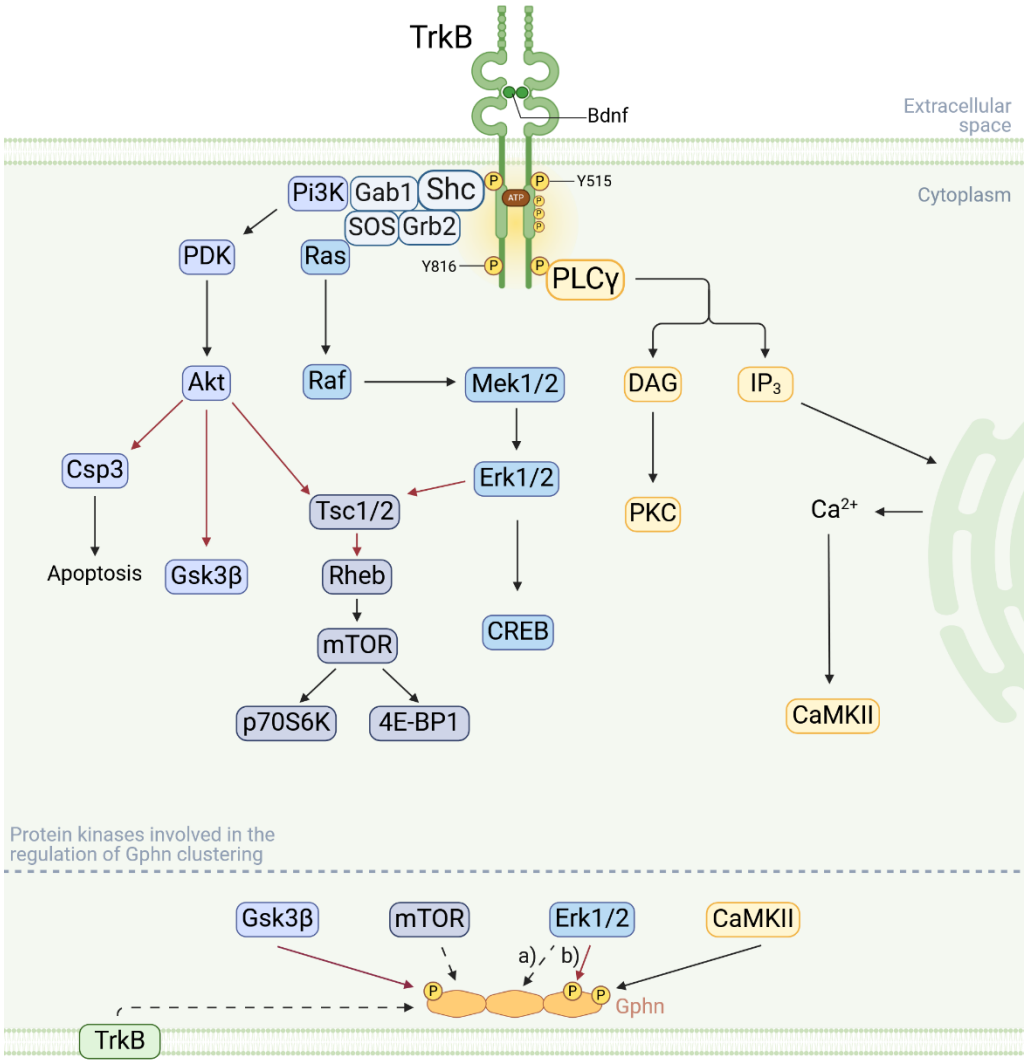

Figure 2: TrkB and its major signaling pathways. Simplified scheme of TrkB and its cognate signaling pathways representing the receptor's mode of action (top part). TrkB and several protein kinases involved in its signaling pathways had been identified as regulators of Gphn clustering (bottom part): TrkB (54, 82); Gsk3β (53, 71, 73, 75); mTOR: (73); Erk1/2: a) (73), b) (53); CaMKII: (46, 71). Red arrows represent a negative impact on gephyrin clustering, whereas black arrows represent a positive impact. Dashed lines represent mechanisms of action that remain to be elucidated. Created in BioRender.com.

The PLCγ pathway

The TrkB-PLCγ pathway participates in the endocytosis and trafficking of TrkB and cell survival but is primarily involved in neuronal plasticity (150-152). Upon rat TrkB activation, tyrosine residue 816 (Y816) in the C-terminal area becomes phosphorylated (see Figure 2) (80). PLCγ binds to this phosphorylated site through a Src-homology 2 (SH2) domain and hydrolyses phosphatidylinositol-4,5-bisphosphate (PIP_2) to generate inositol-1,4,5-trisphosphate (IP_3) and diacylglycerol (DAG) (98). DAG activates PKCs to induce cell survival and enhance synaptic plasticity (80, 103). IP_3 regulates the calcium release from the endoplasmic reticulum (ER), therefore activating Ca^{2+}-dependent enzymes such as CaMKII, which alter synaptic plasticity

and enhance neurotransmission (40, 80, 95, 125). Additionally, at neuronal growth cones, TrkB-PLCγ-signaling has been described to increase cytoplasmatic calcium through transient receptor potential canonical channels (TRPCs) (153). Most importantly, this modulation of intracellular calcium transients and associated proteins allows for TrkB-dependent contribution to different forms of synaptic plasticity, such as LTP (154). Recruitment of PLCγ results in the induction of CREB and CaMKIV phosphorylation, which induces a transcriptional program supporting long-lasting potentiation in excitatory synapses (152). Further, via enhancing autophosphorylation of CaMKII, PLCγ signaling increases CaMKII-dependent phosphorylation of AMPARs and accessory proteins, facilitating receptor trafficking to the postsynaptic density (40, 155). CaMKII also impacts the plasticity of inhibitory synapses by direct phosphorylation of gephyrin at Ser305 and synaptic recruitment of $GABA_A$Rs (discussed in section 1.2.1) (46, 71).

1.3.2. Bdnf/TrkB in Neuropsychiatric Disorders and Inhibitory Synaptic Regulation

The pivotal roles of these pathways in various cellular physiological processes indicate the profound impact of TrkB activation on the formation of precisely connected networks at the level of synapses (86). Via components of its major signaling pathways, TrkB participates in axonal and dendritic differentiation as well as in the formation and maintenance of glutamatergic and GABAergic synapses (discussed in 1.3.1). Furthermore, Bdnf has been associated with various psychiatric and neurological conditions, including MDD, anxiety disorders, schizophrenia, and post-traumatic stress disorder (PTSD) (156-159). Accumulating evidence has revealed that the molecular etiology of numerous neuropsychiatric and neurodegenerative disorders involves synaptic dysfunction (160-165). The accompanying deficit in synaptic plasticity typically results in an imbalance between excitatory and inhibitors (E/I) balance, which had been consistently reported by several studies, therefore emerging as a fundamental principle underlying a variety of neuropsychiatric and neurodevelopmental disorders (166-169). Deficits in Bdnf signaling during development were shown to cause E/I synaptic imbalance, as observed in a mouse model of autism (ASD) (121) and recent studies revealed that several antidepressants act as positive allosteric modulators of TrkB, thereby facilitating Bdnf action and plasticity (170, 171). Additionally, disruption of kinase activity of proteins involved in TrkB-mediated signaling, including MAPK (Erk1/2), Gsk3β, mTOR, and CaMKIIα signaling cascades, contribute to certain schizophrenia, ASD, and PTSD phenotypes (134, 172-178).

In addition, there are indications of impaired Gphn function in several neuropsychiatric disorders, pointing to this inhibitory synapse scaffold protein as a possible target for therapeutic interventions (18). Therefore, TrkB-mediated effects on postsynaptic neurotransmitter clusters may be part of a mechanism that balances inhibitory and excitatory synaptic transmission in neural circuits (179). Additionally, there has been molecular evidence for Bdnf- and GABA-related dysfunctions in MDD, directly linking the neurotrophic and GABA hypotheses of depression (180).

The notion of a Bdnf/TrkB-dependent regulation of inhibitory transmission was further supported by several studies that directly implicated TrkB in the clustering of gephyrin: As already emphasized, Wuchter and colleagues identified TrkB and protein kinases involved in the cognate signaling pathways associated with the stabilization of gephyrin clusters (discussed in 1.2.1 and 1.3.1) (see Figure 2) (54). RNAi-dependent knock-down of TrkB in primary hippocampal neurons impaired Gphn and $GABA_AR$ γ2 subunit clustering and further suggested that Bdnf supports Gphn clustering through MAPK- and PI3K/Akt-mTOR signaling (73, 82). Additionally, several studies showed an increase in the expression and clustering of

Gphn levels after prolonged Bdnf stimulation, an effect that additionally promoted interaction $GABA_A$Rs (63, 119, 181).

Transferring this work *in vivo*, it was able to show that an RNAi-mediated knockdown of TrkB in DG granule cells of rats specifically reduced Gphn clustering at the somata and proximal dendrites (182). These results suggest that TrkB-dependent gephyrin clustering is exclusive to specific inhibitory neuronal subtypes in the DG, such as parvalbumin (PV) and cholecystokinin (CCK) positive basket cells since they differ in the area they target at the principal neurons (183-185). Another supporting study demonstrated that TrkB regulates the assembly and maintenance of GABAergic synapses in the cerebellar cortex by controlling the localization of gephyrin and the cell adhesion molecule Contactin-1, further emphasizing TrkB's essential role in GABAergic synaptic stability (186). This study further proposed that these TrkB-regulated processes are mediated by the PLCγ-binding site, pointing to a calcium-dependent mechanism in the formation of GABAergic synapses (118). Several studies suggest a role for TrkB in the activity-dependent formation and potentiation of these synapses, a crucial process for preserving E/I balance in the brain (29, 31, 187, 188). However, whether this process involves TrkB-dependent regulation of gephyrin remains unclear.

2. AIM

The mechanisms by which TrkB governs inhibitory synapses, specifically at the level of gephyrin, remain unclear. Moreover, the molecular mechanisms of downstream effectors are still under debate, particularly due to contrary observations. Therefore, this study aims to elucidate the role of TrkB in GABAergic synaptic plasticity by dissecting its major signaling pathways and their distinct contributions to the clustering of the inhibitory scaffold protein gephyrin.

To target the individual signaling pathways downstream of neuronal TrkB, mutants of the rat TrkB receptor will be generated and verified using Western Blot analysis. These mutants will be specifically deficient in autophosphorylation or in the induction of PLCγ- or Shc-dependent signaling pathways.

To understand the pathway-specific contributions to inhibitory synapse stabilization under basal conditions, rat primary hippocampal neurons will be transduced with the TrkB mutants to achieve their overexpression. Subsequently, their potential effects on inhibitory synaptic proteins will be evaluated through immunocytochemistry and confocal laser scan microscopy focusing on the scaffold protein gephyrin. In addition, the activation of mTOR and CaMKII, as potential downstream mediators, will be assessed via their phosphorylated forms.

Furthermore, the functional consequences of aberrant signaling and synaptic connectivity will be investigated by analyzing patterns of intracellular calcium transients of neurons overexpressing the TrkB mutants.

Finally, to explore the potential involvement of TrkB in inhibitory synaptic plasticity, inhibitory long-term potentiation will be chemically induced in TrkB mutant overexpressing primary neurons. Inhibitory synaptic proteins will be quantified, and cultures with and without induced iLTP will be compared to determine potential alterations in the associated changes in synaptic protein accumulation. This will illuminate a possible role of TrkB signaling in homeostatic processes that allow neurons to adapt inhibitory synaptic strength to changes in excitatory transmission, using the Bdnf-receptor as a cross-linking mediator.

3. Material and Methods

3.1. Material

3.1.1. Consumables

Table 1 Consumables

Consumables	Manufacturer
0.22 µm PES vacuum filter	Corning Inc., USA
0.22 µm sterile filter	Carl Roth GmbH + Co. KG, Germany
0.45 µm SFCA sterile filter	Corning Inc., USA
100 µm nylon strainer	SPL Life Sciences, Korea
6 well plates	Greiner Bio-One, Germany
96 well µClear® advanced TC, black	Greiner Bio-One, Germany
Cell culture flasks (75, 175 cm^2)	Corning Inc., USA
Cell scrapers	Corning Inc., USA
Cryopreservation tubes	Greiner Bio-One, Germany
Eppendorf Tubes (1.5, 2 ml)	Eppendorf AG, Germany
Falcon Tubes (15, 50 ml)	Greiner Bio-One, Germany
NuPAGE™ 4-12%, Bis-Tris Mini Protein Gels	Thermo Fisher Scientific, USA
Parafilm	Pechiney Plastic Packaging
Petri dishes (5, 10, 25 cm)	Greiner Bio-One, Germany
Pipette reservoir (25, 50 ml)	Cole-Parmer Essentials, USA
Protein LoBind® Tubes	Eppendorf AG, Germany
PVDF Low-Fluorescence Transfer Membranes, 0.2 µm	Thermo Fisher Scientific, USA
PVDF Transfer Membranes, 0.45 µm	Thermo Fisher Scientific, USA
Serological pipettes	Greiner Bio-One, Germany
TipOne® pipette tips (0.1-2.5 µl; 0.5-10 µl; 10-200 µl; 100-1000 µl)	Starlab Internation GmbH, Germany
Via-1 Casettes™	ChemoMetec, A/S, Denmark

3.1.2. Instruments and Devices

Table 2 Instruments and devices

Instrument	Manufacturer
Cell Observer SD	Zeiss, Germany

Centrifuge 5804 R	Eppendorf AG, Germany
CO_2 incubator	WTC Binder, Germany
EVOS XL Core	Thermo Fisher Scientific, USA
Gel electrophoresis chamber	Bio-Rad Laboratories, USA
GelDoc Go Imaging System	Bio-Rad Laboratories, USA
ImageQuant™ LAS-400 mini	GE Healthcare, USA
IncuCyte	Sartorius AG, Germany
Invitrogen™ XCell SureLock™ Mini-Cell und XCell II™ Blot Modul	Thermo Fisher Scientific, USA
LI-COR Odyssey Imager System	LI-COR, Bad Homburg, Germany
Multipette® plus Repeater® plus	Eppendorf AG
Nanodrop, Spectrophotometer ND-100	Thermo Fisher Scientific, USA
Neubauer Counting Chamber	Marienfeld GmbH & Co. KG, Germany
Nucleocounter NC-200	ChemoMetec A/S, Denmark
PerfectBlue Semi-Dry Electro Blotter	Peqlab Biotechnologie GmbH, Germany
pH meter	Mettler Toledo, Germany
Pipette boy ROTILABO®	Carl Roth GmbH + Co. KG, Germany
Pipettes (0.1-2.5 µl; 0.5-10 µl; 10-200 µl; 100-1000 µl)	Eppendorf AG, Germany
PowerEase® 500 Power Supply	Thermo Fisher Scientific, USA
StepOnePlus ™ Real-Time PCR System	Applied Biosystems™, USA
Tecan Plate Reader Spark	Tecan Trading AG, Switzerland
Thermocycler Biometra TOne	Analytic Jena AG, Germany
Thermomixer (comfort)	Eppendorf AG, Germany
Typhoon Trio Variable Mode Imager	GE Healthcare, USA
Ultracentrifuge Sorvall™ MX Plus Mikro	Thermo Fisher Scientific, USA
Vortex Genie 2	Scientific Industries Inc., USA
Water bath	Carl Roth GmbH + Co. KG, Germany

3.1.3. Chemicals and Reagents

Table 3 Chemicals and reagents

Reagent	Manufacturer	Catalogue No.
1 kb Plus DNA Ladder	New England Biolabs, USA	N3200S
2-Mercaptoethanol	Carl Roth GmbH + Co. KG, Germany	4227
Acetic acid	Carl Roth GmbH + Co. KG, Germany	7332
Agar	Carl Roth GmbH + Co. KG, Germany	5210

Agarose Broad Range	Carl Roth GmbH + Co. KG, Germany	T846
Blocking Reagent BMB	Roche, Switzerland	11112589001
Boric acid (H_3BO_3)	Sigma Aldrich, USA	B0252
Bovine Serum Albumin (BSA) Fraction V	Carl Roth GmbH + Co. KG, Germany	1ETA
Calbryte™ 590 AM	AAT Bioquest, USA	20700
Calcium chloride dihydrate	Carl Roth GmbH + Co. KG, Germany	T885
CNQX	MedChem Express, USA	HY-15066
cOmplete™ Mini Protease Inhibitor-Cocktail	Roche, Switzerland	11836153001
CutSmart Buffer	New England Biolabs GmbH, Germany	B6004
Cyclotraxin B	MedChem Express, USA	HY-P1178
Cyclotraxin B	MedChem Express, USA	HY-P1178
D-Glucose	Carl Roth GmbH + Co. KG, Germany	HN06
Dimethylsulfoxid (DMSO)	Carl Roth GmbH + Co. KG, Germany	A994.1
Dulbecco's phosphate buffered saline	Thermo Fisher Scientific, USA	14190094
EDTA solution	Carl Roth GmbH + Co. KG, Germany	1E23
Ethanol	Carl Roth GmbH + Co. KG, Germany	P075
Gel Loading Dye, Purple (6X)	New England Biolabs, USA	B7024
HEPES	Carl Roth GmbH + Co. KG, Germany	HN78
Hydrochloric acid	Carl Roth GmbH + Co. KG, Germany	N076
Isopropanol	Carl Roth GmbH + Co. KG, Germany	0080
KN-62	MedChem Express, USA	HY-13290
LB medium	Carl Roth GmbH + Co. KG, Germany	X964
Lipofectamine™ 2000	Thermo Fisher Scientific, USA	11668019
Magnesium chloride hexahydrate	Carl Roth GmbH + Co. KG, Germany	2189
Methanol	Carl Roth GmbH + Co. KG, Germany	CP43
Midori Green Advance	NIPPON Genetics EUROPE GmbH, Germany	MG04
NaOH	Carl Roth GmbH + Co. KG, Germany	T198
NMDA	MedChem Express, USA	HY-17551
Nuclease-free H_2O	New England Biolabs, USA	B1500S
Nuclease-free Water	New England Biolabs, USA	B1500S
NuPage™ Antioxidans	Thermo Fisher Scientific, USA	NP0005

NuPage™ LDS Loading Buffer	Thermo Fisher Scientific, USA	NP0007
NuPage™ MOPS SDS Running Buffer, 20X	Thermo Fisher Scientific, USA	NP0001
NuPage™ Reducing Agent	Thermo Fisher Scientific, USA	NP0009
NuPage™ Transfer Buffer, 20X	Thermo Fisher Scientific, USA	NP00061
Paraformaldehyd (PFA)	Carl Roth GmbH + Co. KG, Germany	0964
PD98059	MedChem Express, USA	HY-12028
Pierce™ Phosphatase Inhibitor Mini Tablets	Thermo Fisher Scientific, USA	A32957
Ponceau S	Carl Roth GmbH + Co. KG, Germany	5938
Potassium chloride	Carl Roth GmbH + Co. KG, Germany	0601
Q5® High-Fidelity 2X Master Mix	New England Biolabs GmbH, Germany	M0492
RIPA buffer, 1X	Thermo Fisher Scientific, USA	89901
S.O.C. medium	Thermo Fisher Scientific, USA	15544034
Saccharose	Carl Roth GmbH + Co. KG, Germany	4621
SignalFire™ Plus ECL Reagent	Cell Signaling Technology, USA	12630
Sodium azide	Carl Roth GmbH + Co. KG, Germany	4221
Sodium bicarbonate	Carl Roth GmbH + Co. KG, Germany	6885
Sodium chloride	Carl Roth GmbH + Co. KG, Germany	P029
Sodium Pyruvate (100 mM)	Thermo Fisher Scientific, USA	11360070
Sodium tetraborat decahydrate ($Na_2B_4O_7$)	Sigma Aldrich, USA	B9876
T4 Ligase	New England Biolabs GmbH, Germany	M0202
T4 Ligation Buffer, 10X	New England Biolabs GmbH, Germany	B0202
Tris	Carl Roth GmbH + Co. KG, Germany	5429
Triton-X-100	Carl Roth GmbH + Co. KG, Germany	3051
Tween 20	Carl Roth GmbH + Co. KG, Germany	9139

3.1.4. Recombinant Proteins, Restriction Enzymes, and Antibiotics

Table 4 Proteins, restriction enzymes, and antibiotics

Material	Manufacturer	Catalogue No.
Amplicillin	Carl Roth GmbH & Co. KG	HP62
BlpI	New England Biolabs GmbH, Germany	R0585
Geneticin (G418)	Carl Roth GmbH + Co. KG, Germany	2039
Kanamycin	Carl Roth GmbH & Co. KG	T832
Penicillin/Strepomycin	Thermo Fisher Scientific, USA	15140122
Recombinant Human BDNF	PeproTech, Inc., USA	450-02
XhoI	New England Biolabs GmbH, Germany	R0146

3.1.5. Bacterial Strains and Cell Lines

Table 5 Bacterial strains

Cell Line	Manufacturer	Catalogue No.
OneShot™ Stbl3™ chemically competent E.coli	Thermo Fisher Scientific, USA	C737303
OneShot™ Top10 chemically competent E.coli	Thermo Fisher Scientific, USA	C404006
Library Efficiency DB3.1™ chemically competent cells	Thermo Fisher Scientific, USA	11782-018
XL1-Blue supercompetent cells	Agilent Technologies, USA	200518

Table 6 Cell lines

Cell Line	Distributor	Catalogue No.
HEK293	CLS Cell Lines Service GmbH, Germany	300192
HEK293 FT	Thermo Fisher Scientific, USA	R70007
NIH3T3	ATCC, USA	

3.1.6. Cell Culture Media and Supplements

Table 7 Cell culture media and supplements

Medium	Manufacturer	Catalogue No.
B-27™ Supplement	Thermo Fisher Scientific, USA	17504044
BrainPhys™ Imaging Optimized Medium	STEMCELL Technologies, Inc., USA	05796
BrainPhys™ Neuronal Medium and SM1 Kit	STEMCELL Technologies, Inc., USA	05792
DMEM, high glucose, GlutaMAX™ Supplement	Thermo Fisher Scientific, USA	10566016
Fetal Bovine Serum	Thermo Fisher Scientific, USA	10270
Horse Serum	Thermo Fisher Scientific, USA	16050122
L-Glutamine	Thermo Fisher Scientific, USA	25030024
MEM (10X)	Thermo Fisher Scientific, USA	11430030
Non-essential amino acids	Thermo Fisher Scientific, USA	11140035
Opti-MEM™, Reduced Serum Medium	Thermo Fisher Scientific, USA	31985070
Sodium Pyruvate (100 mM)	Thermo Fisher Scientific, USA	11360070
Trypsin/EDTA (0.05 %), with phenol red	Thermo Fisher Scientific, USA	25300054

Table 8 HEK293 cultivation medium

Component	Final concentration
DMEM, high glucose, GlutaMAX™ Supplement	1 X
FBS	10 % v/v
NEAA	1 mM
1 mM	1 mM

Table 9 3T3 standard medium

Component	Final concentration
DMEM, high glucose, GlutaMAX™ Supplement	1 X
FBS	10 % v/v
L-Glutamine	2 mM

Table 10 HEK293FT cultivation medium

Component	Final concentration
DMEM, high glucose, GlutaMAX™ Supplement	1 X
FBS	10 % v/v
NEAAs	1 mM
G418	500 µg/ml

Table 11 HEK293FT pre-transfection medium

Component	Final concentration
Opti-MEM™	1 X
FBS	2% v/v

Table 12 PEI coating and primary neuron seeding medium

Component	Final concentration
PEI-coating	
Sodium borate solution (0.1 M in ddH_2O)	50 mM
Boric acid solution (0.2 M in ddH_2O)	0.1 M
PEI (5%)	0.0005 % v/v
Seeding medium	
NMEM+B27 (see Table 13)	1 X
Horse serum	10 v/v

Table 13 Primary neuron cultivation medium in ddH_2O

Component	Final concentration
MEM	1 X
L-Glutamine	2 mM
Sodium pyruvate	1 mM
$NaHCO_3$ (5,5 % w/v in ddH_2O)	2,2 %
Glucose (20 % w/v in ddH_2O)	6 %
B27, serum free	1 X

3.1.7. Buffer

Table 14 10X TAE buffer in ddH_2O

Component	Concentration
Tris-Acetat	0.4 M
EDTA	0.01 M
Acetic acid	0.2 M

Table 15 1X TBST buffer in ddH_2O

Component	Final concentration
Tris-HCl	15 mM
NaCl	136 mM
Tween-20	0.1 % (v/v)

Table 16 Stripping buffer in ddH_2O

Component	Final concentration
SDS (10% w/v)	2 % (w/v)
Tris-HCl (0.5 M, pH 6.8)	62.5 mM
2-Mercaptoethanol	8 mM

Table 17 TE buffer, pH 8 ddH_2O

Component	Sample
Tris	10 mM
EDTA	1 mM

Table 18 Recording solution in ddH_2O

Component	Final concentration
NaCl	145 mM
KCl	2 mM
$CaClx2H_2O$	2 mM
$MgClx6H_2O$	2 mM
D-Glucose	10 mM
HEPES	10 mM
Saccharose	1 mM

3.1.8. Commercially Available Kits

Table 19 Commercially available kits and enzymes

Kit	Manufacturer	Catalogue No.
Gateway™ BP Clonase™ II Enzyme-Mix	Thermo Fisher Scientific, USA	11789020
Gateway™ LR Clonase™ II Enzyme-Mix	Thermo Fisher Scientific, USA	11791100
Lenti-X™ qRT-PCR Titration Kit	Takara Bio Inc., Japan	631235
NucleoSpin RNA Virus Kit	Macherey-Nagel GmbH & Co. KG, Germany	740956.10
Pierce™ BCA Protein Assay Kit	Thermo Fisher Scientific, USA	23225
Plasmid Mini Kit	Qiagen, Germany	12123
QIAquick Gel Extraction Kit	Qiagen, Germany	12143
QIAquick PCR Purification Kit	Qiagen, Germany	28104
QuikChange Site-Directed Mutagenesis Kit	Agilent Technologies, USA	200518

3.1.9. Antibodies

Table 20 Primary antibodies

Antibody target	Host Species	Manufacturer	Catalogue No.	Dilution
CAMKII α	rabbit	Proteintech Group, Inc, IL, USA	13730-1-AP	1:200
Cleaved Capsase 3	rabbit	Cell Signaling Technology, USA	9661	1:400
GABA	rabbit	Thermo Fisher Scientific, USA	A2052	1:500
GABAA receptor α2 subunit	rabbit	Synaptic Systems, Germany	224103	1:500
Gephyrin	mouse	Synaptic Systems, Germany	147021	1:500
Hoechst 33258		Sigma-Aldrich, USA	861405	1:1000
MAP2	chicken	Thermo Fisher Scientific, USA	PA1-10005	1:2500
p44/42 MAPK	rabbit	Cell Signaling Technology, USA	9102	1:1000

phospho CAMKII α (Thr286)	mouse	Thermo Fisher Scientific, USA	MA1-047	1:100
phospho mTor (ser2448)	rabbit	Cell Signaling Technology, USA	5536	1:50
phospho p44/42 MAPK (Thr202/Tyr204)	mouse	Cell Signaling Technology, USA	9106	1:1000
phospho p70 S6Kinase (Thr389)	rabbit	Cell Signaling Technology, USA	9234	1:1000
phospho PLCγ1 (Y783)	rabbit	Cell Signaling Technology, USA	2821	1:500
phospho-TrkA (Tyr674/675)/TrkB (Tyr706/707)	rabbit	Cell Signaling Technology, USA	4621	1:1000
PLCγ1 (pan)	rabbit	Cell Signaling Technology, USA	2822	1:1000
PSD95	rabbit	Synaptic Systems, Germany	124003	1:500
TrkB	goat	R&D Systems Inc., USA	AF1494	1:2000 (WB)
TrkB	rabbit	Abcam, UK	Ab6180	1:50 (ICC)
vGAT	rabbit	Synaptic Systems, Germany	131003	1:500
vGLUT1	mouse	Synaptic Systems, Germany	135511	1:400
β-Actin	mouse	Sigma-Aldrich, USA	A5316	1:5000

Table 21 Secondary antibodies

Fluorophore/Reporter enzyme	**Host and immunogen species**	**Manufacturer**	**Catalogue No.**	**Dilution**
Alexa Fluor 405	goat anti-chicken IgY (H+L)	Thermo Fisher Scientific, USA	A486260	1:150
Alexa Fluor Plus 555	F(ab')2 goat anti-rabbit IgG (H+L)	Thermo Fisher Scientific, USA	A48283	1:500

Alexa Fluor Plus 647	F(ab')2 goat anti-mouse IgG (H+L)	Thermo Fisher Scientific, USA	A48289	1:500
AlexaFluor 488	goat anti-chicken IgY (H+L)	Thermo Fisher Scientific, USA	A-11039	1:400
Cy3-AffiniPure	goat anti-mouse IgG (H+L)	Jackson ImmunoResearch, UK	115-165-146	1:500
Cy3-AffiniPure	goat anti-rabbit IgG (H+L)	Jackson ImmunoResearch, UK	111-165-144	1:500
Cy5-AffiniPure	goat anti-mouse IgG (H+L)	Jackson ImmunoResearch, UK	115-175-146	1:500
Cy5-AffiniPure	goat anti-rabbit IgG (H+L)	Jackson ImmunoResearch, UK	111-175-144	1:500
HRP	Anti-mouse IgG	Cell Signaling Technology, USA	7076	1:5000
HRP	Anti-rabbit IgG	Cell Signaling Technology, USA	7074	1:5000
IRDye® 680RD	Anit-rabbit IgG	LI-COR Biosciences – GmbH, Germany	926-68071	1:2000
IRDye® 800CW	Anti-mouse IgG	LI-COR Biosciences – GmbH, Germany	926-32350	1:2000

3.1.10. Plasmids

Table 22 Plasmids

Plasmid	Distributor	Catalogue/Reference No.
pDONR™ 221	Thermo Fisher Scientific, USA	12536017
pEGFP-N1	Takara Bio Inc., Japan (former Clontech)	/
pEGFP-N1-TrkB	Addgene	32500
pLenti4CamKII_s/V5-DEST	Martin Kriebel	(189)

pLenti6_sS_WPRE	Martin Kriebel	(189)
pLP/VSVG	Martin Kriebel (based on Cellectas RTX packaging mix)	CPCP-K2A
pLP1	Martin Kriebel (based on Cellectas RTX packaging mix)	CPCP-K2A
pLP2	Martin Kriebel (based on Cellectas RTX packaging mix)	CPCP-K2A

3.1.11. Oligonucleotides

Table 23 Oligonucleotides

Name	Sequence (3'-5')	Applied for
attB1-EGFP_fw	GGGGACAAGTTTGTACAAAAAA GCAGGCTTCCGCCACCATGGT GAGCAAGG	Gateway cloning
TrkB_EGFP_K571A_mut _f	CTGGTGGCCGTGGCGACGCTG AAGGAC	Mutagenesis
TrkB_EGFP_K571A_mut _r	GTCCTTCAGCGTCGCCAC GGCCACCAG	Mutagenesis
TrkB_EGFP_Y515F_mut _f	CATTGAAAACCCCCAGTTCTTC GGTATCACCAAC	Mutagenesis
TrkB_EGFP_Y515F_mut _r	GTTGGTGATACCGAAGAACTGG GGGTTTTCAATG	Mutagenesis
TrkB_EGFP_Y816F_mut _f	GGCGTCGCCCGTCTTCCTGGA CATCCTAG	Mutagenesis
TrkB_EGFP_Y816F_mut _r	CTAGGATGTCCAGGAAGACGG GCGACGCC	Mutagenesis
TrkB-EGFP_attB1_fw	GGGGACAAGTTTGTACAAAAAA GCAGGCTTCACCATGTCGCCCT GGCCGAGGTG	Gateway cloning
TrkB-EGFP_attB2_rev	GGGGACCACTTTGTACAAGAAA GCTGGGTTTTACTTGTACAGCT CGTCCATGCC	Gateway cloning
WPRE-BlpI_rev	ACTACTTGCTTAGCGATGCGGG GAGGCG	Cloning

XhoI-WPRE_fw	TCAATGCTCGAGAATCAACCTC TGGATTACAAAATT	Cloning

3.1.12. Software

Table 24 Software

Software	Company	Version used
Fiji (based on Image J2)	National Institutes of Health, USA (Image J)	2.9
GraphPad Prism	GraphPad Software, USA	10.2
Image Lab	Bio-Rad Laboratories, Inc., USA	6.1
Image Studio	LI-COR Biotechnology, USA	4.0
Imaris Bitplane	Oxford Instruments, UK	10
IncuCyte S3	Sartorius AG, Germany	2019A
Origin	OriginLab Corporation, USA	2015G
SnapGene Viewer	GSL Biotech LLC, USA	5.3.1
ZEN (blue edition)	Zeiss, Germany	3.4

3.2. Methods

3.2.1. Generation of TrkB Mutants

Signaling-deficient TrkB mutants were derived from the pEGFP-N1-TrkB plasmid (a gift from Rosalind Segal (Addgene plasmid # 32500; http://n2t.net/addgene:32500; RRID: Addgene_32500)), which contains the rat full-length *Ntrk2* (TrkB) coding sequence, fused to EGFP at the C-terminus (for Map see Supplementary Figure 1). To verify that the TrkB coding DNA sequence (cds) of pEFGP-N1-TrkB plasmid contains the complete TrkB coding sequence of *Rattus norvegicus*, the sequence was compared to NCBI GenBank ID M55291.1. Further detection of sites critical for Shc, PLCγ, and ATP binding were identified and confirmed based on previous reports (99, 152, 190) and comparison of the amino acid (aa) sequence of pEGFP-N1-TrkB with the rat TrkB aa sequence provided by the universal protein database UniProt (https://www.uniprot.org/; Protein ID: Q63604). Following verification, pEGFP-N1-TrkB was amplified from the original agar stock.

Preparation of LB-Agar Plates

LB-agar plates were prepared by heating 500 ml of LB medium with 7.5 g of agar until fully dissolved. After cooling the medium to below 50°C, either 100 µg/ml ampicillin or 50 µg/ml kanamycin were added, respectively. 10 cm petri dishes were filled with 10-20 ml of LB-antibiotic medium and allowed to cool. The plates were stored at 4°C until needed for growing separate bacterial colonies from agar stocks or transformed cells.

Transformation of OneShot TOP10 Competent Cells

To amplify expression vectors, such as pEGFP-N1-TrkB, 1 ng of the plasmid was added to OneShot™ Top10 chemically competent *E.Coli* bacteria, which were transformed according to the manufacturer's protocol and spread on prewarmed selective LB-agar plates for incubation overnight at 37°C.

Propagation and Purification of Plasmids

To grow bacteria and propagate the plasmid of interest, individual bacterial colonies were picked from selective plates for inoculation of 50 ml LB medium, supplemented with the appropriate antibiotic, followed by incubation overnight at 37°C, shaking at 200 rpm. Plasmids were purified the following day using the Qiagen Plasmid Plus Midi Kit according to the manufacturer's protocol. In the final step, plasmids were eluted in 100 µl ddH_2O by centrifugation at 10 000 x g for 1 min and stored at -20°C until needed.

Restriction Digest of Plasmid DNA

To verify purified plasmids, a small amount was enzymatically digested with the appropriate set of restriction enzymes at 37°C for 1.5-2 h. In case of pEGFP-N1-TrkB this involved digestion with *BlpI* (see Table 25).

Table 25 Reaction of analytical plasmid digestion

Component	Quantity
pEGFP-N1-TrkB	0.5 ng
CutSmart Buffer (10X)	1 µl
BlpI (10,000 units/ml)	1 µl
ddH_2O	Filled up to 10 µl

Gel Electrophoresis

To confirm plasmid digestion, the fragments of digested DNA were separated by gel electrophoresis. Agarose gels (1-2 % w/v) were prepared by dissolving 1.5-3 g agarose in 150 ml of 1X Tris-acetat-EDTA (TAE) buffer (see Table 14). After adding Midori Green (25 000 x), the gel mixture was poured into a chamber and allowed to solidify for at least 20 min at RT. Each plasmid sample was mixed with 6X purple loading dye and loaded into the gel pockets. For reference, additional pockets were loaded with 5-10 µl of 1 kb Plus DNA Ladder. DNA fragments were separated by applying 120 V for at least 45 min. DNA bands were visualized using the UV-light tray of the Gel Doc Pro. Only plasmids displaying the expected fragment sizes were used for subsequent mutagenesis.

Site-Directed Mutagenesis

TrkB sites of interest were targeted using the QuikChange Site-Directed Mutagenesis Kit. Mutagenic primers were designed according to the manufacturer's protocol and following primer pairs were used: TrkB_EGFP_Y515F_mut_f and TrkB_EGFP_Y515F_mut_r (TrkBY515F); TrkB_EGFP_Y816F_mut_f and TrkB_EGFP_Y816F_mut_r (TrkBY816F); TrkB_EGFP_K571A_mut_f and TrkB_EGFP_K571A_mut_r (K571A) (for sequences see Table 23).

Site-directed mutagenesis was performed by preparing PCR reactions using pEGFP-N1-TrkB as the template for the respective mutagenic primer pairs (see Table 26 and Table 27).

Table 26 PCR reaction for site-directed mutagenesis

Component	Quantity
Reaction buffer, 10X	5 µl
pEGFP-N1-TrkB	50 ng
TrkB_EGFP_X_mut_f	125 ng
TrkB_EGFP_X_mut_r	125 ng
dNTP mix	1 µl
ddH_2O	Filled up to 50 µl
PfuTurbo DNA polymerase	1 µl

Table 27 PCR cycling parameters

Segment	Cycles	Temperature	Time
1	1	95°C	30 s
2	12	95°C	30 s
		55°C	1 min
		68°C	3 min

Following PCR, the reactions were stored on ice for *DpnI* digestion. The *DpnI* enzyme digests methylated DNA, such as the non-mutated pEGFP-N1-TrkB template but does not degrade the mutated PCR amplified DNA. 1 µl of *DpnI* was added to each reaction and incubated for 1 h at 37°C.

Next, 1 µl of *DpnI*-treated DNA was added to 50 µl of supercompetent XL1-Blue cells (included in the mutagenesis kit) for transformation according to the manufacturer's protocol. Bacteria were plated onto 2x LB-kanamycin agar plates and incubated overnight at 37°C.

The following day, several isolated clones were picked and processed for plasmid amplification and extraction as described before (see Propagation and Purification of Plasmids). Following restriction digest (see Restriction Digest of Plasmid DNA), plasmids displaying the expected fragments were further validated for their mutation via Sanger Sequencing at 4baselab AG, Germany (https://4base-lab.de/).

3.2.2. Characterization of TrkB Mutants

Cultivation of HEK293 and NIH3T3 Cells

HEK293 and NIH3T3 cells were cultured in T175 flasks with standard HEK293 or NIH3T3 medium (see Table 8 and Table 9) at 37°C and 5% CO_2 in humidified atmosphere. Cells were dissociated when reaching approximately 70-80 % confluency by treatment with Trypsin-EDTA (0.05%) after a single wash with DPBS to remove the remaining FBS from the cells. Once detached from the vessel, HEK293 medium or NIH3T3 medium was added to stop further trypsinization, and cells were harvested via centrifugation at 300 g for 3 min. Subsequently, the cells were resuspended in the respective standard cultivation medium and seeded in a 1:20 ratio for preservation of the cell lines or at 0.5 $x10^6$ cells/well in a 6-well format for transfection with the TrkB plasmids.

Transfection of HEK293 and NIH3T3 Cells and Protein Extraction

At 70% confluency, cells were transfected with DNA using Lipofectamine 2000 according to the manufacturer's protocol. For each well, 10 µl of Lipofectamine 2000 was added to 250 µl of Opti-MEM and incubated for 5 min at RT. Further 250 µl of Opti-MEM were mixed with 2 µg of the respective plasmids, combined with the Lipofectamine 2000 mixture, and added to the cells after a 20-min incubation at RT. Subsequently, cells were incubated at 37°C and 5 % CO_2 until the next day, when the media was exchanged for serum-free cultivation medium for 24 h. Prior to lysis, the cells were stimulated with 100 ng/ml Bdnf for 30 min at 37°C under humidified atmosphere. After washing with DPBS, cells were lysed in RIPA buffer supplemented with cOmplete™ mini protease inhibitors and Pierce™ Phosphatase inhibitors for 30 min on ice. To remove debris, the cells were centrifuged for 20 min at 14 000 x g and 4°C. The protein-containing supernatant was collected and stored in protein low-bind tubes at -20°C until further processed.

Determination of Protein Concentration

Protein concentrations of the collected extracts were determined in triplicates using the Pierce™ BCA Protein Assay Kit according to the manufacturer's protocol. Samples were prepared in protein low-bind tubes with 10X NuPage™ Sample Reduction Agent and 4x NuPage™ LDS-Sample Buffer to a final concentration of 1.5 µg/µl and a total volume of 20 µl. As a final step, the cells were heated for 10 min at 70°C and either used immediately or stored for further processing at -20°C. In the latter case, the samples were thawed and heated again for 10 min at 70°C before loading.

SDS-PAGE

Prepared cell extracts were separated by SDS-PAGE with 30 µg of protein per lane on NuPAGE™ 4-12 % Bis-Tris gels with 20X NuPage™ MOPS running buffer, following the manufacturer's protocol. Electrophoresis was performed in a XCell SureLock™ Mini Cell Module, initially at 150 V for 10 min, and subsequently at 200 V for 50-60 min.

Western Blot

After separation, proteins were transferred to PVDF membranes. Proteins of HEK293 cells were transferred using semi-dry blotting in NuPAGE™ Transfer Buffer, which was prepared according to the manufacturer's protocol and blotted with a PerfectBlue Semi-Dry Electro Blotter at 2 mA/cm^2 and constant 250 V for 80 min. Proteins of NIH3T3 were transferred using wet tank blotting with identical transfer buffer but in a XCell II™ Blot Module, at 30 V, 200 mA, and 17 W for 75-120 min powered by PowerEase® 500 Power Supply.

Immediately after blotting, membranes were stained with 0,1 % Ponceau/1% Acetic acid for 10 min to confirm protein transfer. After two washes with 1X TBST (pH 7.6) (see Table 15), membranes were dried and imaged with the GelDoc Go device.

Immunolabeling and Detection of Proteins

Proteins of interest were visualized using indirect immunolabeling. Membranes were blocked with 1 % TBST/5 % (w/v) BSA for 60 min at RT on a rolling shaker. Primary antibodies were incubated overnight at 4°C on a rolling shaker (for primary antibody dilutions, see Table 20). Except for phosphorylated PLCγ1 and total (pan) PLCγ1, membranes were washed three times for 5 min each with 1X TBST before incubation with fluorescently labeled secondary antibodies diluted in 1X TBST/5 % (w/v) BSA for 1 h at RT (for secondary antibody dilutions, see Table 21). After three additional washing steps with 1X TBST for 5 min each, membranes were dried and protected against light until imaging.

The signals related to phospho-TrkB and pan TrkB were detected using the Typhoon Trio Variable Mode Imager with excitation at 543 nm and 633 nm and detection of signals with 580BP30 and 670BP30 filters, respectively. Fusion protein weights were estimated using the 'Protein Molecular Weight' online tool (https://www.bioinformatics.org/sms/prot_mw.html). Signals related to phospho-Erk1/2 and pan Erk1/2 were detected using the 700 nm and 800 nm channels of the LI-COR Odyssey Imager System, respectively. For the detection of phosphorylated PLCγ1 and pan PLCγ1, HRP-labeled secondary antibodies were applied as described above. After the final washing step, the membranes were kept in 1X TBST and wrapped in foil to prevent drying. To develop chemiluminescent signals, membranes were

incubated with fresh SignalFireTM Plus ECL Reagent mix for 1 min at RT and protected from light. Signals were subsequently acquired using the ImageQuantTM LAS-400 mini.

Since both primary antibodies used for the detection of PLCγ1 proteins react with the same species IgG, the antibodies used for the detection of phosphorylated PLCγ1 were removed by stripping after detection. For this purpose, membranes were incubated in 50 ml stripping buffer (see Table 16) at 50°C for 45 min on an orbital shaker. To remove any excess 2-mercaptoethanol, the membranes were rinsed under tap water for 1-2 min before being washed for 5 min in 1X TBST. Membranes were now blocked and re-probed as described above but for total PLCγ1.

Quantification of Protein Bands

To quantify protein bands, densitometric analysis was conducted using the Image Lab software. Subsequently, the ratio of phosphorylated protein to the corresponding pan protein signal was calculated.

3.2.3. Construction of Lentiviral Expression Vector

For the transfer of transgenes into primary hippocampal neurons, an appropriate lentiviral backbone was constructed. For this purpose, the previously modified lentiviral vector pLenti4/V5-DEST® was used. The CMV-promotor of the original plasmid was replaced with a functional mouse α-CaMKII promotor fragment (189), resulting in a pLenti4CAMKII/V5-DEST plasmid suitable for Gateway cloning (for Map see Supplementary Figure 2).

PCR Cloning of WPRE into pLenti4CAMKII/V5-DEST

To enhance the expression of transgenes delivered by pLenti4CAMKII/V5-DEST, the plasmid was modified to include a Woodchuck Hepatitis Virus Posttranscriptional Regulatory Element (WPRE) (191, 192). This was achieved by recombination of pLenti4CAMKII/V5-DEST with the WPRE sequence using PCR cloning. The plasmid was digested with *BlpI* and *XhoI* to remove the V5-epitope, EM7 promoter, and sequences encoding for the Blasticidin resistance. The reaction (see Table 28) was incubated for 4 h at RT to receive a 949 and a 7504 bp fragment, respectively, which was validated via gel electrophoresis (see Gel Electrophoresis).

Table 28 BlpI/XhoI Digestion of pLenti4CAMKII/V5-DEST

Component	Quantity
pLenti4CAMKII/V5-DEST	5 µg
CutSmart Buffer (10X)	5 µl
BlpI (10 000 units/ml)	1 µl
XhoI (20 000 units/ml)	1 µl
ddH_2O	up to 50 µl

Gel Extraction

To isolate the opened lentiviral backbone, the corresponding 7504 bp was collected by excising the appropriate gel section using a clean, sharp scalpel. The excised DNA fragment was extracted using the QIAGEN Gel Extraction Kit according to the manufacturer's protocol and was finally eluted in 50 µl ddH_2O and stored at -20°C until further processing.

PCR Cloning of XhoI-WPRE-BlpI

To generate a WPRE fragment flanked by *BlpI and XhoI* restriction sites, a previously constructed WPRE-containing plasmid (pLenti6_sS_WPRE, kindly provided by Martin Kriebel) was used as a template. Oligonucleotides used to amplify the WPRE sequence were designed to include the restriction sites of *BlpI* and *XhoI*, respectively (see Table 23). The PCR for fragment amplification was performed using Q5 High-Fidelity 2X Master Mix according to the manufacturer's protocol (see Table 29 and Table 30).

Table 29 Q5 PCR reaction for the generation of XhoI-WPRE-BlpI-fragment

Component	Quantity
Q5 High-Fidelity 2X Master Mix	25 µl
pLenti6_sS_WPRE	1 ng
10 µM XhoI-WPRE_fw	2.5 µl
10 µM BlpI-WPRE_rev	2.5 µl
ddH_2O	to 50 µl

Table 30 Program for Q5 PCR

Phase	Temperature	Duration
Initial denaturation	98°C	30 s
PCR x 40 cycles	98°C	10 s
	50-72°C	20 s

	72°C	20 s
Final extension	72°C	2 min
Hold	4-10°C	

PCR Sample Purification and Generation of Cohesive Ends

Following PCR, the amplified DNA was purified using the QIAGEN PCR Purification kit according to the manufacturer's protocol and was finally eluted in 47 µl ddH_2O and stored at -20°C until needed. Next, the entire reaction of purified XhoI-WPRE-BlpI fragment was digested with 1µl *Xho* and *BlpI* in a 50 µl reaction to generate cohesive ends (according to the reaction in Table 28). Next, the digested fragment was verified through gel electrophoresis (see Gel Electrophoresis) and the corresponding 589 bp fragment was excised from the gel and extracted as described before (see Gel Extraction).

DNA-Ligation and Transformation of OneShot™ Stbl3

To insert the XhoI-WPRE-BlpI fragment into the opened XhoI-pLenti4CAMKII-BlpI-vector, both DNA fragments were ligated in a 1:3 molecular ratio using T4 DNA Ligase. The ligation reaction (see Table 31) was prepared according to the manufacturer's protocol and incubated at 16°C overnight. To terminate the enzymatic activity, the reaction was heat-inactivated at 65°C for 10 min and stored at -20°C until needed.

Table 31 T4 ligation reaction

Component	Quantity
T4 DNA ligase Buffer	2 µl
XhoI-pLenti4CAMKII-BlpI	50 ng
XhoI-WPRE-BlpI	13 ng
Nuclease-free H_2O	to 20 µl
T4 DNA Ligase	1 µl

1 µl of the ligation reaction was added to 50 µl OneShot™ Stbl3 cells, which were transformed according to the manufacturer's protocol. Subsequently, 70-100 µl were spread onto 2 x LB-ampicillin plates (see Preparation of LB-Agar Plates). Propagation and purification of pLenti04CAMKII//WPRE were performed as described before but in 50 ml of LB medium supplemented with ampicillin (see Propagation and Purification of Plasmids). Likewise, to verify successful ligation, restriction digest was applied with *NotI-HF* in CutSmart buffer according to the previous description (see Restriction Digest of Plasmid DNA). The expected

fragmentation of the plasmid (1412, 1597, and 5094 bp-fragments) was assessed using gel electrophoresis (see Gel Electrophoresis), followed by validation of successful recombination via Sanger Sequencing.

Further propagation of verified, *ccdB* gene-bearing pLenti4CAMKII//WPRE (for Map see Supplementary Figure 3) was performed using LIBRARY EFFICIENCY® DB.1 competent cells according to the manufacturer's protocol and propagation with ampicillin selection as described before.

Gateway Recombination

To insert the EGFP-N1-TrkB wild-type and mutant transgenes into pLenti4CAMKII//WPRE, Gateway® technology was utilized. Using the Q5® High-Fidelity Master Mix, the TrkB transgenes were amplified with TrkB-EGFP_attB1_fw and TrkB-EGFP_attB2_rev (for sequences see Table 23) to add site-specific attachment (att) sites needed for recombination and was performed as described before (see PCR Cloning of WPRE into pLenti4CAMKII/V5-DEST). Following the manufacturer's protocol for successful Gateway® recombination, equimolar ratios of the attB-PCR fragments and the pDONR™ 221 vector were used for BP recombination with BP Clonase II (see Table 32) and incubated overnight at 25°C.

Table 32 BP recombination reaction

Component	Sample
attB-EGFP-TrkB PCR fragments (WT/SHC-/PLC-/KD)	50 fmol
pDONR™ vector	50 fmol
TE Buffer, pH 8 (see Table 17)	Filled up to 8 µl
BP Clonase™ II	2 µl

The following day, the BP reaction was terminated using 1 µl Proteinase K at 37°C for 10 min. 1 µl of each reaction was transformed into One Shot® TOP10 chemically competent *E.coli* as previously described (see Transformation of OneShot TOP10 Competent Cells) and selected with LB + 50 µg/ml kanamycin. The plasmids were purified using the Qiagen Plasmid Midi Kit as described before (see Propagation and Purification of Plasmids).

To create the final expression clones, LR recombination was performed. The purified entry clone was recombined with the pLenti4CAMKII//WPRE vector (see Table 33) using LR Clonase™ II overnight at 25°C.

Table 33 LR recombination reaction

Component	Sample
Entry clone	150 ng
pLenti4CAMKII//WPRE	150 ng
TE Buffer, pH 8 (see Table 17)	Filled up to 8 µl
LR Clonase™ II	2 µl

The following day, the LR reaction was terminated according to manufacturer's protocol, transformed into One Shot® Stbl3 competent cells and processed as previously described (see DNA-Ligation and Transformation of OneShotTM Stbl3). All lentiviral plasmids were verified for their correct sequence via Sanger sequencing (for Map see Supplementary Figure 4).

3.2.4. Lentiviral Production

Cultivation of HEK293FT Cells

HEK293FT cells were cultured in a T175 with standard HEK293 medium (see Table 10) at 37°C and 5% CO2 in humidified atmosphere. For subcultivation the cells were dissociated with Trypsin-EDTA (0.05%) when reached 70-80 % confluency. Once the cells were detached from the vessel, HEK293FT standard culture medium was added to stop further trypsinization and the cells were harvested via centrifugation at 300 g for 3 min. Subsequently, the cells were resuspended in their standard cultivation medium and seeded in a 1:10 ratio for preservation in T175 flasks.

Transfection of HEK293FT Cells

To produce lentiviral particles HEK293FT cells were employed. They were cultured as described before until reaching 80 % confluency. At this point, the standard medium of the cells was replaced with a pre-transfection medium (see Table 11) for 24 h in humidified atmosphere at 37°C and 8 % CO_2 to prepare the cells for the transfection under serum-free conditions. The following day, the cells were harvested as previously described (see Cultivation of HEK293FT Cells), using pure Opti-MEM™. Cells were counted with a Neubauer chamber, and approximately 3.8 x 10^7 cells were seeded in a new T175 flask containing 13.5 ml of prewarmed Opti-Mem™. Transfection was performed using Lipofectamine 2000 based on the manufacturers' protocol. For each reaction, 4.5 ml of Opti-Mem™ was mixed with 108 µl Lipofectamin2000 and incubated for 5 min at RT. Simultaneously, 4.5 ml of Opti-MEM™ was mixed with 27 µg of a third-generation packaging mix (pLP1, pLP2 and pLP_VSGV in a 1:1:1

molar ratio) and 18 µg of the respective plasmids of the TrkB mutants (pEGFP-N1-TrkB (WT), SHC-, PLC- or KD) were added. Subsequently, the Lipofectamine2000-Opti-Mem-Mix was added to the plasmid mix and incubated for 20 min at RT before the entire mix was added to the HEK293FT cell suspension and incubated in humidified atmosphere at 37°C and 8 % CO_2.

24 h post-transfection, the medium was replaced with fresh 30 ml. 48 h post-transfection, the Opti-MEM containing the viral particles was collected and replaced with fresh 30 ml, which was again collected at 72 h after transfection. After the second collection, the HEK293FT cells were briefly monitored for EGFP expression with the EVOS cell imaging system and subsequently discarded. The collected supernatants were filtered through a 45 µm SFCA filter and stored at -80°C until further processing.

Lentivirus Concentration

After thawing at RT, the stored supernatants were transferred to ultracentrifugation tubes and centrifuged for 90 min at 19 600 rpm and 4°C. Following centrifugation, supernatants were discarded, leaving the viral particles, which were overlaid with 50 µl 0.1 % BSA/DPBS overnight at 4°C. The next day, the viral particles were gently resuspended in the 50 µl 0.1 % BSA/DPBS, and collections from 48 h and 72 h were pooled. Viral stocks were stored as 10 µl aliquots at -80°C until needed.

Titration of Lentiviral Suspensions

To quantify the concentration of virions in the produced suspensions, lentiviral RNA copies were assessed using the Lenti-X qRT-PCR kit. Each virus suspension was diluted 1:200 in Opti-MEM, and 150 µl of this dilution was processed with the corresponding NuleoSpin RNA virus Kit according to the manufacturer's protocol for cell-free biological fluids, omitting the initial 70°C incubation step.

Since transiently transfected HEK293FT cells were used for lentiviral production, the RNA samples were further treated with DNase I to remove any potentially remaining DNA, following the manufacturer's protocol. Amplification and quantification of lentiviral genomic RNA were performed using qRT-PCR with ROX reference Dye LMP on a StepOne qPCR instrument. All samples were measured in duplicates.The qRT-PCR reaction cycle program was set, as shown in Table 34.

Table 34 Program for lentiviral RNA titration according to manufacturer's protocol

Phase	Temperature	Duration
RT Reaction	42°C	5 min
	95°C	10 s
qPCR x 40 cylces	95°C	5 s
	60°C	30 s
Dissociation curve	95°C	15 s
	60°C	30 s
	60°C-95°C	∞

To determine the respective Ct values, the average Ct values of the samples were analyzed in comparison to the corresponding standard according to the manufacturer's suggestions. Viral titers are defined as viral copies per ml (VC/ml).

3.2.5. Cultivation of Primary Hippocampal Neurons

Preparation of Primary Hippocampal Neurons

Culture vessels were prepared a day before neuronal preparation by coating the respective wells with sterile filtered PEI-coating (see Table 12) and incubated overnight at 37°C and 5% CO_2 in humidified atmosphere. The next day, the coated wells were washed twice with ddH_2O and prepared with 100 µl of seeding medium (see Table 12).

For primary hippocampal neuron preparation, adult pregnant female Sprague–Dawley rats were supplied by Janvier Labs, Le Genest-Saint-Isle, France. The housing of animals and submission to surgical procedures were performed in accordance with the European Union recommendations for the care and use of laboratory animals (2010/63/EU) and were approved by the regional authority (Regierungspräsidium Tübingen) (193). On embryonic day 18 (E18) the dam was sacrificed by CO_2 narcotization and subsequently decapitated. The embryos were removed and immediately decapitated. Independent of sex, the brains were extracted and both hippocampi were dissected. During the whole procedure, brain tissues were stored on ice in DPBS + 1% P/S.

The hippocampal tissues were dissociated with Trypsin/EDTA (0.05%) for 10 min at 37°C. After removal of the enzymatic solution, tissues were further dissociated by gently triturating in 2 ml of seeding medium. After the addition of 8 ml medium, the cells were separated via a 100 µm cell strainer. Cells were further diluted in seeding medium, counted at the NucleoCounter®, and assessed for viability using Via1-Cassettes™.

Primary hippocampal neurons were seeded at 4 x 10^4 cells/well in a volume of 100 µl/well on PEI-coated 96-well plates and incubated under humidified atmosphere at 37°C and with 5 % CO_2 for 4 h before exchanging the medium to serum-free cultivation medium (see Table 13).

Cultivation, Transduction, and Fixation of Primary Hippocampal Neurons

On day *in vitro* 1 (DIV1), the medium was replaced by fresh cultivation medium, and neurons were further maintained at 37°C with 5% CO2 in humidified atmosphere.

On DIV3, the primary neurons were transduced with lentiviral constructs. To this end, 50 % of the medium was replaced with 50 µl of fresh cultivation medium, containing viral particles at a final concentration of 2 x 10^6 viral copies/well. The removed conditioned medium was saved, sterile filtered, and stored at 4°C.

On DIV6, the stored conditioned medium was mixed 1:1 with BrainPhys™+SM1 to replace the medium containing viral particles. At this point, 50 % of the medium was replaced by fresh BrainPhys™+SM1 every other day until DIV14.

Fo immunocytochemical analysis, DIV14 neurons were fixed by replacing their medium with 100 µl/well of 4 % (w/v) PFA/DPBS solution for 15 min at RT, followed by extensively washing the cells three times with 200 µl/well DPBS for 5 min each. Cells were stored in 200 µl DPBS + 0.02% NaN_3 in the dark at 4°C.

Chemical Induction of Inhibitory LTP and Pharmacological Treatment

To chemically induce inhibitory long-term potentiation (chem iLTP) in primary hippocampal cultures, the protocol from Petrini and colleagues was adapted (48).

For this purpose, 0.1 M stocks of N-methyl-D-aspartate (NMDA) and cyanquixaline (CNQX) were prepared freshly on the day of treatment. NMDA was diluted in recording solution (pH 7.4), (78), (see Table 18), whereas CNQX was diluted in DMSO in an ultrasonic bath. Subsequently, both substances were diluted and combined to receive final concentrations of 20 µM and 10 µM, respectively. Likewise, as a control, recording solution with an identical DMSO concentration but omitting NMDA+CNQX was prepared (sham). Hippocampal neurons were treated by replacing the cultivation medium with 100 µl of either the sham or NMDA+CNQX-containing media for 2 min at 37°C. Subsequently, treatment media were replaced by 100 µl pure recording solution for 18 min at 37°C before PFA fixation (see Cultivation, Transduction, and Fixation of Primary Hippocampal Neurons).

To evaluate the role of TrkB, MAPK, and CaMKII signaling during chem iLTP, hippocampal neurons were treated with specific inhibitors during NMDA+CNQX treatment. For this purpose,

inhibitor stocks were prepared in either H_2O (Cyclotraxin, CtxB) or DMSO (PD98059 and KN-62) and stored at -20°C until needed. For chem iLTP induction with concurrent interference of TrkB, Mek1/2 and CaMKII signaling, neurons were pretreated for 30 min at 37°C with either 1 µM CtxB, 50 µM PD98059, 3 µM KN-62 or a DMSO control diluted in BrainPhys + SM1. Chem iLTP was then induced as previously described, but in the continued presence of inhibitors or DMSO control at identical concentrations during the 2 min treatment phase and subsequent recovery phase. For this, the inhibitors or DMSO control were diluted in the same concentrations as during pre-treatment but diluted in the recording solution. Following the recovery phase, the cells were fixed in PFA (see Cultivation, Transduction, and Fixation of Primary Hippocampal Neurons).

3.2.6. Calcium Imaging

For measuring calcium transients, transduced primary hippocampal neurons were stained with a red fluorescent Ca^{2+} indicator at DIV14 by replacing 50% of the neuronal medium with fresh BrainPhys + SM1 containing 2 µM CalBryte™* 590 AM. The cells were incubated for 30 min in humidified atmosphere at 37°C, 5 % CO_2, and washed once with DBPS before calcium transients were recorded in 100 µl/well imaging optimized BrainPhys + SM1, using the Cell Observer SD. 3 min recordings of multiple cells within a microscopic field were obtained with a framerate of 50 ms. Per experiment, two acquisitions/well were conducted for a total of three wells per experimental group. To identify EGFP-positive neurons and enable cell-specific analysis, snapshots of the microscopic field with the Calbryte and EGFP signals were taken directly before each recording. Somatic calcium transients were measured from individual neurons by manually drawing ROIs with Fiji and extracting the mean fluorescence intensity over time. A minimum of three spontaneously active EGFP-positive neurons (at least two calcium transients/recording) per recording were analyzed.

Analyzation of Calcium Transients

Traces were subsequently analyzed using the Origin 2015G Peak Analyzer module. Baseline normalization was applied to all traces, maintaining peak detection threshold and minimum peak distance across all replicates. Somatic calcium fluctuations were analyzed for the event rate, which reflects the frequency of occurring calcium transients, the peak amplitude (ΔF/F0) for the magnitude of the calcium responses, the area under the curve (AUC) as a proxy for calcium flux dynamics, and the full-width half maximum (FWHM). The respective data were averaged across all peaks of a single neuron. Data points in the graphs are normalized to the WT and represent the mean values of multiple cells per well.

3.2.7. Immunocytochemistry

For indirect immunofluorescence DPBS + 0.02% NaN_3 was removed, and the cells were blocked and permeabilized at room temperature in 0.1 % Triton X-100/DPBS containing 1 X BMB blocking reagent for 30 min. Subsequently, the cells were incubated with the respective primary antibodies diluted in the blocking solution on an orbital shaker, in the dark overnight at 4°C (for dilutions of primary antibodies, see Table 20). The following day, primary antibodies were removed, and cells were washed three times for 5 min with 200 µl DPBS each. Afterward, fluorophore-conjugated secondary antibodies diluted in blocking solution were added for 2 h at RT and further placed on an orbital shaker, protected from light (for dilutions of primary antibodies, see Table 21). After another three washing steps of 5 min with 200 µl DPBS each, cells were stored in 200 µl DPBS + 0.02% NaN_3 in the dark at 4°C until image acquisition. In some cases, nuclei were additionally stained with Hoechst Dye 33258 diluted in DPBS. This involved replacing the second washing step after secondary antibody removal with the incubation of Hoechst dilution for 30 min at RT.

3.2.8. Image Acquisition and Analysis

Images of labeled proteins were retrieved using a spinning disc confocal microscope (Cell Observer SD, Carl Zeiss Microscopy) equipped with a plan-apochromat 20x air objective and a plan-apochromat 63x oil immersion objective (N.A. 1.4, Carl Zeiss Microscopy). Z-stacks were obtained from the somata of EGFP-positive neurons.

For all recordings, acquisition settings, including exposure time, laser intensity, and gain, were kept constant across samples from different experimental groups. Each representative image depicted in this study is a maximum intensity projection of the corresponding z-stack.

For analysis, image stacks were loaded into IMARIS 10 for the generation of three-dimensional ROIs of the EGFP-positive neuronal somata using IMARIS' surface creation functionality.

Quantification of Fluorescence Intensities

To assess protein expression levels of TrkB, phospho-CaMKIIα, CaMKIIα, phosphor-mTOR, phospho-S6K, cleaved caspase 3, and GABA in transduced neurons, ROIs of the somata were used to determine mean gray value intensities of the corresponding immunoreactivity after background subtraction. For cleaved caspase 3 and GABA, a mean intensity threshold for immunoreactivity was set across all replicates. Neurons with mean grey values above this threshold were defined as cleaved caspase or GABA-positive. The ratio of cleaved caspase 3 or GABA-positive neurons to all transduced neurons was further calculated as a proxy for

induced apoptosis in these cells and to assess the amount of GABAerig cells within EGFP-positive neurons.

Quantification of Synaptic Marker Densities and Size

To quantify synaptic marker protein clusters per neuron, ROIs were used to exclude signals outside of the EGFP signal. Synaptic marker structures were quantified using IMARIS' spot detection functionality, with a threshold set and maintained constant across samples from different experimental groups. Within a single ROI, the number of structures was normalized to its volume to determine the marker density. To assess the mean cluster size of the individual synaptic markers, three-dimensional renderings of the synaptic marker structures were generated from the respective image channels by using IMARIS' surface creation tool. The mean cluster volume for each neuron was analyzed. To identify colocalized pre- and postsynaptic markers, the IMARIS XTention MATLAB-based plugin 'Spots Colocalize' was used. A maximum distance threshold of 0.7 µm between local intensity maxima of pre- and postsynaptic marker structures was set to exclude signals that were above the hypothetical axial resolution limit of the Cell Observer SD microscope. All quantified parameters were normalized to the WT values.

For the quantification of excitatory and inhibitory synaptic proportions, the mean densities for each group within each experiment were determined and summarized to receive a value for each synapse type per group. Both means were summarized to calculate the respective proportions.

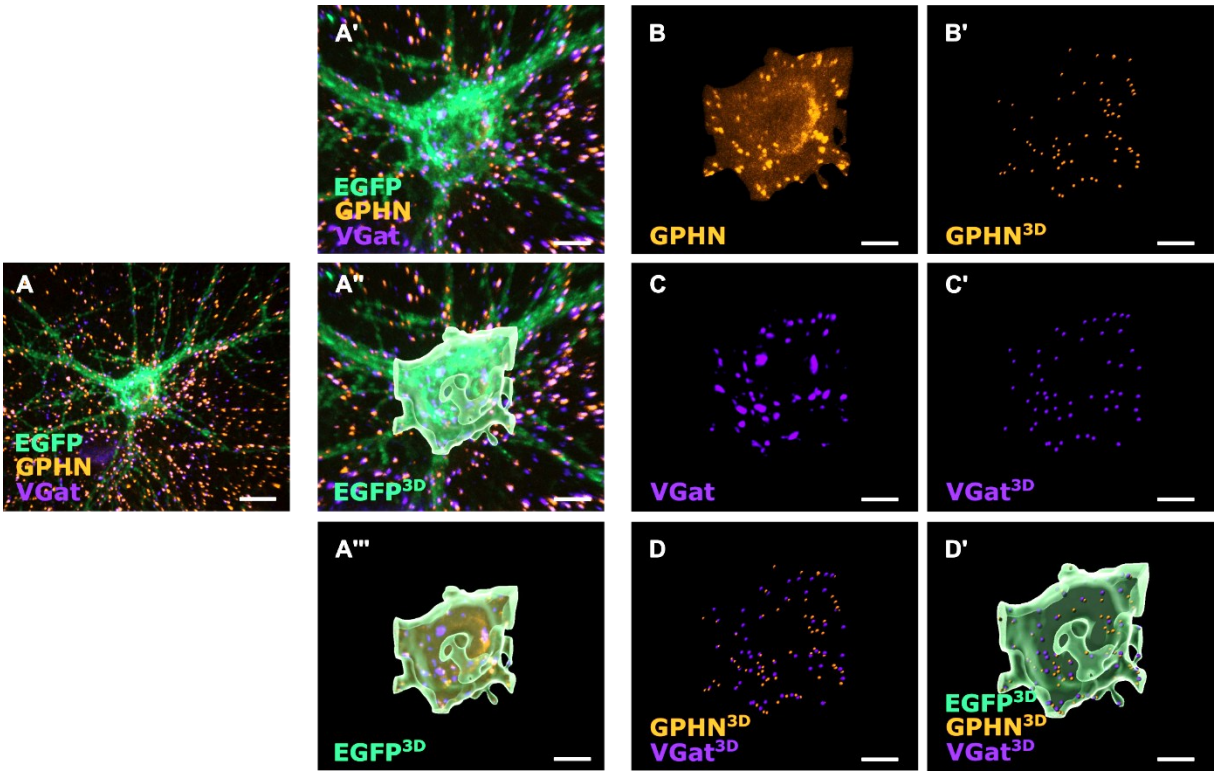

Figure 3: Analysis of synaptic marker density quantification. **A** Representative image of a microscopic z-stack, represented in the IMARIS software, showing a TrkB-EGFP expressing primary hippocampal neuron stained for the post- and presynaptic marker gephyrin (GPHN) and VGat. **A'** Enlarged section of A, highlighting the soma of the corresponding neuron. **A"** 3D rendering of the soma depicted in A' based on the EGFP signal ($EGFP^{3D}$) which defined the ROI. **A"'** All signals outside of the $EGFP^{3D}$ rendering were excluded. **B** Gephyrin related signals residing in the $EGFP^{3D}$ rendering. **B'** Based on the remaining gephyrin signals within the soma-rendering, the gephyrin spots above a certain signal intensity threshold were 3D rendered resulting in $GPHN^{3D}$ representing the individual gephyrin spots. **C** VGat related signals residing in the $EGFP^{3D}$ rendering. **C'** Based on the remaining VGat signals within the soma-rendering, the VGat spots above a certain signal intensity threshold were 3D rendered resulting in $VGat^{3D}$, representing the individual VGat spots. **D** Representation of $GPHN^{3D}$ and $VGat^{3D}$ that were analyzed for colocalization with the IMARIS XTention MATLAB-based plugin 'Spots Colocalize'. **D'** To calculate densities of $GPHN^{3D}$ and $VGat^{3D}$ spots, the number of spots was divided by the volume of the corresponding $EGFP^{3D}$ volume to obtain the number of spots/μm^3.

3.2.9. Statistics

Statistical analysis was performed using GraphPad Prism 10 (GraphPad Software). All data sets were identified for outliers using Prism's 'Robust regression and Outlier removal' (ROUT) with a coefficient Q = 1%. Afterwards, all data sets were tested for Gaussian distribution using the D'Agostino-Pearson test. Normally distributed data were analyzed using an unpaired One-way ANOVA with Dunn's multiple comparison, while nonparametric data sets were analyzed using a Kruskal-Wallis test with Dunn's multiple comparison test. Experiments with two variables were analyzed with a 2way ANOVA and Tukey's multiple comparisons test.

If not stated differently, all values are represented as mean ± SEM. The p-values were assigned as follows: *$p < 0.05$; **$p < 0.01$; ***$p < 0.001$, ****$p < 0.0001$. The values of mean and SEM,

as well as sample size, are stated in the respective figure legends. For primary neuron experiments, an independent experiment is defined as an individual neuron preparation and associated culture. Detailed statistical data is shown in Table 37.

4. Results

4.1. Targeting TrkB Signaling: Vectors for the Expression of Mutant TrkB

4.1.1. Site-directed Mutagenesis Induced Nucleotide Exchanges in Rat *Ntrk2* (TrkB) Coding Sequence

To dissect the individual contributions of TrkB signaling pathways in neurons, mutants of the rat TrkB receptor were generated deficient in autophosphorylation or in the induction of PLCγ- or Shc-dependent signaling pathways. For this purpose, the respective amino acids, identified as critical for the recruitment of Shc (Y515), PLCγ (Y816), and ATP-binding (K571) (99, 152, 190) were replaced in the rat *Ntrk2* (*TrkB*) coding sequence (cds) of pEGFP-N1-TrkB using site-directed mutagenesis of the corresponding base pair triplets.

Before inducing site-directed mutagenesis, the correct *TrkB* sequence of the EGFP-N1-TrkB transgene was verified by comparing the included *TrkB* cds in pEGFP-N1-TrkB with the mRNA of rat neural *TrkB* (NCBI GenBank ID: M55291.1). Alignment of both sequences confirmed the correct rat *TrkB* cds present in the plasmid (Figure 4).

Since the mutations had previously been described only for the TrkB protein in mice (*Mus musculus*), the aa sequence of the rat TrkB protein (based on M55291.1) was compared with the mouse TrkB protein sequence (NCBI GenBank ID: NM_001025074.3). This alignment demonstrated that the critical residues Y515, K571, and Y816 are identical in their positions within the rat TrkB protein (Supplementary Figure 6).

Finally, to further verify these conserved functional residues, the TrkB protein aa sequence, translated from pEGFP-N1-TrkB cds, was compared with the rat TrkB protein aa sequence of Uniprot entry Q63604. The alignment further confirmed the functional residues, strengthening their roles in Shc, ATP, and PLCγ binding (Figure 5).

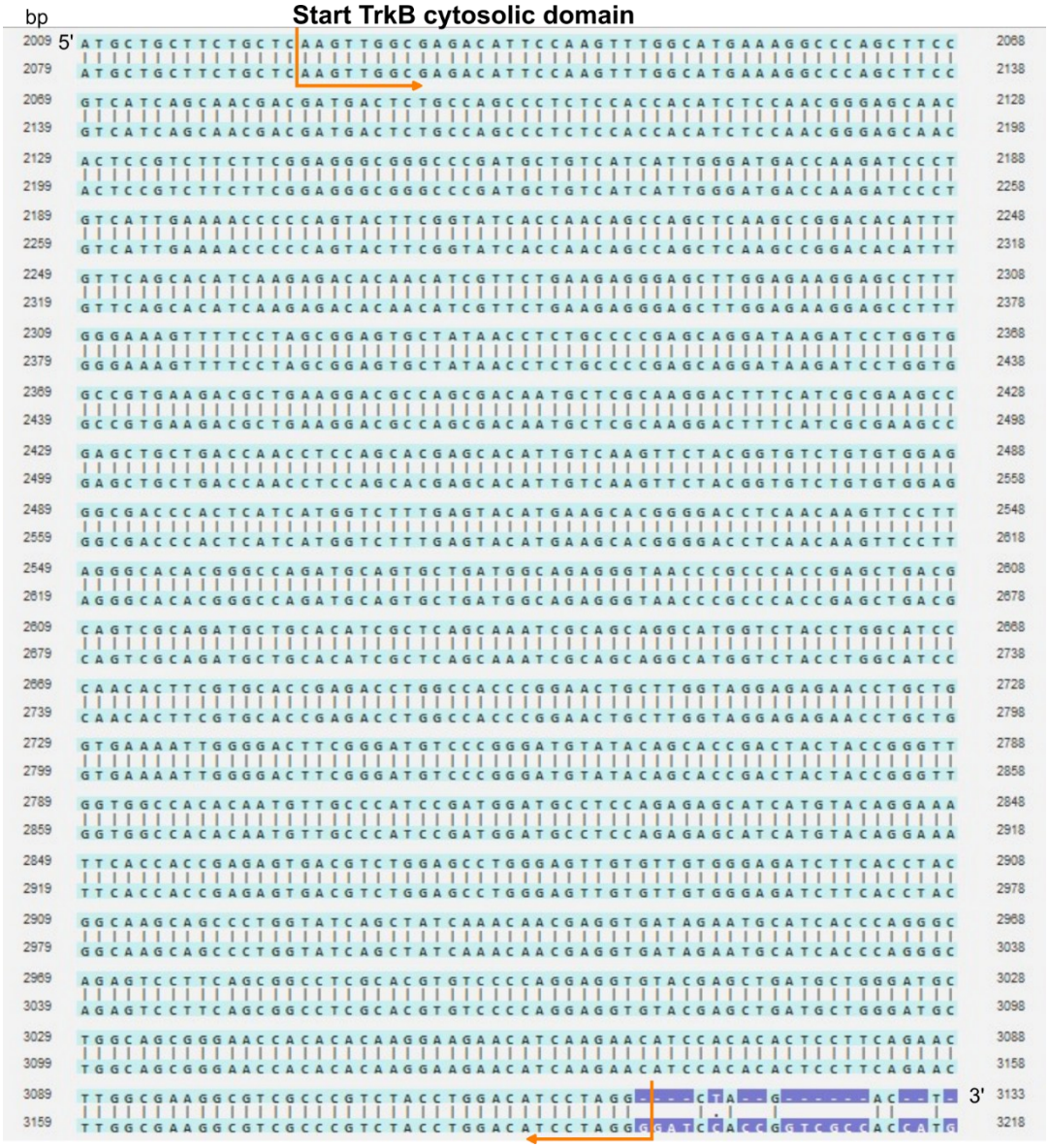

Figure 4: Sequence alignment of *TrkB* cytosolic domain from pEGFP-N1-TrkB and M55291.1. Partial alignment of *TrkB* cds from pEGFP-N1-TrkB (top sequence) with the complete *TrkB* cds from NCBI reference sequence M55291.1 (bottom sequence), showing the cytosolic domain of the receptor. The orange arrows indicate the start and stop sequences of the cytosolic domain. The full alignment is shown in Supplementary Figure 5. *Bp: basepair number; Sequence alignment was performed with the alignment tool of Vectorbuilder.com.*

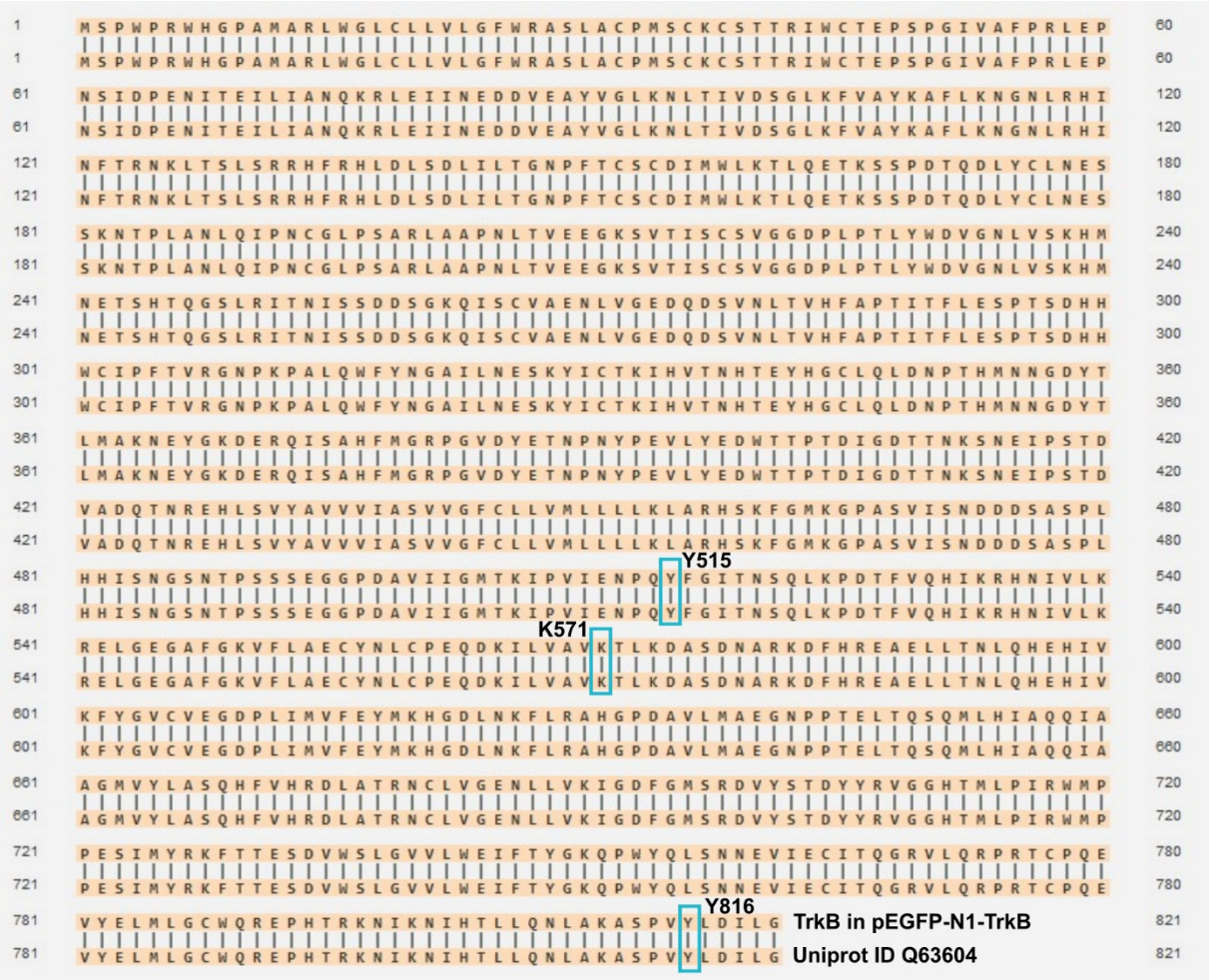

Figure 5: Comparison of the TrkB protein sequence encoded by pEGPF-N1-TrkB with the Uniprot rat TrkB protein sequence confirmed positions of amino acids responsible for Shc, ATP, PLCγ. The alignment of the TrkB protein sequence translated from pEGFP-N1-TrkB with the native TrkB protein sequence of *Rattus norvegicus* (Uniprot ID Q63604) confirms the position of critical amino acid residues responsible for Shc (Y515), ATP (K571) and PLCγ binding (Y816). This comparison validates the functional integrity of the TrkB construct in pEGFP-N1-TrkB. The numbers indicate the sequence positions of amino acids. *Sequence alignment was performed with the alignment tool of Vectorbuilder.com.*

Following this initial sequence verification, confirmed sites of interest underwent mutagenesis, to generate signaling-deficient TrkB mutants. For the generation of the TrkB mutant, deficient in Shc-dependent signaling, the adenine at position 2278 of the codogenic strand of the expression vector pEGFP-N1-TrkB was replaced by thymine to induce a change in the triplet code from TAC to TTC (Figure 6, top panel). As confirmed by Sanger sequencing, this exchange resulted in the switch of tyrosine (Y) to phenylalanine (F) at position 515, resulting in the TrkBY515F mutant. Likewise, for the PLCγ-signaling deficient TrkB mutant, adenine at vector bp-position 3181 was replaced with thymine to generate the TrkBY816F mutant (Figure 6, bottom panel). For the ATP-binding deficient TrkB mutant, adenine nucleobases at the positions 2445 and 2446 were replaced with guanine and cytosine, respectively, converting

the triplet code from AAG to GCG and therefore resulting in a switch from lysine (K) to arginine (A) at amino acid sequence 571 (TrkBK571A) (Figure 6, middle panel).

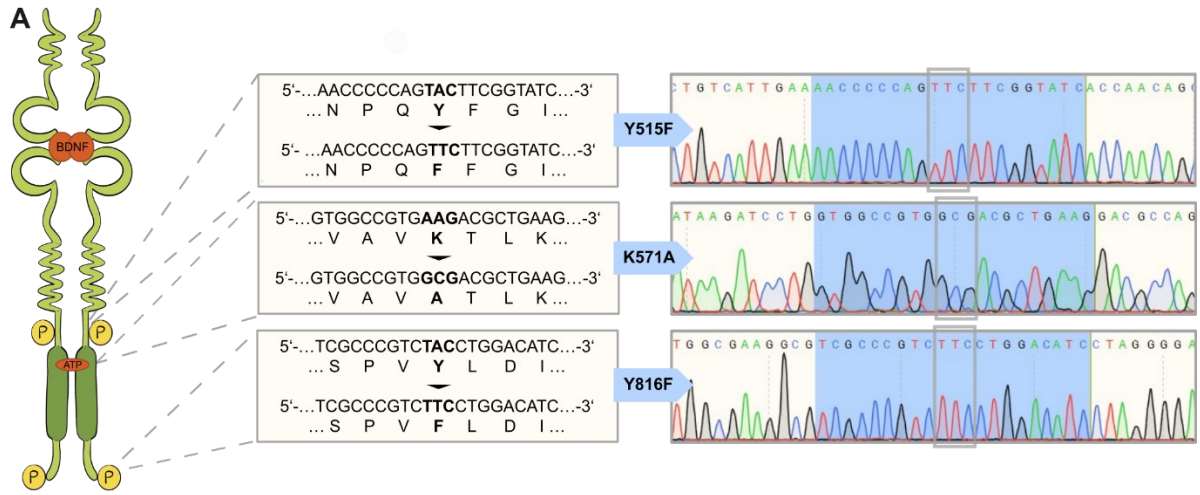

Figure 6: Site-directed mutagenesis generates TrkB mutants by induction of nucleotide exchanges in the coding sequence. Schematic illustration of the full-length, wild-type TrkB receptor, depicting its extracellular Bdnf binding site, the cytosolic phosphorylation, and ATP binding sites (left). Dashed lines indicate zoomed-in views of the DNA sequences corresponding to the amino acids Y515, K571, and Y816, respectively (middle). These sequences schematically indicate the exchange of nucleotides and the associated switch in the respective amino acids resulting in Y515F (top panel), K571A (middle panel), and Y816F (bottom panel). Nucleotide exchanges were confirmed via Sanger sequencing, as indicated by the respective chromatogram sections, depicted in the right panel. Grey boxes highlight the mutated sites within the corresponding chromatogram. Figure adapted from (193).

To summarize, site-directed mutagenesis was successfully employed on the rat TrkB receptor, resulting in TrkB Y515F, K571A, and Y816F mutants. In the following sections, these mutants will be referred to based on their impact on TrkB signaling, resulting in SHC- (Y515F, TrkB deficient in Shc-dependent signaling), PLC- (Y816F, TrkB deficient in PLCγ-dependent signaling), and KD (K571A, kinase-dead TrkB mutant).

4.1.2. Mutation of TrkB Phosphorylation and ATP Binding Sites Reduced Site-Specific Signaling Pathway Induction

To study the functional consequences of TrkB site-directed mutagenesis in SHC-, PLC- and KD mutants, the catalytic function of these TrkB receptors and the activation of the associated signaling components Erk1/2 and PLCγ1 were analyzed via Western Blot analysis of the respective phosphorylated forms. To assess this, EGFP-tagged TrkB WT and mutants were expressed in HEK293 and NIH3T3 cells, stimulated with Bdnf, and analyzed for the respective ratio of phosphorylated protein to overall protein.

After transfection of HEK293 and NIH3T3 cells with either a control plasmid (CTR, pEGFP-N1) or plasmids containing the TrkB WT or mutants, they were monitored for EGFP expression. As representatively shown for HEK293 cells in Figure 7, cells transfected with CTR (B), WT (C), SHC- (D), PLC- (E), and the KD mutant (F) all widely display an expression of EGFP, which is not observed in mock-transfected cells (WO, A).

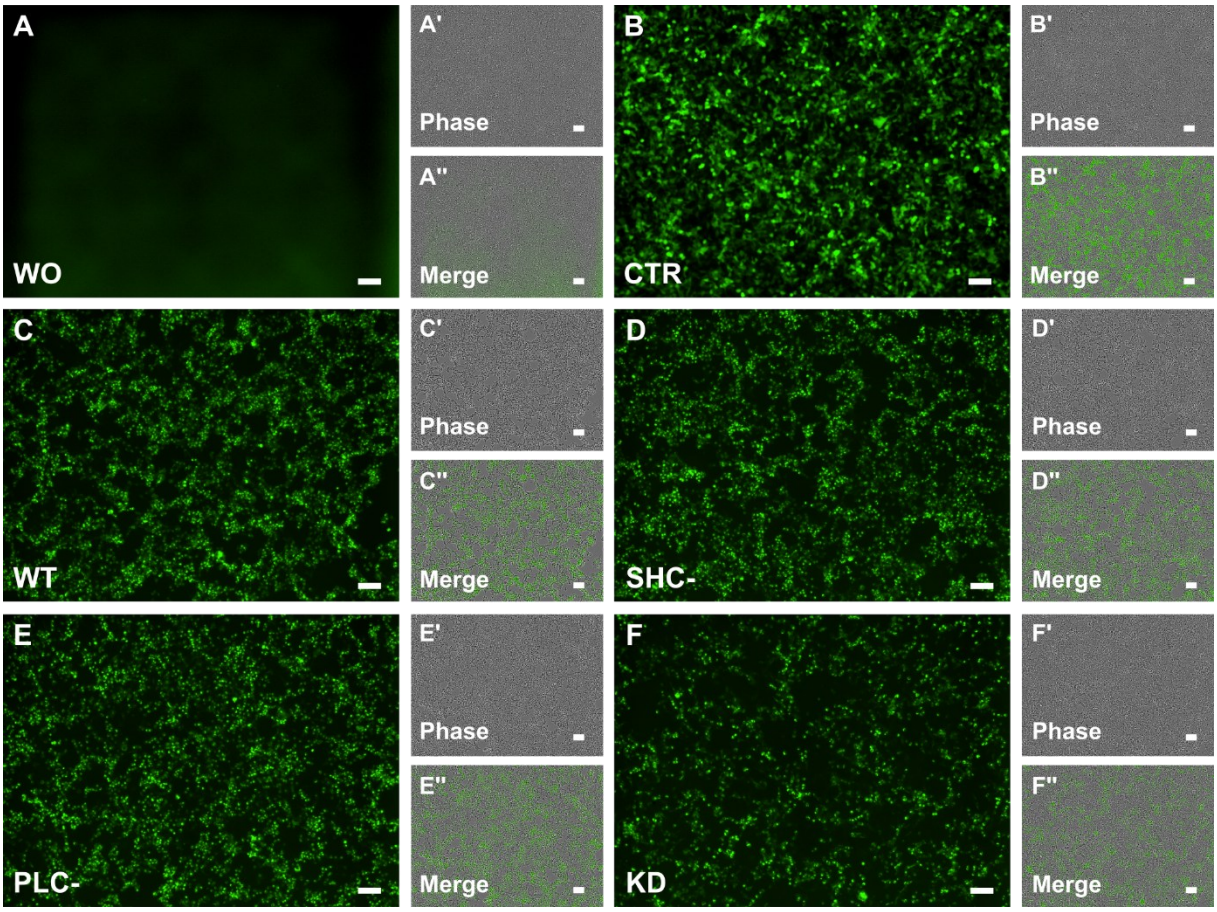

Figure 7: HEK293 cells express EGFP after transfection with EGFP-tagged TrkB WT and mutants or CTR. A Representative image of mock-transfected HEK293 cells (WO) monitored for their EGFP expression, two days post-transfection. **A'-A''** Separate phase channel (A') corresponding to A and merge of A and A' (A''). **B-F''** As described in A and A'-A'' but for cells transfected with pEGFP-N1 (CTR, B-B''), pEGFP-N1-TrkB (WT, C-C''), SHC- (D-D''), PLC- (E-E'') and KD (F-F''), respectively. Scale bars: 100 µm.

Western Blot analysis and immunolabelling of proteins extracted from transfected HEK293 cells revealed the successful expression of TrkB-EGFP at the predicted size of approximately 120 kDa (Figure 8, A, TrkB panel). Since HEK293 cells do not express the TrkB receptor endogenously, no TrkB protein was detected in mock (WO) or pEGFP-N1 (CTR) transfected cells.

To assess the catalytic activity of the TrkB mutants, the blots were additionally labeled for TrkB phosphorylated in its catalytic loop at Tyr706/707. The results revealed that TrkB WT, as well as SHC- and PLC- mutants maintain their ability to autophosphorylate. In contrast, the kinase-dead mutant showed no signs of TrkB catalytic activity, comparable to the results observed with mock- and CTR-transfected cells (Figure 8, A, pTrkB panel). Quantifying the ratio of pTrkB to total TrkB further demonstrated a comparable ratio of activated TrkB between TrkB WT and SHC- and PLC- mutants and further highlighted the lack of autophosphorylation in the KD mutant with K571A (Figure 8, B).

The stimulation of cells with 100 ng/ml Bdnf for 30 min did not alter the ratio of pTrkB/TrkB (Figure 8 B) in comparison to sham-treated cultures, indicating that TrkB overexpression in the cells is sufficient to induce homodimerization and, consequently, activation of TrkB WT, SHC- and PLC- .

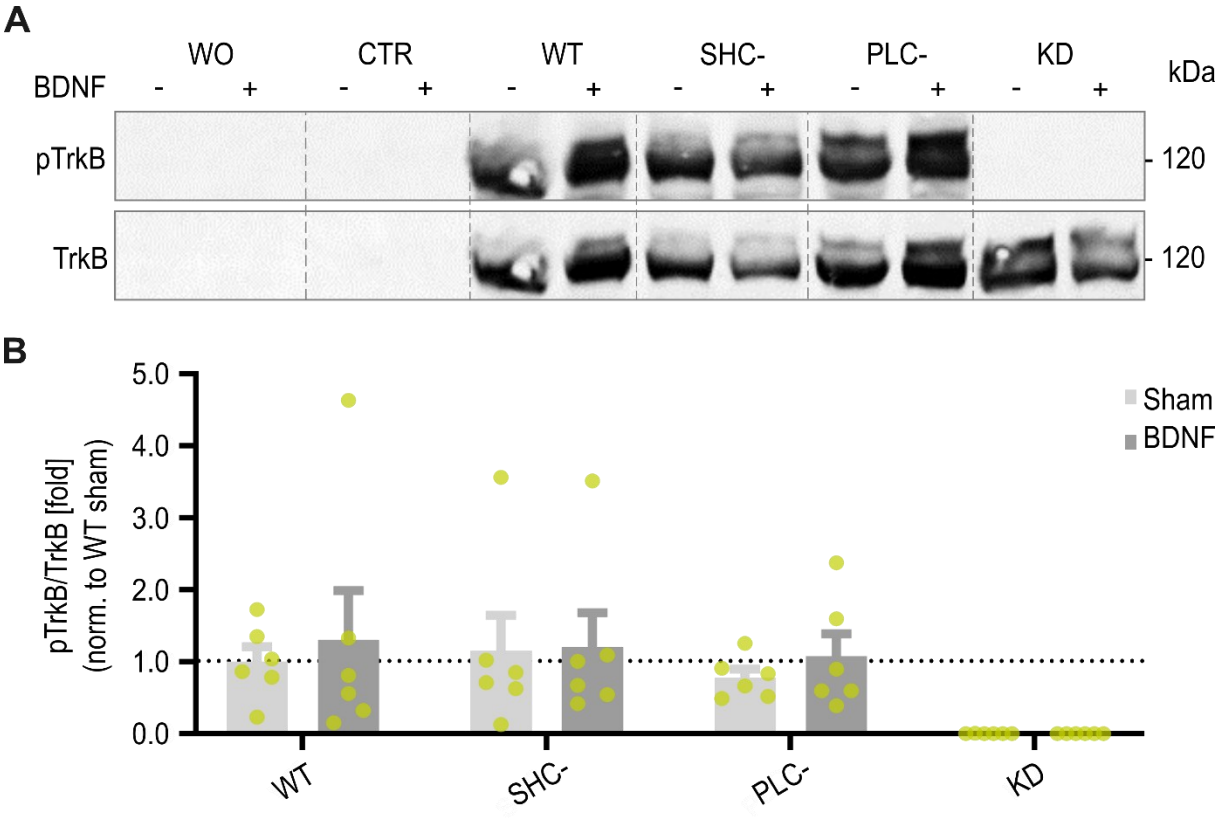

Figure 8: HEK293 cells expressed TrkB WT and mutants and showed Bdnf-independent receptor activation, except for the KD mutant. **A** Representative immunoblot of protein extracts of HEK293 cells, transfected with either no plasmid (WO), pEGFP-N1 (CTR), or the EGFP-tagged TrkB WT, SHC-, PLC- and KD receptors. The cells were either treated with Bdnf-solvent (-, sham) or 100 ng/ml Bdnf (+, BDNF) for 30 min prior to lysate collection. The top panel represents blots labeled for phospho-TrkB (Tyr706/707; pTrkB), whereas the bottom panel displays total TrkB protein levels. **B** Quantification of the pTrkB/TrkB ratio in cells transfected with TrkB WT and mutants. All data are normalized to the sham WT group. Data represents mean ± S.E.M. from 6 independent experiments (n = 6). WT sham: 1 ± 0.21,

WT Bdnf: 1.30 ± 0.69, SHC- sham: 1.15 ± 0.50, SHC- Bdnf: 1.21 ± 0.47, PLC- sham: 0.78 ± 0.12, PLC- Bdnf: 1.08 ± 0.31, KD sham: 0.002 ± 0.31, KD Bdnf: 0.001 ± 0.0006. Figure adapted from (193).

To further assess how site-directed mutagenesis of TrkB impacts cognate signaling, the protein extracts of HEK293 and NIH3T3 cells were analyzed for the activation of Erk1/2 and PLCγ as proxies for Shc- and PLCγ-dependent pathway induction. Since Bdnf stimulation did not alter TrkB activity, only the protein extracts of Bdnf-treated cells were further analyzed.

Transfection of NIH3T3 cells with TrkB WT revealed an increased phosphorylation of Erk1/2 (pErk1/2) compared to CTR-transfected cells, which was also observed with the transfection of PLC- (Figure 9 A, top panel). In contrast, the protein bands observed with SHC- and KD transfection did not show this increased Erk1/2 activation. Quantification of the pErk1/Erk1 ratio revealed that the Y515F mutation reduced the proportion of activated Erk1 by 54 % compared to TrkB WT transfected cells (Figure 9 B). Conversely, the ratio of phosphorylated Erk1 in the PLC- variant remained comparable to that of the WT, indicating no interference of Shc-dependent signaling induction with the Y816F mutation. On the other hand, the mutation of the TrkB-ATP binding site reduced the ratio of phosphorylated Erk1 in cells transfected with the KD mutant by 24 % compared to the WT.

Likewise, to evaluate the impact of mutations on TrkB-PLCγ-dependent signaling, the ratio of phosphorylated PLCγ1 (pPLCγ1) to total PLCγ1 was analyzed. Phosphorylation of Tyr783 reflects TrkB-dependent activation of PLCγ1 and was increased in HEK293 cells expressing TrkB WT compared to CTR cells (Figure 9 C, top panel)(98). A similar increase in detected pPLCγ1 protein was observed with SHC-, whereas PLC- as well as KD showed a reduced amount of activated PLCγ1 protein. Quantification of the pPLCγ1 to total PLCγ1 ratio demonstrated that with the mutation Y816F, as well as with K571A, the proportion of activated PLCγ1 was reduced by 73 % and >99 % compared to the WT cells, respectively (Figure 9 D). In contrast, with the mutation Y515F, the ratio of pPLCγ1/PLCγ1 remained comparable to WT-expressing cells.

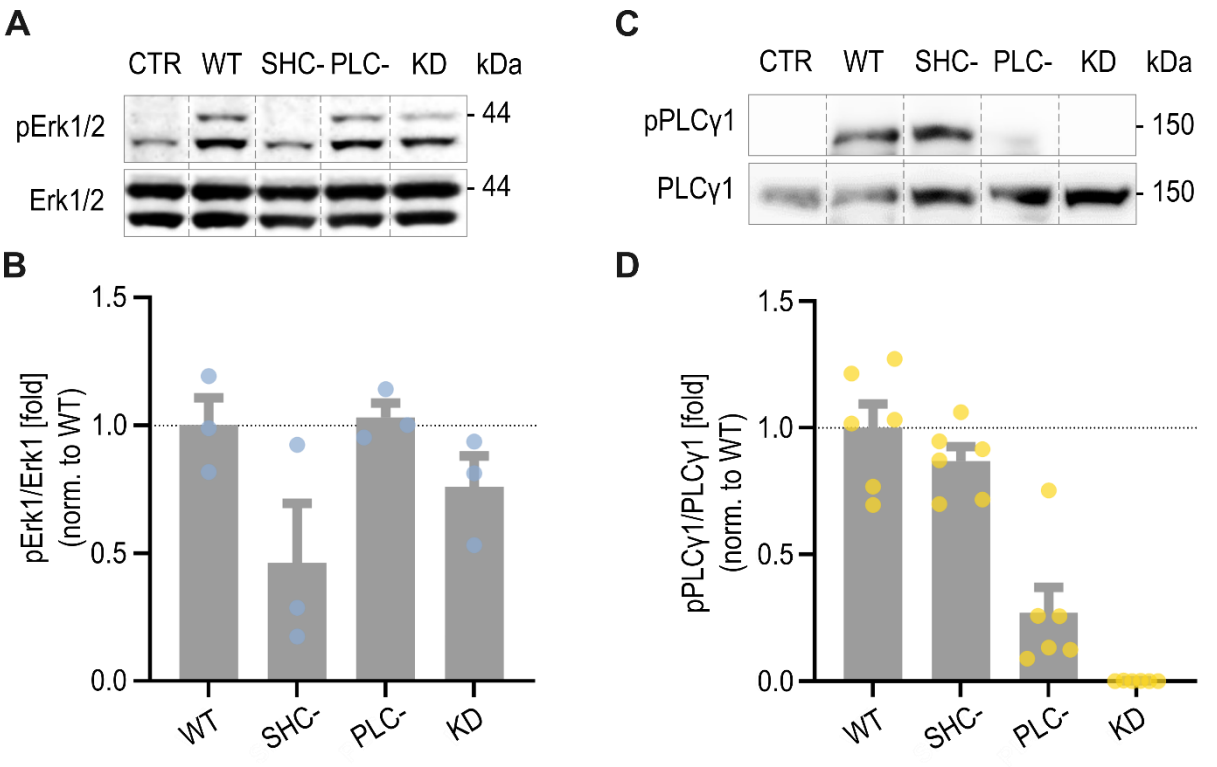

Figure 9: Mutations Y515F (SHC-), Y816F (PLC-), and K571A (KD) differently reduce the activation of TrkB-associated downstream signaling components. **A** Representative immunoblot of protein extracts from NIH3T3 cells transfected with an EGFP control plasmid (CTR) or the TrkB WT and mutants. The top panel represents blots probed for phosphorylated Erk1/2 (Thr202/Tyr204; pErk1/2), while the bottom panel displays total Erk1/2 protein levels in these cells. **B** Quantification of the pErk1/total Erk1 ratio, normalized to WT. Data represent the mean ± S.E.M. from 3 independent experiments (n = 3). WT: 1 ± 0.11; SHC-: 0.46 ± 0.23; PLC-: 1.03 ± 0.06; KD: 0.76 ± 0.12. **C** Representative immunoblot of protein extracts from HEK293 cells transfected with an EGFP control plasmid (CTR) or the TrkB WT and mutants. The top panel represents blots probed for phospho-PLCγ1 (Tyr783, pPLCγ1), while the bottom panel displays total PLCγ1 protein levels. **D** Quantification of the phospho-PLCγ1/total PLCγ1 ratio, normalized to WT. Data represent the mean ± S.E.M. from 6 independent experiments (n = 6). WT: 1 ± 0.09; SHC-: 0.87 ± 0.06; PLC-: 0.27 ± 0.10; KD: 0.001 ± 0.0005. Figure adapted from (193).

Overall, site-directed mutagenesis of TrkB, in addition to the evaluation of associated functional consequences in signaling induction confirmed the successful generation of the following TrkB mutants based on rat TrkB WT (Figure 10 A):

SHC-: A TrkB mutant that retains the protein kinase activity through autophosphorylation and the ability to bind and activate PLCγ1, but exhibits impaired Shc-dependent signaling induction, including reduced Erk1/2 activation (Figure 10 B).

PLC-: This mutant equally preserves protein kinase activity and the ability to activate Shc-dependent signaling but displays diminished PLCγ1 activation (Figure 10 C)

KD: A TrkB mutant deficient in autophosphorylation, resulting in a complete loss of TrkB activation and diminished Shc- and PLCγ-dependent signaling (Figure 10 D).

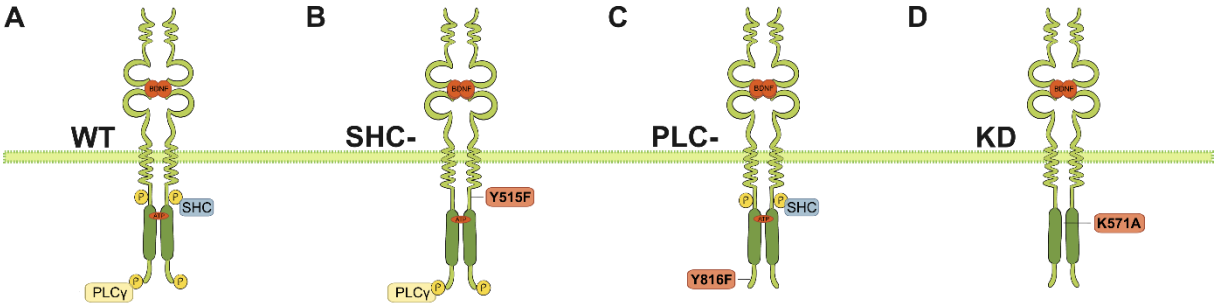

Figure 10: Generated TrkB mutants and their impact on cognate signaling pathway induction. A Schematic representation of the full-length wild-type (WT) TrkB receptor, emphasizing its extracellular Bdnf binding site, intracellular phosphorylation sites, and ATP binding site within the catalytic domain. Bdnf-induced autophosphorylation triggers the binding of adaptor protein Shc at Y515, thereby activating associated pathways, including PI3K-Akt and Ras-MAPK cascades (not shown). Phosphorylation of Y816 binds PLCγ1 and initiates cognate signaling. **B** Point-mutation of Y515 (here Y515F) interferes with Shc binding, thereby preventing Shc-dependent signaling (SHC-). **C** Point-mutation of Y816 (here Y816F) prevents PLCγ1 binding and induction of associated signaling (PLC-). **D** Mutation of the K571 site (here K571A), responsible for ATP-binding, prevents its binding, resulting in a kinase-dead TrkB receptor (KD), which is incapable of autophosphorylation and diminished in further pathway induction.

4.1.3. Generation of Lentiviral Transfer and Expression Vectors

To transfer the TrkB mutants specifically to excitatory neurons, the EGFP-N1-TrkB transgenes of WT and mutants were recombined with a lentiviral vector for transgene expression under the control of a CaMKII promotor. Figure 11 schematically depicts the process of lentiviral expression vector generation.

To this end, the previously constructed lentiviral transfer vector pLenti4CamKII_s/V5-DEST, kindly provided by Martin Kriebel, was equipped with a woodchuck hepatitis virus posttranscriptional regulatory element (WPRE). This ensured enhanced expression of the transgenes in target cells, and the recombination resulted in the 8103 bp lentiviral transfer vector pLenti4CAMKII//WPRE (Figure 11 A to B) (192).

Gateway recombination of the EGFP-N1-TrkB WT or mutant transgenes with pLenti4CAMKII//WPRE resulted in the 9655 bp large vectors pLenti4CAMKII/EGFP-TrkB/WPRE, pLenti4CAMKII/EGFP-TrkBSHC-/WPRE, pLenti4CAMKII/EGFP-TrkBPLC-/WPRE, and pLenti4CAMKII/EGFP-TrkBKD/WPRE (Figure 11 C). Flanked by the long terminal repeats (LTRs) of the lentiviral expression vector, the shortened 04CAMKII-promotor was followed by EGFP-tagged TrkB WT, SHC-, PLC- or KD, and WPRE. Sanger Sequencing confirmed successful recombination by assessing each purified lentiviral vector for the respective recombination and mutation sites (not shown).

With the improved vector pLenti4CAMKII//WPRE and its recombination with EGFP-TrkB WT and mutant transgenes, lentiviral vectors for the transduction of target cells and expression of the WT and mutant receptors in neurons were generated.

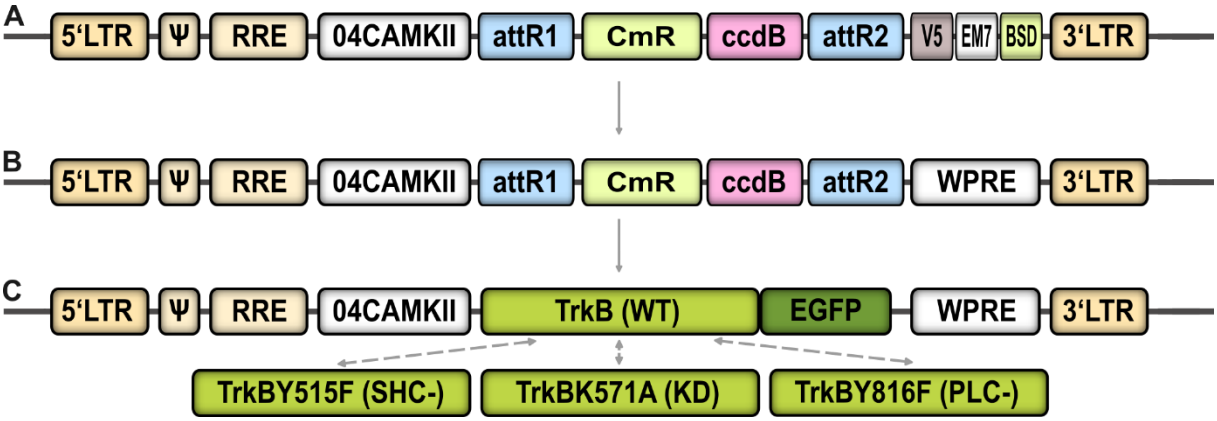

Figure 11: Generation of Lentiviral Transfer and Expression Vectors. A Schematic representation of the elements within the LTR regions of pLenti4CamKII_s/V5-DEST. The V5-tag, EM7 promotor, and the Blasticidin resistance were replaced by a WPRE fragment, resulting in the modified transfer vector pLenti4CAMKII//WPRE (B). **C** Representative lentiviral TrkB vector of pLenti4CAMKII/EGFP-TrkB/WPRE. Through Gateway recombination, EGFP-N1-TrkB transgenes encoding TrkB WT and mutants were inserted into pLenti4CAMKII//WPRE, generating lentiviral vectors for TrkB WT and mutant transgene expression under the control CaMKII control. Full Maps are shown in Supplementary Figure 2 to Supplementary Figure 4. *LTR: long terminal repeat, ψ: packaging signal of human immunodeficiency virus type 1, RRE: Rev response element of HIV-1, 04CAMKII: shortened CaMKII promotor, attR1 and R2: attachment sites for Gateway recombination, CmR: chloramphenicol acetyltransferase, ccdB: coding for bacterial toxin that poisons DNA gyrase, WPRE: woodchuck hepatitis virus posttranscriptional regulatory element, V5: epitope tag from simian virus 5, EM7: synthetic bacterial promoter, BSD: blasticidin S deaminase.* Figure adapted from (193).

4.2. Characterization of TrkB Mutant Vectors in Neurons

4.2.1. TrkB WT and Mutants were Overexpressed in Both Excitatory and Inhibitory Primary Hippocampal Neurons

To assess the successful transduction of neurons and the associated expression of EGFP-tagged TrkB WT and mutants, primary hippocampal neurons were transduced at DIV3 with the corresponding lentiviral vectors and subsequently assessed for the EGFP expression pattern.

After six days post-transduction, it was possible to detect the EGFP-associated fluorescence in neurons transduced with either TrkB WT or mutant forms. At DIV14, EGFP-fluorescence was observed distributed across the whole membrane of primary neurons (Figure 12), transduced with either TrkB WT (A), SHC- (B), PLC- (C), or KD (D). Comparison with neuron-specific MAP2 labeling (Figure 12, A''-D'') revealed that the main EGFP fluorescence was detectable at the somata and proximal neurites but was also observed in proximal neurites.

The observed EGFP expression in primary hippocampal neurons not only confirmed the successful transduction of target cells and expression of the induced transgenes but also showed the correct localization and integration of the TrkB receptors into the cell membrane of the infected neurons.

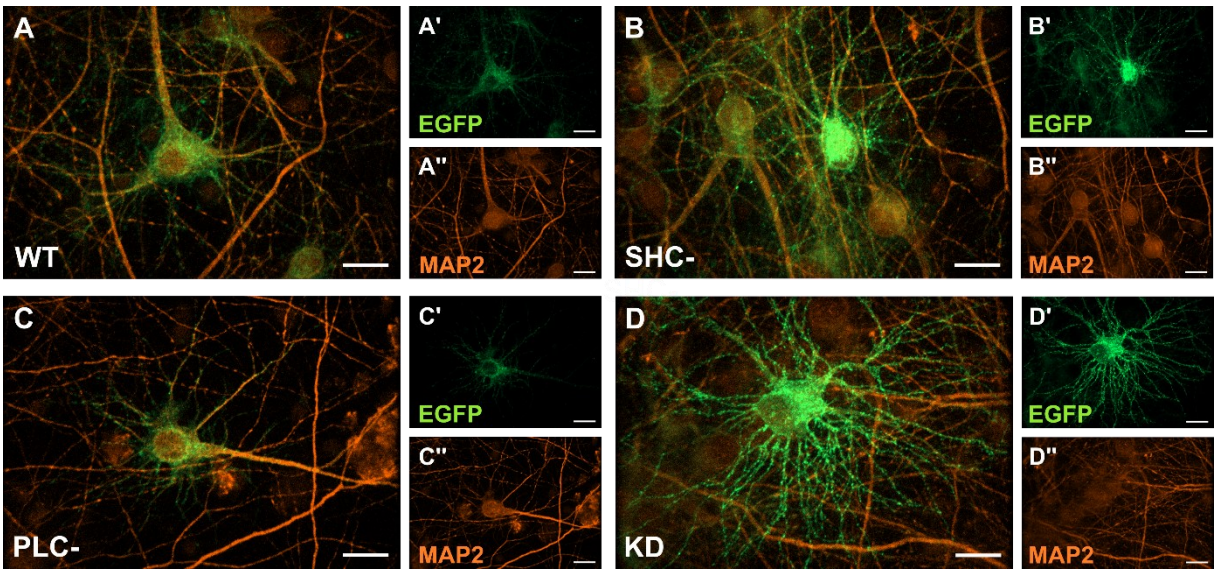

Figure 12: Primary hippocampal neurons express EGFP after lentiviral transduction with TrkB WT and mutants. **A** Representative image of primary hippocampal neurons at DIV14, 11 days post-transduction with pEGFP-N1-TrkB (WT). **A'-A''** Individual channels corresponding to the merged image in A, highlighting the EGFP expression resulting from the viral transduction (A', green) and the expression of immunolabelled MAP2 (A'', orange). **B D''** As described in A-A'' but for the TrkB mutants SHC-, PLC- and KD, as indicated. Scale bars: 10 µm. Figure adapted from (193).

CaMKII-driven gene expression was commonly believed to be primarily restricted to excitatory neurons *in vivo,* however there is accumulating evidence showing that the expression can also occur in inhibitory neurons (194, 195). To assess whether the CaMKII promotor-driven expression of transgenes was exclusive to excitatory neurons *in vitro*, WT transduced neurons were stained for the neuronal marker MAP2 and the inhibitory neurotransmitter GABA (Figure 13 A). Upon quantification of EGFP-single positive and GABA/EGFP-double positive neurons, results showed that the expression of TrkB-EGFP was not limited to excitatory neurons *in vitro* (Figure 13 B). Approximately 11% of all EGFP-positive neurons were additionally positive for GABA, demonstrating that CaMKII-driven transgene is not exclusive to excitatory neurons *in vitro*.

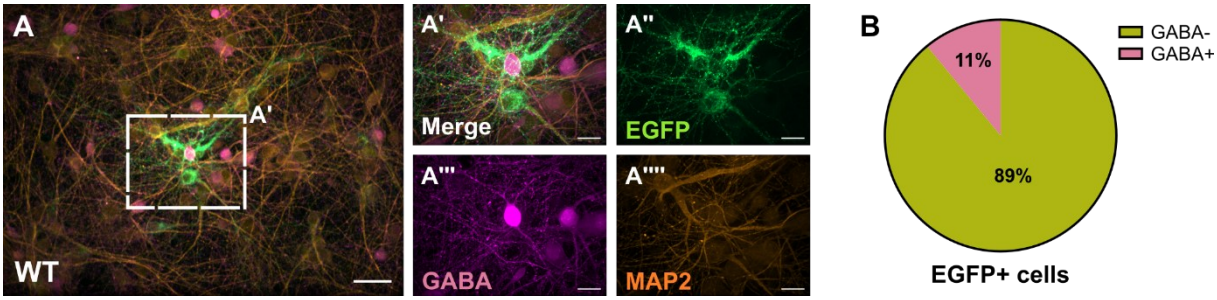

Figure 13: CaMKII-driven expression of TrkB-EGFP transgenes in primary neurons is not specific to excitatory neurons. A Representative image of primary hippocampal neurons transduced with TrkB WT and stained for neurotransmitter GABA and neuronal marker MAP2. The dashed rectangle implies the section depicted enlarged in A'. **A''** shows the individual expression pattern of EGFP-tagged TrkB. **A'''** highlights the staining pattern of GABA, which is labeled inhibitory neurons. **A''''** shows the staining pattern of MAP2**. B** Number of GABA-positive neurons (inhibitory neurons) among all EGFP-positive neurons. Figure adapted from (193).

To further verify the overexpression of TrkB with lentiviral transduction of primary neurons with TrkB-EGFP transgenes, the cells were stained for total TrkB protein (Figure 14). To this end, cells were transduced with a lentiviral control vector only containing the EGFP sequence (pLenti/04CAMKII/EGFP/WPRE, CTR) next to TrkB WT and mutant vectors. The expression pattern of CTR-EGFP was contrary to the pattern observed with TrkB-EGFP transgenes, as it concentrated within the somata and nuclei of transduced cells (Figure 14 A and B-E). Quantification of the mean grey values of TrkB staining showed a significantly increased fluorescence signal with TrkB WT and mutant form transduction compared to CTR (Figure 14 F). Notably, the mean fluorescence signal among TrkB WT and mutants did not differ significantly. Collectively these results confirm the successful overexpression of TrkB with lentiviral transduction of TrkB-EGFP transgenes, which was comparable across all TrkB forms.

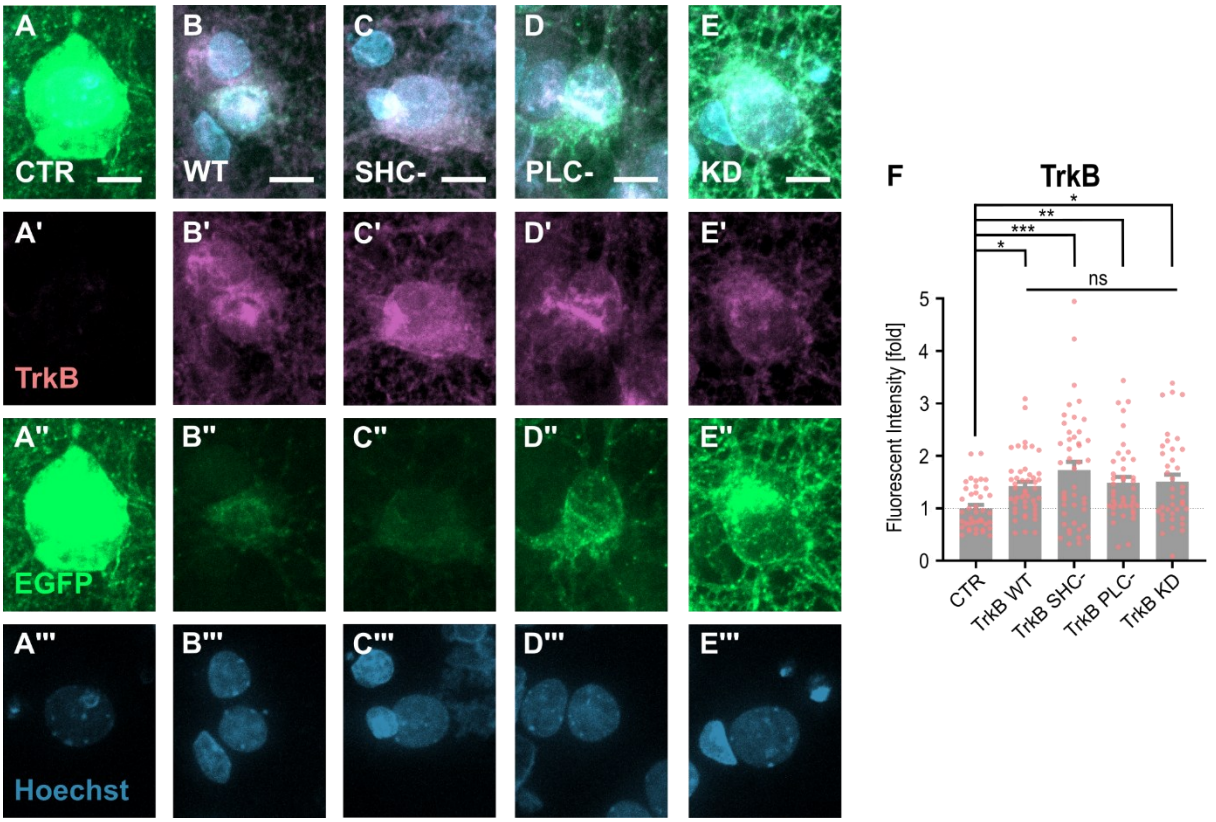

Figure 14: Expression of TrkB WT and mutants increased total TrkB immunoreactivity but was comparable among TrkB forms. A Representative enlarged section of a primary hippocampal neuron at DIV14, 11 days post-transduction with an EGFP-control virus (CTR), stained for TrkB (A'), EGFP (A'') and Hoechst (A'''). **B-E** As described in A, but for TrkB WT (B), SHC- (C), PLC- (D), and KD (E). Scale bars: 5 µm. Corresponding overview microscopic images are shown in Supplementary Figure 7. **F** Quantification of total somatic TrkB fluorescence intensity in CTR, TrkB WT, and mutants. Data represent mean ± S.E.M and are normalized to CTR. n ≥ 38 somata per group from three independent experiments. CTR = 1 ± 0.07, TrkB WT = 1.42 ± 0.08, TrkB SHC- = 1.73 ± 0.16, TrkB KD = 1.51 ± 0.13. Statistical significance was assessed by Kruskal-Wallis with Dunn's multiple comparison test (*p < 0.05, **p < 0.01, ***p < 0.001; ns = not significant). Detailed statistical data is stated in Table 37. Figure adapted from (193).

4.2.2. Mutation of TrkB does not Alter Apoptosis Induction

TrkB is known for promoting cell survival through anti-apoptotic mechanisms via its Shc-dependent signaling pathways (127, 128, 196). Since overexpression of mutant TrkB may alter the anti-apoptotic effects, it was important to exclude cell death-dependent effects for consecutive experiments. Therefore, the activity of Csp3 was assessed by staining transduced primary hippocampal neurons for cleaved Caspase 3 (Cl.Csp3) (Figure 15 A).

Quantification of Cl.Csp3-positive cells within EGFP-positive neurons showed no significant changes in the proportions among TrkB WT and mutants (Figure 15 B), suggesting no alteration of TrkB-dependent anti-apoptotic effects with the mutations, respectively.

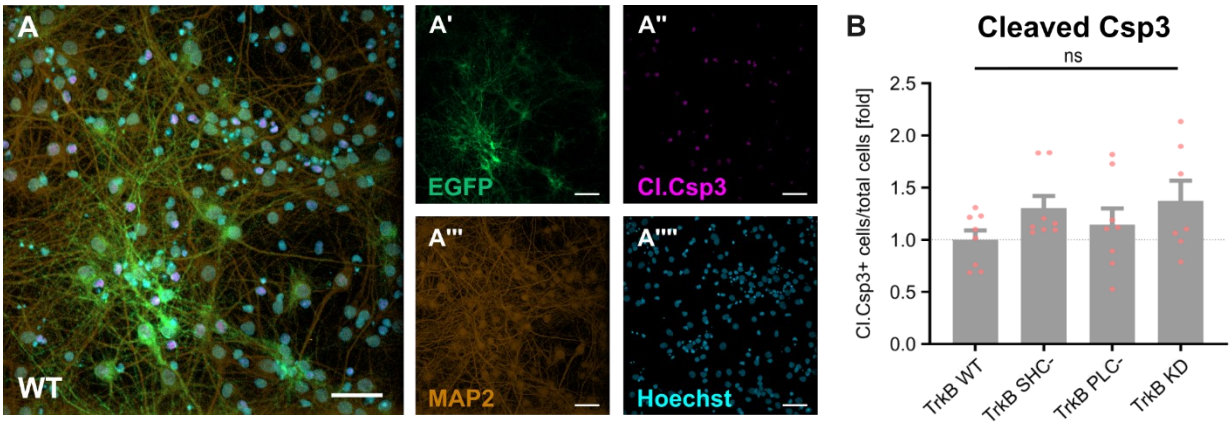

Figure 15: TrkB mutants do not alter the proportion of Cl.Csp+ neurons in transduced cells. A Representative image of primary hippocampal neurons at DIV14, 11 days post-transduction with TrkB WT, stained for cleaved Caspase 3 (Cl.Csp3, A''), MAP2 (A''') and Hoechst (A''''). Scale bars: 50 µm. **B** Quantification of the proportion of Cl.Csp3 positive EGFP-neurons/total EGFP-neurons. Data represent the mean ± S.E.M., obtained from multiple images within an individual well and a total of >7 wells per group from three independent experiments. WT: 1 ± 0.09; SHC-: 1.30 ± 0.12; PLC-: 1.14 ± 0.16; KD: 1.37 ± 0.19; n = 7-8 wells from 3 independent experiments. Statistical significance was assessed by Kruskal-Wallis with Dunn's multiple comparison test; ns = not significant). Detailed statistical data is stated in Table 37. Figure adapted from (193).

4.3. Impact of Mutant TrkB to Synaptic Marker Protein Expression

4.3.1. Distinct Roles of TrkB Signaling Pathways in the Regulation of Gphn Clustering

To dissect the specific impact of TrkB signaling pathways on inhibitory synapses, TrkB mutant transduced primary hippocampal neurons were assessed for the expression of the pre- and postsynaptic markers VGat and gephyrin (Gphn), respectively. Since previous reports highlighted the impact of TrkB specifically on inhibitory synapses at the soma and proximal dendrites of principal cells in the hippocampus (182, 197), the analysis was focused on the synaptic markers at the somata of primary neurons (Figure 16).

To evaluate the role of TrkB mutants on synaptic protein marker density and size, transduced primary hippocampal neurons were stained for Gphn and VGat. The labeling of both markers revealed their abundant expression in TrkB WT (Figure 16 A), SHC- (B), PLC- (C), and KD (D). Quantifying the overall Gphn density, which reflects the total number of extra- and intrasynaptic gephyrin clusters, showed a significant increase, specifically after overexpression of SHC- when compared to WT (Figure 16, E). Neither PLC- nor KD induced any significant changes in total somatic gephyrin density. Likewise, investigation of the total Gphn cluster size demonstrated a significant increase after overexpression of SHC- (Figure 16 F). Again, the PLC mutant remained ineffective regarding changes in total gephyrin cluster size. However, overexpression of TrkB KD significantly increased the size of Gphn clusters, likewise to SHC.

To investigate a potential selectivity of TrkB-dependent Gphn clustering regulation regarding its subcellular localization, extra- and intrasynaptic Gphn cluster densities were quantified separately. To this end, Gphn clusters located within a synapse (syn) were dissected from extrasynaptic clusters (extrasyn), based on the close apposition of a VGat-positive presynaptic cluster. Colocalized pre- and postsynaptic protein markers were further defined as morphological synapses, and, therefore, the associated Gphn clusters as synaptic. Vice versa, Gphn clusters that were not in apposition to a VGat cluster were defined as extrasynaptic.

Quantification of extrasynaptic Gphn cluster density only showed a minor increase in Gphn cluster density after overexpression with SHC- no longer reaching significance compared to TrkB WT (Figure 16 G). Like quantification of total Gphn densities, overexpression of PLC- and KD did not change the density of extrasynaptic gephyrin marker expression.

In contrast, the specific quantification of synaptic Gphn cluster density demonstrated a significant decrease after overexpression of both PLC- and KD, respectively (Figure 16 H), showing a specific contribution of TrkB-PLCγ signaling to synaptic Gphn clustering.

The decrease of inhibitory synapse marker Gphn observed with PLC- was also reflected in the quantification of total VGat-positive presynaptic terminal density (Figure 16 I), highlighting the

significant reduction of GABAergic synapses with PLC- overexpression. In contrast, KD mutant overexpression remained ineffective for VGat marker density.

Overall, dissection of TrkB signaling pathways with site-directed mutation revealed the distinct contributions of Shc- and PLCγ signaling to extra- and intrasynaptic gephyrin clustering in primary hippocampal neurons. Overexpression of SHC- significantly increased total Gphn cluster density and size, while PLC- specifically decreased the density of synaptic Gphn and VGat clusters. Notably, after kinase-dead TrkB overexpression, the neurons displayed a mixture of both phenotypes, including the increased total Gphn cluster size and specific reduction of synaptic Gphn clusters.

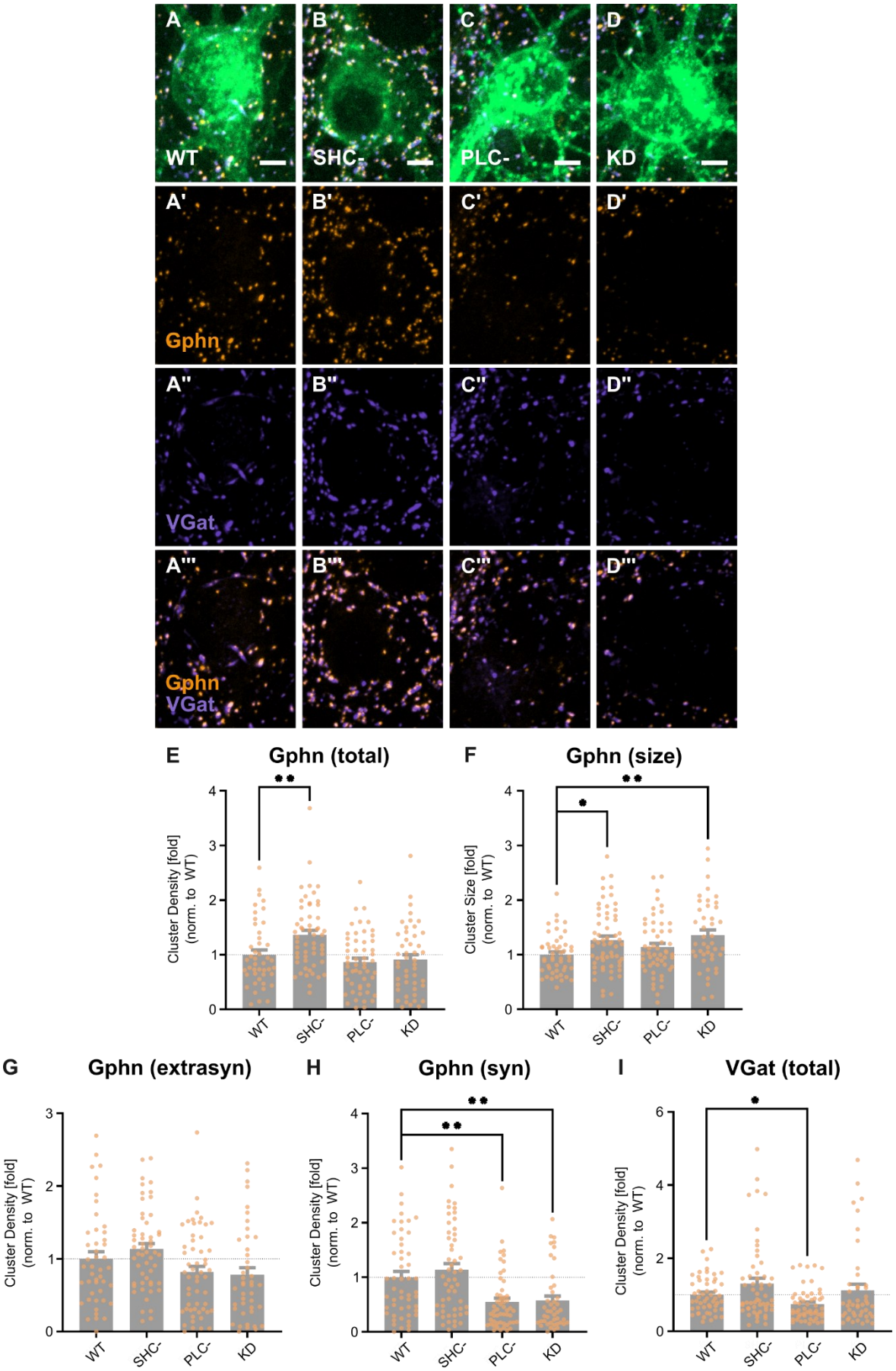
A
B
C
D
WT
SHC-
PLC-
KD
A'
B'
C'
D'
Gphn
A''
B''
C''
D''
VGat
A'''
B'''
C'''
D'''
Gphn
VGat
E
Gphn (total)
Cluster Density [fold] (norm. to WT)
F
Gphn (size)
Cluster Size [fold] (norm. to WT)
G
Gphn (extrasyn)
H
Gphn (syn)
I
VGat (total)
WT
SHC-
PLC-
KD

Figure 16: Dissection of TrkB signaling pathways revealed their distinct roles in regulating gephyrin clustering. **A** Representative enlarged section of primary hippocampal neuron cell body at DIV14, 11 days post-transduction with TrkB WT, stained for gephyrin (Gphn, A') and VGat (A''). Colocalized markers represent GABAergic synapses (A'''). **B-D** According to A but for SHC- (B), PLC- (C) and KD (D). Scale bars 2.5 µm. Corresponding full microscopic images are shown in Supplementary Figure 8. **E** Quantification of total somatic gephyrin cluster densities. WT = 1.00 ± 0.09, SHC- = 1.36 ± 0.08, PLC- = 0.87 ± 0.07; KD = 0.91 ± 0.09. **F** Quantification of total gephyrin cluster size. WT = 1.00 ± 0.05, SHC- = 1.27 ± 0.07, PLC- = 1.14 ± 0.07; KD = 1.36 ± 0.10. **G** Quantification of extrasynaptic gephyrin cluster densities. WT = 1.00 ± 0.10, SHC- = 1.13 ± 0.07, PLC- = 0.82 ± 0.08; KD = 0.78 ± 0.10. **H** Quantification of synaptic gephyrin (apposition of Gphn + VGat). WT = 1.00 ± 0.11, SHC- = 1.14 ± 0.11, PLC- = 0.54 ± 0.07, KD = 0.57 ± 0.08. **I** Quantification of total VGat-positive presynaptic terminals. WT = 1.00 ± 0.07, SHC- = 1.30 ± 0.15, PLC- = 0.74 ± 0.06; KD = 1.12 ± 0.16. Data represents mean ± S.E.M, normalized to WT with n ≥ 45 somata per group obtained from four independent experiments (3 independent experiments for KD). Statistical significance was assessed by Kruskal-Wallis with Dunn's multiple comparison test (only significant comparisons are shown, *p < 0.05, **p < 0.01). Detailed statistical data is stated in Table 37. Figure adapted from (193).

4.3.2. Diminished TrkB-PLCγ Signaling Reduced Total α2-$GABA_AR$ Density

Gephyrin facilitates tethering of $GABA_A$ receptors ($GABA_ARs$) at synaptic sites (14), and $GABA_ARs$ containing α2 and α3- subunits are reduced upon knockdown of Gphn (62). Therefore, to investigate if the decrease in synaptic gephyrin cluster density observed with PLC- and KD might result in an accompanied reduction of $GABA_ARs$, the total density of $GABA_AR$ subunit α2 (α2) and the colocalization with Gphn was assessed (Figure 17).

Immunolabelling of the $GABA_AR$ α2 subunit showed the abundant expression of the GABA receptor across the whole neuron, colocalizing with Gphn clusters in TrkB WT (Figure 17 A), as well as SHC- (B), PLC- (C), and KD (D) overexpressing neurons. Quantifying the total α2 density in these neurons demonstrated a significant decrease after overexpression with PLC- , compared to WT (Figure 17 E). In contrast, SHC- remained ineffective regarding the total α2 subunit density. Like the previous findings of the unaltered VGat-positive terminal density with KD transduction, the overexpression of the kinase-dead TrkB mutant had no effect on α2 subunit density. Upon quantification of α2 subunits colocalizing with Gphn, none of the TrkB mutants showed a change in the overall density when compared to TrkB (Figure 17, F).

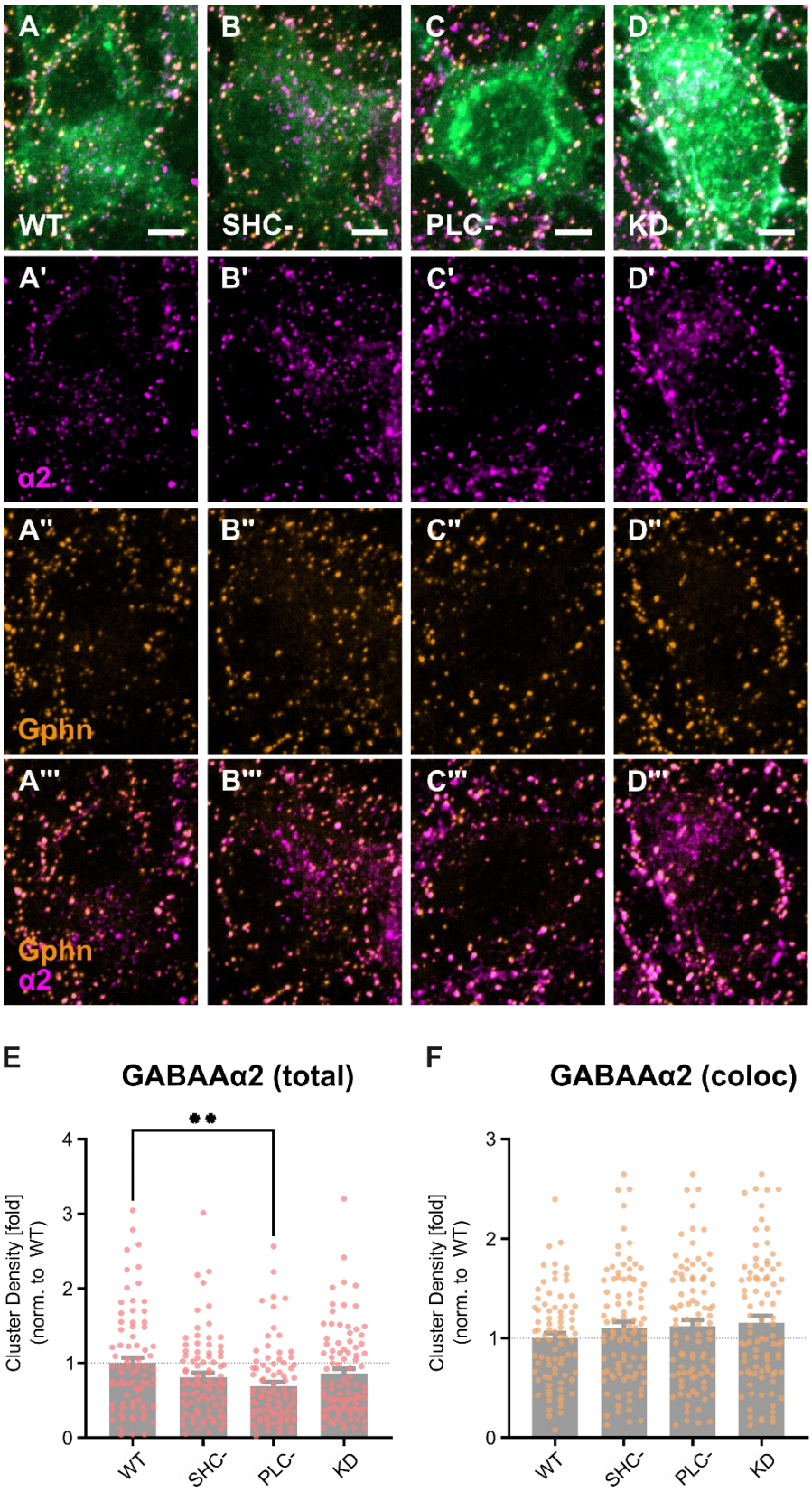

Figure 17: PLC- overexpression reduced GABAAR α2 subunit density at the somata. A Representative enlarged section of primary hippocampal neuron cell body at DIV14, 11 days post-transduction with TrkB WT, stained for $GABA_AR$ α2 subunit (α2, A') and Gphn (A''). Colocalized markers are shown in A'''. **B-D** According to A but for SHC- (B), PLC- (C), and KD (D). Scale bars 2.5 µm. Corresponding full microscopic images are shown in Supplementary Figure 9. **E** Quantification of total somatic α2 cluster densities. WT = 1.00 ± 0.08, SHC- = 0.81 ± 0.06, PLC- = 0.69 ± 0.06; KD = 0.86 ±

0.06. **F** Quantification of α2 clusters colocalized with gephyrin clusters. WT = 1.00 ± 0.05, SHC- = 1.11 ± 0.06, PLC- = 1.12 ± 0.06; KD = 1.16 ± 0.07. Data represent mean ± S.E.M, normalized to WT with n ≥ 80 somata per group obtained from three independent experiments. Statistical significance was assessed by Kruskal-Wallis with Dunn's multiple comparison test (only significant comparisons are shown, **p < 0.01). Detailed statistical data is stated in Table 37.

4.3.3. Excitatory Synaptic Marker Expression Remained Unaltered with Overexpression of TrkB Mutants

TrkB signaling is widely known for regulating synaptic plasticity at excitatory synapses (80, 196, 198) by controlling PSD95 localization, which involves all three major signaling pathways (139). Therefore, to evaluate the impact of TrkB mutations in excitatory synapses, pre- and postsynaptic marker expression of VGlut1 and PSD95 was investigated (Figure 18).

Like inhibitory synaptic markers, both VGlut1 and PSD95 were expressed abundantly across the whole neuron overexpressing TrkB WT (Figure 18, A), SHC- (B), PLC- (C), and KD (D). The total somatic PSD95 cluster density, which includes extra- and intrasynaptic PSD95 clusters, was unaltered after overexpression of TrkB mutants compared to WT (Figure 18, E). Dissection of intra- and extrasynaptic PSD95 clusters, defined by the apposition of PSD95 clusters to VGlut1-positive presynaptic terminals, also revealed no changes in excitatory synapse density (Figure 18, F). Likewise, the total density of VGlut1-positive presynaptic terminals remained unchanged, demonstrating no TrkB mutant-dependent effects on excitatory synaptic marker expression at primary neuronal somata (Figure 18, D).

Overall, none of the investigated pre- and postsynaptic markers were changed after overexpression of TrkB mutants.

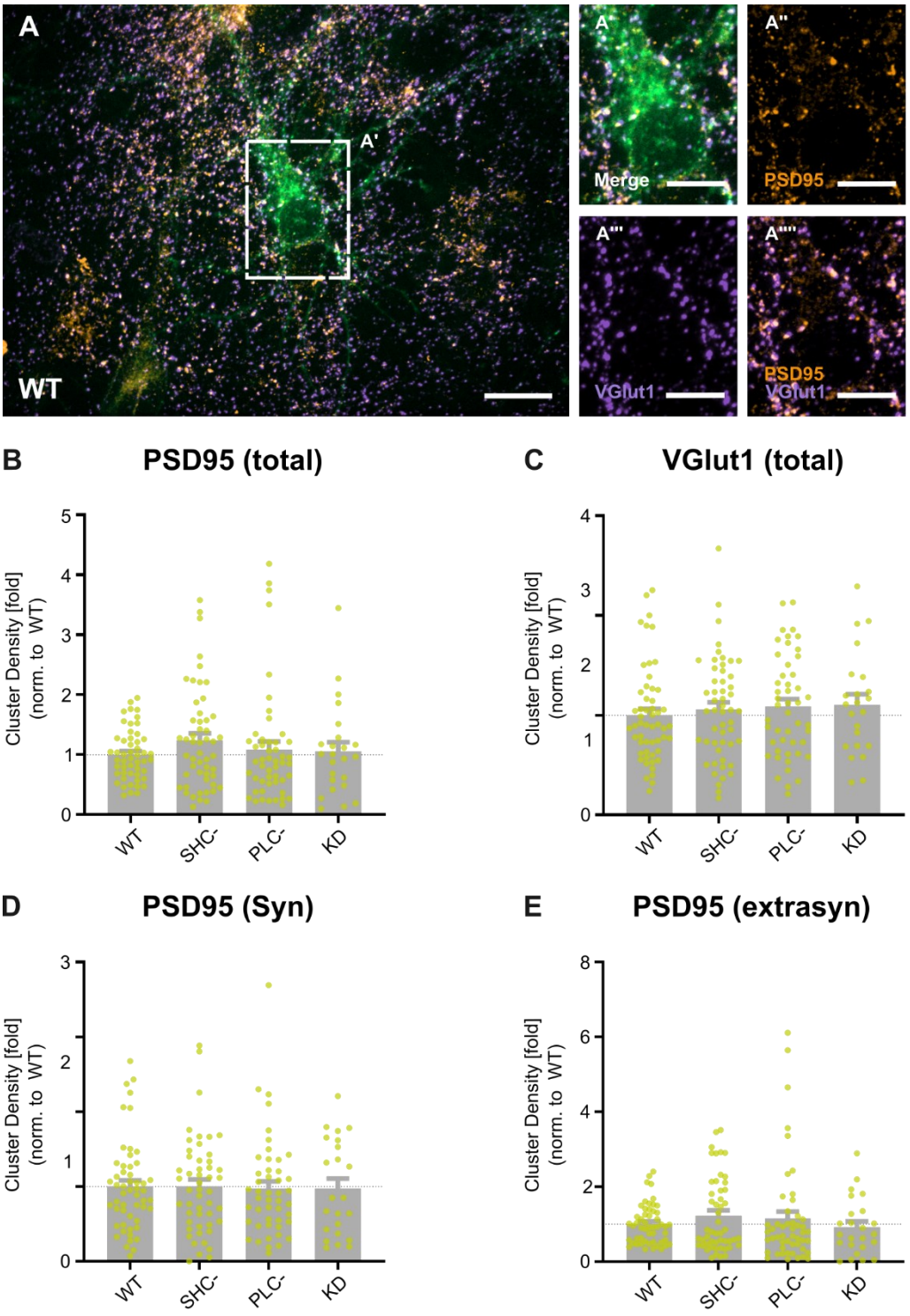

Figure 18: TrkB mutants did not alter excitatory synaptic marker densities. A Representative image of primary hippocampal neurons at DIV14, 11 days post-transduction with TrkB WT, stained for PSD95 (A'), VGlut1 (A''). Colocalized markers represent excitatory synapses (A'''). **B** Quantification of total somatic PSD95 cluster densities. WT = 1.00 ± 0.06, SHC- = 1.24 ± 0.12, PLC- = 1.09 ± 0.13; KD = 1.05 ± 0.16. **C** Quantification of total VGlut1 cluster densities. WT = 1.00 ± 0.06, SHC- = 1.06 ± 0.07, PLC- = 1.09 ± 0.07; KD = 1.1 ± 0.11. **D** Quantification of synaptic PSD95 cluster densities (apposition of PSD95 and VGlut1); WT = 1.00 ± 0.08, SHC- = 1.01 ± 0.09, PLC- = 0.97 ± 0.1; KD = 0.97 ± 0.13. **E** Quantification of extrasynaptic PSD95. WT = 1.00 ± 0.17, SHC- = 1.23 ± 0.14, PLC- = 1.15 ± 0.19, KD = 0.92 ± 0.15. Data represent mean ± S.E.M, normalized to WT with n ≥ 47 somata per group obtained from four independent experiments except for the KD group (n ≥ 23 somata obtained from two independent experiments). Statistical significance was assessed by Kruskal-Wallis with Dunn's multiple

comparison test (ns = not significant). Detailed statistical data is stated in Table 37. Figure adapted from (193).

4.3.4. Reduction of Inhibitory Synapses after PLC- Overexpression Results in a Shift in E/I Synaptic Proportions

The specific reduction in inhibitory synapses, alongside unaltered excitatory synaptic marker expression, as observed after overexpression of PLC- and KD, might result in imbalanced excitatory-inhibitory input at the cell bodies of transduced primary neurons. Therefore, the proportions of excitatory to inhibitory synapses at the somata of TrkB mutant transduced neurons were assessed (Figure 19).

Figure 19 A summarizes the densities of excitatory and inhibitory synapses quantified in Figure 16 H and Figure 18 D, further highlighting the significant reduction of inhibitory synapses (orange) after overexpression of PLC- and KD mutants compared to TrkB WT. The reduction in GABAergic synapses reduced its proportion of total synapses at the somata by 15.8 % (PLC-) and 11,8 % (KD), respectively, whereas it remained unaltered after SHC- overexpression (Figure 19 B). Consequently, the proportion of excitatory synapses found on transduced neurons increased with PLC- and KD to the same degree.

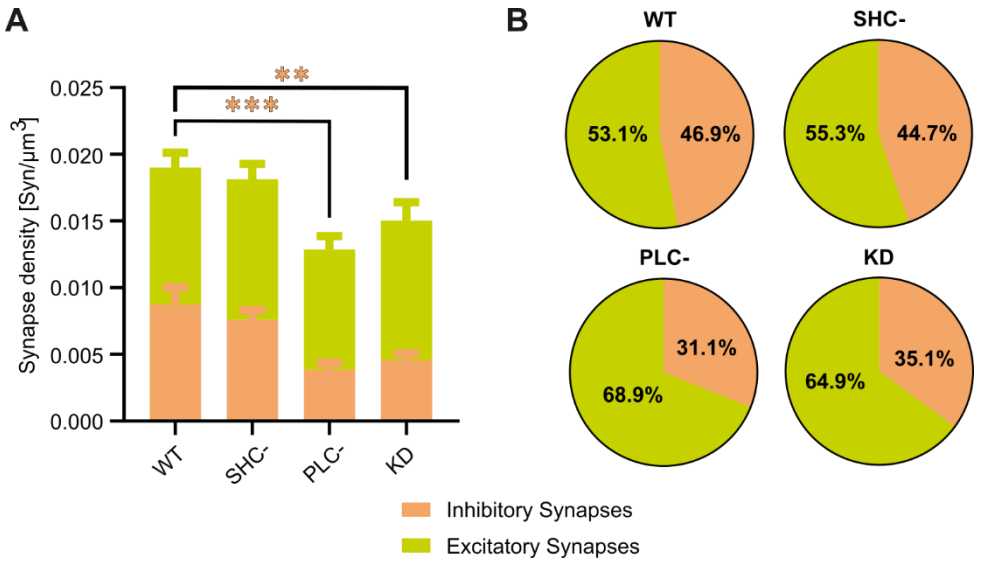

Figure 19: Reduction in inhibitory synapse density shifts the ratio of somatic inhibitory and excitatory synapses towards excitatory synapses. A Average total synaptic density/ µm^3 combined of inhibitory (orange) and excitatory synapses (green) at the somata of EGFP-positive neurons. The number of inhibitory synapses significantly decreased after overexpression of PLC- and KD mutants. *Inhibitory Synapses (orange)*: WT = 0.009 ± 0.001, SHC- = 0.008 ± 0.0007, PLC- = 0.004 ± 0.0005; KD = 0.005 ± 0.0005. *Excitatory Synapses (green)*: WT = 0.01 ± 0.001, SHC- = 0.01 ± 0.001, PLC- = 0.009 ± 0.001; KD = 0.01 ± 0.001. Data represent mean ± S.E.M, Inhibitory Synapses: n ≥ 51 somata per group obtained from four independent experiments except for the KD group (here n = 44 somata obtained from three independent experiments). Excitatory Synapses: n ≥ 47 somata per group obtained from four independent experiments except for the KD group (n = 23 somata obtained from two independent experiments). Statistical significance was assessed by 2way ANOVA with Dunn's multiple

comparison test (only significant comparisons are shown, **p < 0.01, ***p < 0.001). Orange stars indicate significant changes resulting from the comparison of inhibitory proportions. **B** Pie charts showing the average proportions of inhibitory and excitatory synapses among all synapses of the somata of WT, SHC-, PLC-, and KD transduced neurons.

Collectively, quantifying somatic excitatory and inhibitory pre- and postsynaptic markers and their proportions in primary neurons overexpressing TrkB WT and mutants revealed the specific role of TrkB-dependent synaptic regulation to inhibitory synapses and the pathway-specific roles in regulating gephyrin clustering. While SHC- overexpression resulted in alterations of total Gphn accumulation, overexpression of PLC- and KD specifically affected synaptic Gphn and, therefore, inhibitory synapses. This specific reduction in inhibitory synaptic density shifted the ratio of excitatory to inhibitory synapses towards an increased proportion of morphological excitatory synapses at the somata of primary hippocampal neurons.

4.4. Functional Consequences of TrkB Mutant Overexpression

To investigate functional changes alongside the reduced inhibitory morphological synapse densities observed with the overexpression of PLC- and KD, spontaneous calcium transients were analyzed in TrkB WT and mutant transduced primary hippocampal neurons since intracellular somatic calcium transients reflect electrical events in neurons (199).

To this end, to observe calcium fluctuations in neuronal cultures, they were stained with the red fluorescent chemical calcium indicator Calbryte 590 AM, as representatively shown in Figure 20 A. Subsequently, somatic calcium fluctuations were recorded in red fluorescent/EGFP double-positive neurons. Traces were analyzed for the event rate, the peak amplitude (ΔF/F0), the area under the curve (AUC), and the full-width half maximum (FWHM).

At DIV14, 11 days post-transduction, calcium transients were measurable in cultures, irrespective of the transduced TrkB variant. The representative calcium transients are shown in Figure 20 B. Quantifying the calcium transient frequency revealed a significant increase in event frequency after overexpression of PLC-, as compared to TrkB WT (Figure 20 C), while SHC- and KD remained ineffective. The increased event frequency in PLC- cells was accompanied by a reduced calcium transient amplitude (Figure 20 D), which was also reflected in the AUC of these cells (Figure 20 E). Again, SHC- overexpression remained ineffective for these parameters. Notably, the KD mutant did not share these functional observations with the PLC-mutant overexpression, although showing a reduction in morphologically inhibitory synapses. The full-width half-maximum remained unchanged with all TrkB mutants (Figure 20 F).

Taken together, analysis of spontaneous calcium transients of TrkB mutant overexpressing neurons demonstrated the functional consequences of diminished TrkB-PLCγ-dependent signaling and reduced inhibitory synapse density, by showing increased excitability in transduced neurons under basal conditions.

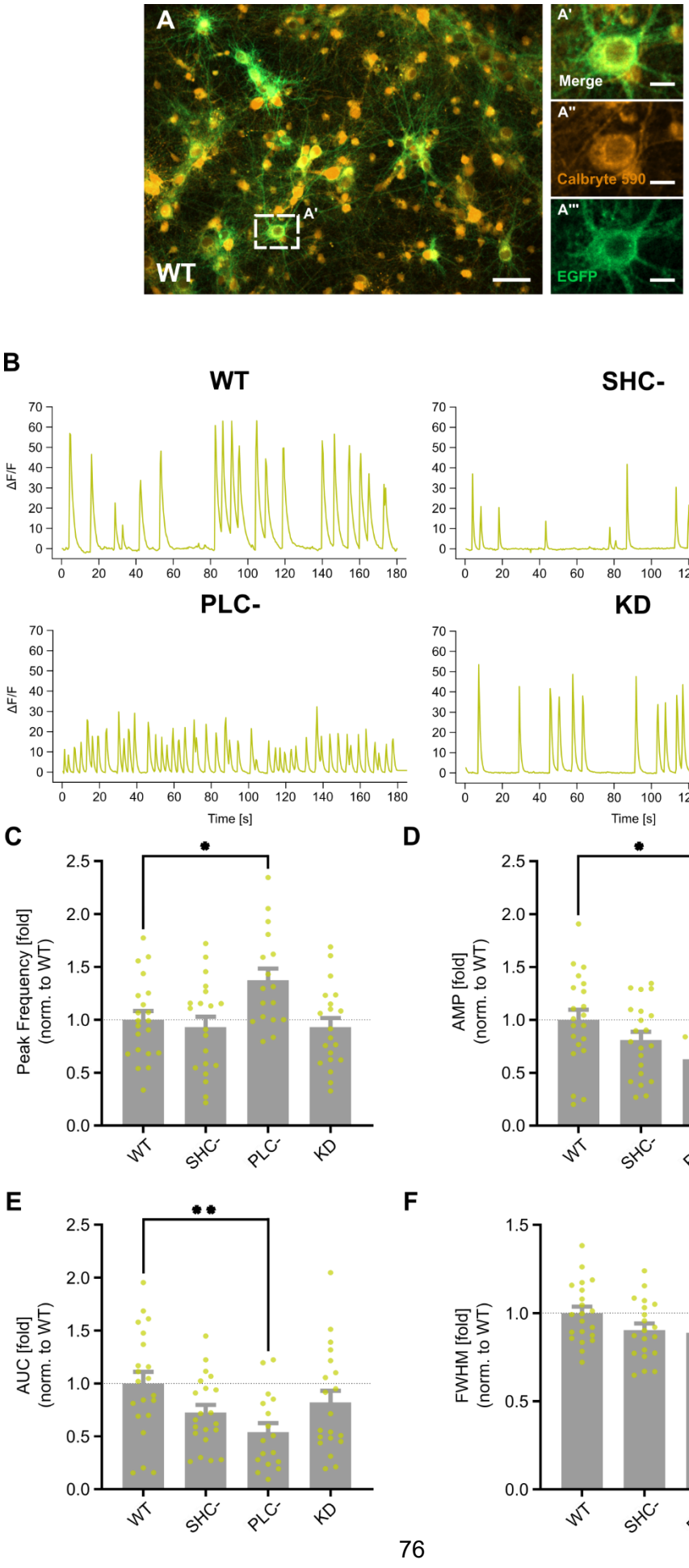
A
A'
WT
A'
Merge
A''
Calbryte 590
A'''
EGFP
B
WT
SHC-
PLC-
KD
ΔF/F
Time [s]
C
Peak Frequency [fold] (norm. to WT)
D
AMP [fold] (norm. to WT)
E
AUC [fold] (norm. to WT)
F
FWHM [fold] (norm. to WT)
WT
SHC-
PLC-
KD

Figure 20: Overexpression of PLC- increased calcium peak frequency in primary hippocampal neurons. **A** Representative confocal image of non-fixated TrkB WT-transduced primary hippocampal neurons at DIV14, stained for calcium using Calbryte 590 AM. The dashed rectangle represents the enlarged section depicted in A' and the individual channels for CalBryte 590 AM (A'') and the TrkB-related EGFP signal (A''') Scale bars: 10 µm (A) and 2.5 µm (A'-A'''). **B** Representative traces of spontaneous somatic calcium transients measured in neurons positive for EGFP. **C** Quantification of the event frequency; WT = 1.00 ± 0.08, SHC- = 0.93 ± 0.10, PLC- = 1.38 ± 0.11; KD = 0.93 ± 0.09. **D** Quantification of amplitudes; WT = 1.00 ± 0.10, SHC- = 0.81 ± 0.08, PLC- = 0.63 ± 0.09; KD = 0.86 ± 0.10. **E** Quantification of AUCs: WT = 1.00 ± 0.11, SHC- = 0.72 ± 0.07, PLC- = 0.54 ± 0.09; KD = 0.82 ± 0.11. **F** Quantification of FWHMs; WT = 1.00 ± 0.04, SHC- = 0.90 ± 0.04, PLC- = 0.89 ± 0.05; KD = 0.99 ± 0.06. Numerical data are values ± SEM normalized to WT. n = 17-21 wells from 7 independent experiments. Statistical significance was assessed by one-way ANOVA with Dunn's multiple comparison test (**p < 0.01; nonsignificant comparisons are not noted). Detailed statistical data is stated in Table 37. Figure adapted from (193).

4.5. The Role of mTOR and CaMKII Signaling in TrkB Dependent Gephyrin Clustering

Various protein kinases have been described as regulating gephyrin clustering, either through phosphorylation or by associating with gephyrin (46, 48, 73, 149). Additionally, similar kinases are described as downstream effectors of TrkB signaling (discussed in 1.3.1). To understand the molecular mechanism underlying the TrkB-dependent changes observed in this study at both morphological and functional levels, two potential downstream mediators were assessed next: mTOR and CaMKII. Both protein kinases were assessed for their signaling after overexpression of TrkB mutants to evaluate their potential involvement in the TrkB-dependent alterations of Gphn clustering.

4.5.1. mTOR Signaling was Reduced after SHC- Overexpression

Gphn has been described to be associated with mTOR and to be released upon Bdnf-dependent mTOR-activation, promoting gephyrin clustering (73). In turn, the induction of mTOR signaling is regulated by the TSC1/2 complex on which both Shc-dependent signaling pathways Pi3K/Akt and Ras/MAPK converge (142, 143). To investigate if mTOR is potentially involved in the SHC- dependent increase in gephyrin clustering, primary hippocampal neurons were assessed for their activation of mTOR signaling after TrkB mutant overexpression. Therefore, cells were stained for mTOR phosphorylated at Serine 2448 (Ser2448), the amino acid, targeted by the Pi3K-Akt pathway (200). Additionally, mTOR substrate S6K, phosphorylated at Threonine 389 (Thr389), the site most closely correlating with its activity, was labeled as well, together serving as a proxy measure of mTOR pathway induction (201).

Immunolabelling of mTOR Ser2448, as well as S6K Thr389, revealed both proteins being abundantly expressed in cultures transduced with TrkB WT (Figure 21 A & E), SHC- (B & F), PLC- (C & G), and KD (D & H). Quantifying the somatic expression of phosphorylated mTOR showed a significant reduction in fluorescence intensity in neurons overexpressing SHC- and KD mutants, compared to TrkB WT (Figure 21 I). In contrast, neurons transduced with PLC-, did not show any significant change in the mean fluorescence intensity of mTOR Ser2448. Likewise, PLC- transduced neurons did not show an altered mean fluorescence intensity in phosphorylated S6K, whereas the overexpression of SHC- and KD mutants significantly reduced the fluorescence intensity of labeled S6K Thr389 (Figure 21 J).

Taken together, these results demonstrate a reduced activation of mTOR and S6K with diminished TrkB activity, particularly Shc-dependent signaling.

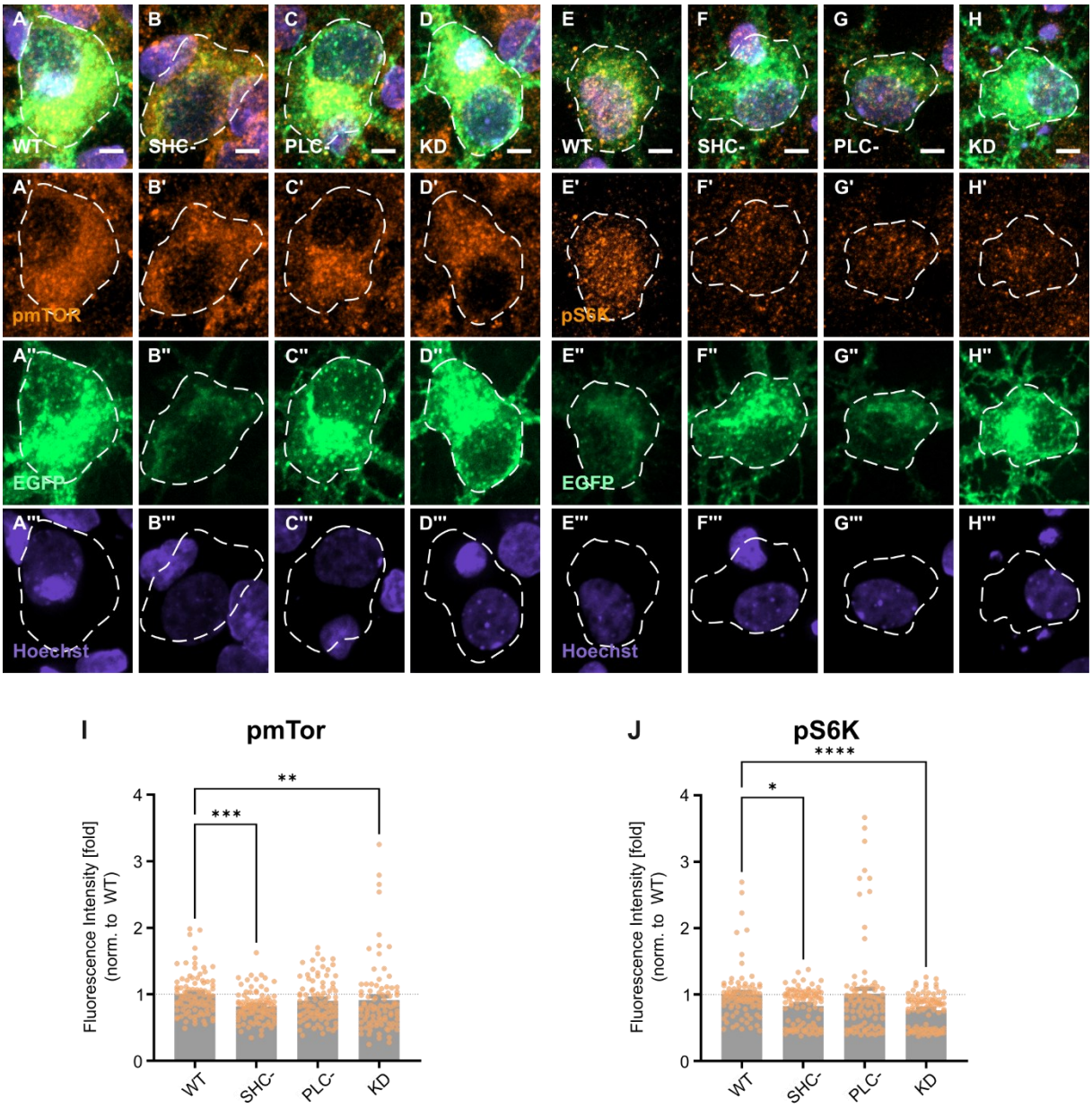

Figure 21: SHC- and KD overexpression reduced the phosphorylation of mTOR and S6K. A Representative enlarged section of primary hippocampal neuron cell body at DIV14, 11 days post-transduction with TrkB WT, stained for phosphorylated mTOR (Ser2448, pmTOR, A') and Hoechst (A'''). The corresponding expression of TrkB-EGFP is depicted in A''. **B-D** According to A but for overexpression of SHC- (B), PLC- (C) and KD (D). **E** Representative enlarged section of primary hippocampal neuron cell body at DIV14, 11 days post-transduction with TrkB WT, stained for phosphorylated p70-S6 kinase (Thr389, pS6K, E') and Hoechst (E'''). The corresponding expression of EGFP is depicted in E''. **F-H** According to F but for overexpression of SHC- (F), PLC- (G) and KD (H). Scale bars: 2.5 µm. The corresponding full images are shown in Supplementary Figure 10. **I** Quantification of the mean somatic fluorescence intensity of pmTOR in EGFP- positive neurons. WT = 1.00 ± 0.03, SHC- = 0.82 ± 0.03, PLC- = 0.90 ± 0.03; KD = 0.91 ± 0.06. **J** Quantification of the mean somatic fluorescence intensity of pS6K in EGFP- positive neurons. WT = 1.00 ± 0.04, SHC- = 0.83 ± 0.03, PLC- = 1.01 ± 0.07; KD = 0.76 ± 0.03. Data represent mean ± S.E.M, normalized to WT with n ≥ 86 somata per group obtained from three independent experiments. Statistical significance was assessed by Kruskal-Wallis with Dunn's multiple comparison test (only significant comparisons are shown, *p < 0.05, **p < 0.01, ***p < 0.001, ****p < 0.0001). Detailed statistical data is stated in Table 37.

4.5.2. PLC- and KD Overexpression Reduced CaMKII Activity

Autophosphorylated CaMKII has been described as translocating to inhibitory synapses, facilitating the insertion of GABAARs (47). Further reports revealed that CaMKII is crucial for regulating the localization of synaptic Gphn clusters through phosphorylation (46, 48). Furthermore, TrkB has been described to enhance CaMKII activity via its PLCγ-dependent impact on intracellular Ca^{2+} concentrations (discussed in 1.3.1.) Therefore, to determine whether CaMKII is involved in the TrkB PLC- dependent reduction in synaptic gephyrin density, the level of autophosphorylated CaMKII was assessed in TrkB WT and mutant transduced neurons. To this end, the cells were immunolabelled for total CaMKIIα and CaMKIIα phosphorylated at Threonine 285 (Thr286, pCaMKII). Activated CamKII further autophosphorylates at this site, which renders the kinase constitutively active (37, 202).

Neurons overexpressing TrkB WT (Figure 22 A), as well as SHC- (B), PLC- (C), and KD (D), all showed expression of total and autophosphorylated CaMKII. Following background subtraction, quantification of the mean fluorescence intensity in cell bodies of EGFP-positive neurons revealed no alterations in the expression of autophosphorylated CaMKIIα after overexpression of SHC- (Figure 22 E). In contrast, neurons transduced with PLC- and KD showed a significant reduction in autophosphorylated CaMKII-related fluorescence intensity. To verify these results and confirm that overexpression of TrkB mutants did not alter the overall CaMKII protein expression, total CaMKII fluorescence was additionally quantified (Figure 22 F). Except for KD, none of the TrkB point mutants altered the overall CaMKII expression, demonstrating a decreased activation of CaMKII in neurons after PLC- overexpression.

The results showed that neurons transduced with TrkB mutants, which are associated in this study with the decrease of synaptic Gphn density, exhibited reduced levels of autophosphorylated CaMKII. Whereas PLC- overexpression reduced the amount of the constitutively active form of CamkII, overexpression of KD further decreased the overall expression of CaMKII in transduced neurons

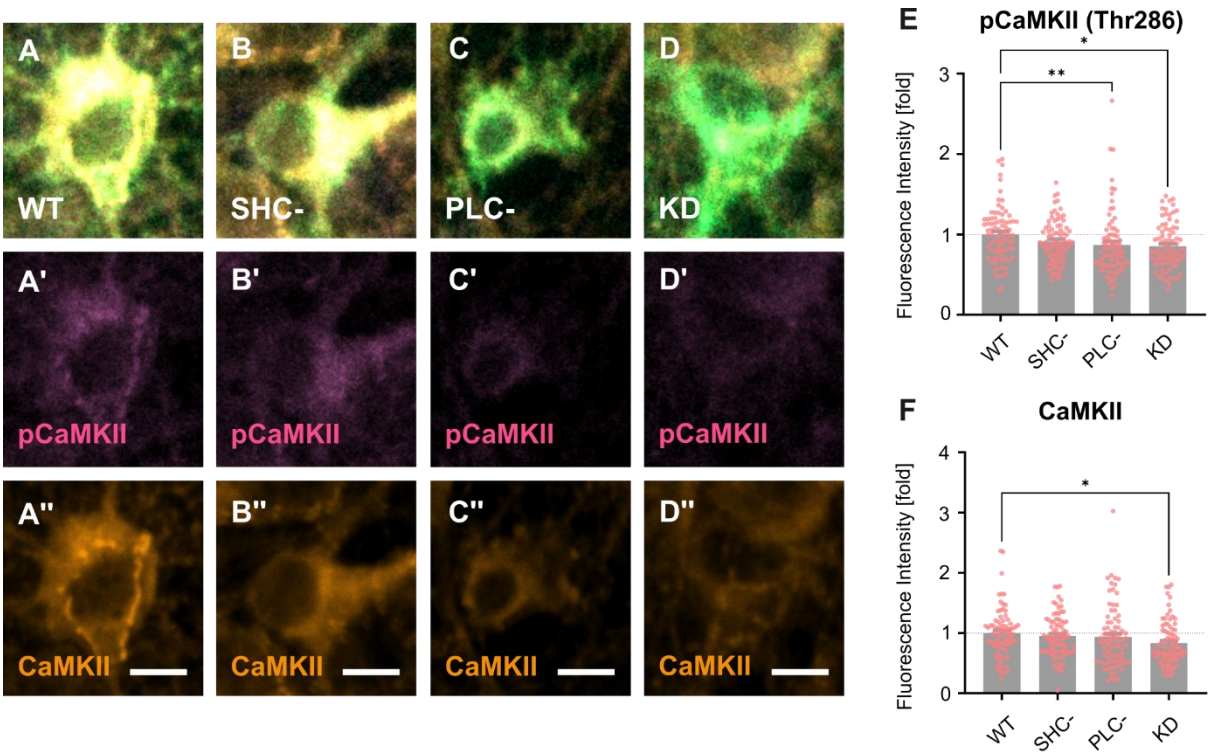

Figure 22: Autophosphorylation of CAMKII is reduced with overexpression of PLC- and KD mutants. **A** Representative enlarged section of an EGFP-positive primary hippocampal neuron cell body at DIV14, 11 days post-transduction with TrkB WT, stained for autophosphorylated CAMKIIα (Thr286, pCAMKII, A') and total CaMKIIα (A''). **B-D** According to A, but for neurons overexpressing SHC- (B), PLC- (C), and KD (D). Scale bars: 2.5 µm. The corresponding full images are shown in Supplementary Figure 11. **E** Quantification of the mean somatic fluorescence intensity of pCAMKIIα after background subtraction in EGFP- positive neurons. WT = 1.00 ± 0.04, SHC- = 0.94 ± 0.04, PLC- = 0.85 ± 0.03; KD = 0.85 ± 0.04. **F** Quantification of the mean somatic fluorescence intensity of total CAMKIIα after background subtraction in EGFP- positive neurons. WT = 1.00 ± 0.05, SHC- = 0.95 ± 0.04, PLC- = 0.94 ± 0.06; KD = 0.83 ± 0.04. Data represent mean ± S.E.M, normalized to WT with n ≥ 78 somata per group obtained from three independent experiments. Statistical significance was assessed by Kruskal-Wallis with Dunn's multiple comparison test (only significant comparisons are shown, *p < 0.05, **p < 0.01). Detailed statistical data is stated in Table 37**.** Figure adapted from (193).

4.6. Summarized Results I: TrkB-Dependent Gephyrin Regulation under Basal Conditions

Creating several mutations of the rat TrkB receptor (4.1) allowed the dissection of TrkB signaling pathways (4.2) and the investigation of their specific impact on Gephyrin clustering in primary hippocampal neurons *in vitro* (for overview see Table 35).

Under basal conditions, signaling pathways of TrkB receptors appeared to have distinct roles regarding the regulation of gephyrin clustering. Reduction of TrkB-Shc-dependent signaling increased the overall gephyrin clustering by density and size, while TrkB-PLCγ dependent signaling was needed to cluster Gphn specifically at synaptic sites and to maintain the overall α2-$GABA_AR$ density (4.3). Consequently, the kinase activity of TrkB was important for both overall Gphn clustering and localization at synaptic sites.

Since the impact of TrkB mutant overexpression was exclusive to inhibitory synaptic proteins, TrkB-PLCγ signaling was further important to maintain the E/I balance at the somata of neurons as the increased proportion of morphological excitatory synapses was functionally accompanied by an increased calcium peak frequency (4.4).

Analysis of potential downstream mediators revealed that increased mTOR signaling was not required to increase total Gphn accumulation (4.5). In contrast, TrkB catalytic activity, particularly PLCγ-dependent signaling, was important for the autophosphorylation of CaMKIIα.

Table 35 Main summarized observations made under basal conditions

BASAL CONDITIONS			
Observation	**TrkB SHC-**	**TrkB PLC-**	**TrkB KD**
Gphn cluster size	↑	-	↑
Gphn cluster density	↑	-	-
Gphn syn. cluster density	-	↓	↓
VGat cluster density	-	↓	-
$GABA_AR$ α2 cluster density	-	↓	-
E/I balance	-	↑E	↑E
Calcium Freq	-	↑	-
mTOR signaling	↓	-	↓
CaMKII autophosphorylation	-	↓	↓

4.7. The Contribution of TrkB to Gephyrin Clustering during iLTP

TrkB is known for the induction and maintenance of excitatory LTP (eLTP) (80), mediated by all three major signaling pathways (139, 152). Whereas a long-standing focus on the persistent strengthening of excitation and its role to learning and memory continued, the importance of inhibitory LTP (iLTP) has become increasingly apparent(24). Relative local calcium levels facilitate glutamatergic and GABAergic synaptic crosstalk and plasticity responses through an intersection of downstream signaling pathways (24). Moderate intracellular calcium concentration results in CaMKIIα translocation to inhibitory synapses and facilitates inhibitory long-term potentiation (iLTP) through synaptic gephyrin recruitment and enhanced $GABA_AR$ forward trafficking and membrane insertion (46, 48). Regarding the results observed with the investigation of TrkB-dependent Gphn clustering under basal conditions, the question arose, whether TrkB could contribute to processes involved in gephyrin recruitment during iLTP as an upstream mediator. To address this question, neurons expressing the TrkB mutants were exposed to chemically induced iLTP, adapted from Petrini and colleagues (48).

To chemically induce iLTP (chem iLTP), Petrini et al. induced a moderate calcium increase in their target cells by mild stimulation of NMDA receptors (NMDARs) with parallel inhibition of AMPA receptors (AMPARs) (48). With the brief NMDAR stimulation, they observed potentiation of inhibitory synapses via redistribution and accumulation of gephyrin at synaptic sites through increased size and density of Gphn clusters, further showing the necessity of this accumulation for chem iLTP. To reproduce the accumulation of gephyrin via chem iLTP in the here-used culture system, the protocol by Petrini et al. was adapted in TrkB WT expressing primary hippocampal neurons by performing the same mild NMDAR stimulation but in a recording solution that Pennachietti and colleagues described in 2017 (48, 78). The neurons were assessed for inhibitory synaptic marker expression to assess the consequences of adapted chem iLTP in the here used cultures.

Immunolabelling of Gphn and VGat in stimulated primary neurons revealed an overall increased expression of both markers after chem iLTP (Figure 23 A & B). Quantification of the total somatic Gphn density in EGFP-positive neurons showed a significant increase of 14.4 % ± 3.3 % with chem iLTP compared to the sham-treated neurons (Figure 23 C). In addition, total Gphn cluster size significantly increased by 16.8 % ± 3.1 % with moderate NMDAR stimulation (Figure 23 D). Whereas the effects of chem iLTP remained ineffective for the density of extrasynaptic Gphn (4.1 % ± 4.6 %, Figure 23 E), they increased the density of synaptic gephyrin cluster significantly by 24.2 % ± 7.3 % (Figure 23 F). In contrast, the density of VGat-positive presynaptic terminals remained unaltered, compared to sham-treated neurons (5 % ± 4.3 %, Figure 23 G), emphasizing the selective postsynaptic effects of chem iLTP.

Overall, the adaptation of Petrini's chem iLTP protocol to the here-used neuronal cultures allowed the successful replication of chem iLTP-dependent effects of gephyrin clustering, by increasing its accumulation, specifically at synaptic sites.

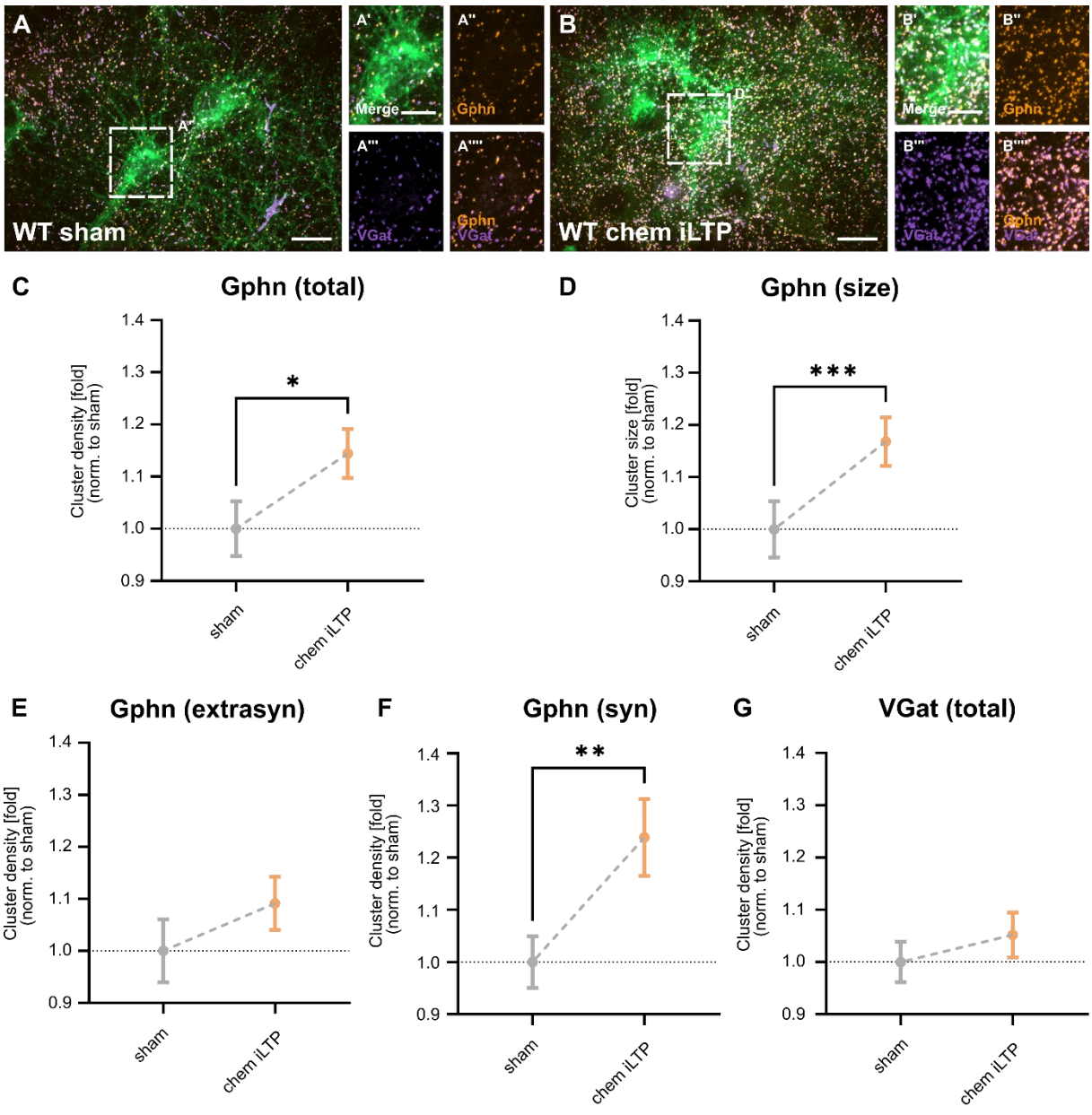

Figure 23: Adaption of chem iLTP protocol in TrkB WT expressing primary hippocampal neurons resulted in increased total Gphn cluster density and size and increased synaptic Gphn density. **A** Representative confocal image of TrkB WT-transduced primary neurons at DIV14, treated with the sham solution. The dashed rectangle indicates the enlarged section depicted in A' and the individual staining patterns for Gphn (A'') and VGat (A'''), and their colocalization (A''''). **B** According to A but for neurons treated with NMDA+CNQX (chem iLTP). Scale bars: 10 µm (A & B) and 5 µm (A'-B''''). **C** Quantification of total somatic Gphn cluster density of neurons treated with sham or chem iLTP solution. Sham = 1.00 ± 0.05, chem iLTP = 1.14 ± 0.05. **D** Quantification of the mean cluster size of total somatic Gphn. Sham: 1.00 ± 0.05, chem iLTP: 1.17 ± 0.05. **E** Quantification of extrasynaptic Gphn clusters. Sham = 1.00 ± 0.06, chem iLTP: 1.04 ± 0.05. **F** Quantification of synaptic Gphn clusters. Sham = 1.00 ± 0.05, chem iLTP = 1.24 ± 0.07. **G** Quantification of total somatic VGat-positive presynaptic terminals. Sham = 1.00 ± 0.04, chem iLTP = 1.05 ± 0.04. All values are normalized to the sham treated group.

Data represents mean ± S.E.M, normalized to sham with n ≥ 78 somata per group obtained from three independent experiments. Statistical significance was assessed by one-tailed Mann-Whitey test (only significant comparisons are shown, $p < 0.05$*, $p < 0.01$**, $p < 0.001$***). Detailed statistical data is stated in Table 37.

4.7.1. TrkB Catalytic Activity is Required for chem iLTP-induced Gphn Clustering and Involves Shc- and PLCγ-dependent Pathways

To now investigate if TrkB contributes to chem iLTP-dependent Gphn accumulation and further dissect potential TrkB-pathway-dependent effects, the results shown with TrkB WT were extended by inducing chem iLTP in primary hippocampal neurons transduced with either the SHC-, PLC-, or KD mutant. After chem iLTP, neurons were immunolabelled for inhibitory pre- and postsynaptic markers Gphn and VGat (Figure 24 A and B).

Quantification of total somatic Gphn cluster density revealed that the significant increase observed in the presence of TrkB WT was absent in neurons that overexpressed any of the TrkB mutants (Figure 24 C). While the mutation of the TrkB-ATP or Shc- binding site completely prevented the chem iLTP-dependent increase in Gphn cluster density (4.7 % ± 4.8 % and -6.4 % ± 4.4 %), neurons with diminished TrkB-PLCγ signaling still exhibited a trend towards an increase in the density of total gephyrin clusters following chem iLTP (11.5 % ± 4.6 %).

Additionally, quantifying the mean total Gphn cluster size further confirmed the importance of TrkB signaling to iLTP-dependent Gphn accumulation (Figure 24 D). Again, neurons overexpressing the SHC and KD mutant were unable to increase the mean cluster size following chem iLTP (-6.5 % ± 3.8 % and -2.3 % ± 3.9 %), whereas a significant increase was still observed in PLC neurons (21.7 % ± 4.8 %).

To dissect the TrkB-dependent effects on chem iLTP-associated Gphn clustering in a site-specific manner, Gphn clusters were again assessed in their intra- and extrasynaptic densities separately. Quantification of extrasynaptic Gphn cluster density revealed a significant chem iLTP-dependent increase in cluster density with neurons overexpressing either the SHC- (28 % ± 6.7 %) or PLC- mutants (24.0 % ± 6.0 %). This effect was not observed with chem iLTP treatment of WT and KD neurons (6.2 % ± 4.7 %) (Figure 24 E). In contrast, the significant increase in synaptic Gphn density observed with chem iLTP in WT neurons was completely abolished with all three TrkB mutants, further highlighting the importance of TrkB signaling to the synaptic effects of chem iLTP (Figure 24 F). Whereas overexpression of SHC- and PLC- failed to significantly change synaptic cluster density with chem iLTP (-7.5 ± 5.6 % and 3.0 % ± 4.9 %, respectively) as observed in WT neurons, the reduction of TrkB kinase activity even further reversed these effects by significantly decreasing the synaptic Gphn density with chem iLTP by 15.7 % ± 5.3 %. This KD-dependent significant reduction in postsynaptic marker expression was also reflected in the density of VGat-positive presynaptic terminals after chem

iLTP (Figure 24 G). Here, the density was decreased by 13.7 % ± 4.3 %, whereas no significant changes were observed in SHC- (-8.6 % ± 4.1 %) and PLC- (-0.1 % ± 4.0 %) neurons, compared to WT.

Overall, the chemical induction of iLTP in neurons overexpressing TrkB mutants revealed the requirement of TrkB to the iLTP-associated processes of gephyrin accumulation. Not only was the receptor's catalytic activity necessary to increase the total density and size of Gphn clusters, but it was also needed to specifically increase synaptic gephyrin clustering. Increasing total and synaptic Gphn densities involved both Shc and PLCγ pathways, and malfunction of either one of both cascades resulted in excess accumulation of extrasynaptic Gphn. Since chem iLTP did not positively alter the density of the presynaptic marker VGat, these processes were exclusive to postsynaptic markers.

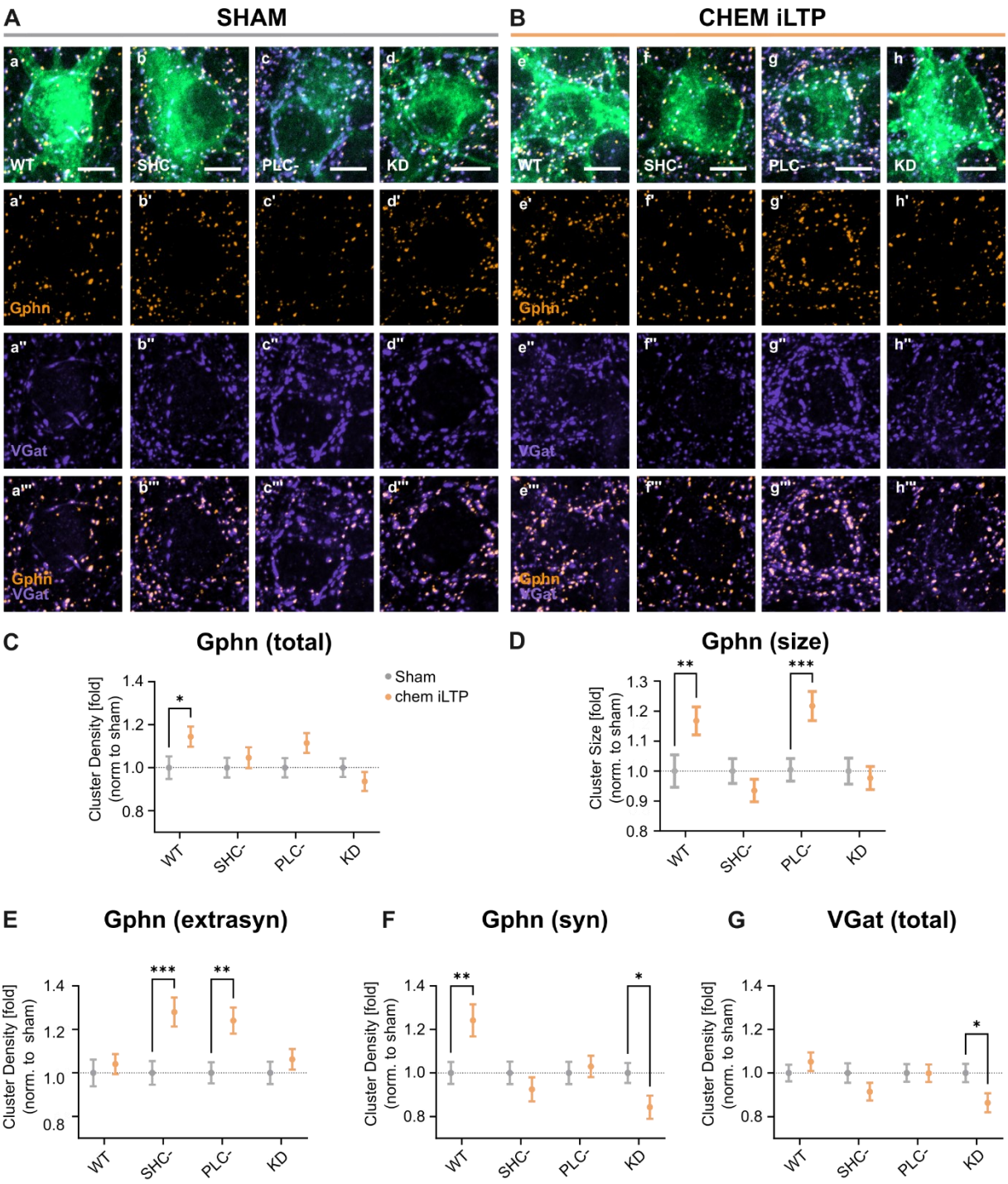

Figure 24: TrkB is necessary for chem iLTP induction of gephyrin clustering. **A** Representative enlarged sections of primary hippocampal neuron cell bodies at DIV14, 11 days post-transduction with TrkB WT (a), SHC- (b), PLC- (c) and KD (d), treated with sham solution and stained for gephyrin (Gphn, a'-d') and VGat (a''-d''). Colocalized markers represent GABAergic synapses (a'''-d'''). **B** According to A but for primary neurons transduced with either TrkB WT (e), SHC- (f), PLC- (g) and KD (h) and treated with NMDA+CNQX (chem iLTP). Scale bars: 5 µm. Full microscopic images are shown in Supplementary Figure 12. **C** Quantification of the total somatic Gphn cluster density, either treated with sham solution (sham, grey) or NMDA+CNQX (chem iLTP, orange). WT sham: 1.00 ± 0.05, chem iLTP = 1.14 ± 0.05; SHC- sham: 1.00 ± 0.05, chem iLTP: 1.05 ± 0.05; PLC- sham: 1.00 ± 0.04, chem iLTP: 1.12 ± 0.05, KD: 1.00 ± 0.04, chem iLTP: 0.93 ± 0.04. **D** Quantification of mean cluster size of total Gphn. WT sham: 1.00 ± 0.05, chem iLTP = 1.17 ± 0.05; SHC- sham: 1.00 ± 0.04, chem iLTP: 0.93 ± 0.04; PLC- sham: 1.00 ± 0.04, chem iLTP: 1.22 ± 0.05, KD: 1.00 ± 0.04, chem iLTP: 0.98 ± 0.04. **E** Quantification of extrasynaptic Gphn cluster density. WT sham: 1.00 ± 0.06, chem iLTP = 1.04 ± 0.05; SHC- sham: 1.00 ± 0.05, chem iLTP: 1.28 ± 0.07; PLC- sham: 1.00 ± 0.05, chem iLTP: 1.24 ± 0.06, KD: 1.00 ± 0.05,

chem iLTP: 1.06 ± 0.05. **F** Quantification of synaptic Gphn cluster density (colocalized Gphn + VGat marker). WT sham: 1.00 ± 0.05, chem iLTP = 1.24 ± 0.05; SHC- sham: 1.00 ± 0.05, chem iLTP: 0.93 ± 0.06; PLC- sham: 1.00 ± 0.05, chem iLTP: 1.03 ± 0.05, KD: 1.00 ± 0.05, chem iLTP: 0.84 ± 0.05. **G** Quantification of VGat-positive presynaptic terminals. WT sham: 1.00 ± 0.04, chem iLTP = 1.05 ± 0.04; SHC- sham: 1.00 ± 0.04, chem iLTP: 0.91 ± 0.04; PLC- sham: 1.00 ± 0.04, chem iLTP: 1.00 ± 0.04, KD: 1.00 ± 0.04, chem iLTP: 0.86 ± 0.04. All values are normalized to respective sham treated group. Data represent the mean ± S.E.M. with n ≥ 78 somata obtained from three independent experiments. Statistical significance was assessed by Two-way ANOVA with Tukey's multiple comparisons test (only significant comparisons between sham and the respective chem iLTP group are shown, $p < 0.05$*, $p < 0.01$**, $p < 0.001$***). Detailed statistical data is stated in Table 37. Figure adapted from (193).

4.7.2. TrkB, Mek1/2, and CaMKII Signaling all Contribute to Gphn Accumulation during chem iLTP

To further confirm the role of TrkB in iLTP-dependent gephyrin accumulation, chem iLTP was induced in neurons expressing TrkB WT, alongside the presence of the non-competitive TrkB antagonist Cyclotraxin B (Ctx B). Likewise, to elucidate potential downstream mechanisms, Mek1, which is upstream of Erk1/2, as well as CaMKII were inhibited during chem iLTP with PD98059 and KN-62, respectively. Following these treatments, cells were again stained for gephyrin and VGat (Figure 25 A and B).

Consistent with the findings in Figure 24, chem iLTP again significantly increased total Gphn cluster density at the cell bodies of transduced neurons (Figure 25 C). In addition, a comparison of the unstimulated groups revealed that none of the inhibitors modified the baseline protein marker densities compared to the DMSO control but inhibition of Mek1 as well as CtxB reduced the overall cluster sizes (Supplementary Figure 13 C-F). The increase in Gphn accumulation following chem iLTP was completely abolished by Ctx B treatment, confirming the critical role of TrkB signaling in the associated gephyrin regulation. Likewise, inhibition of Mek1 and CaMKII with PD98059 and KN-62, respectively, prevented the iLTP-induced increase in gephyrin density. Additionally, the increase in cluster size, typically observed after chem iLTP, was absent once any of the inhibitors was applied (Figure 25 D).

Co-staining of gephyrin with the inhibitory presynaptic marker VGat allowed to distinguish between extra- and intrasynaptic gephyrin clusters. As observed previously, chem iLTP had no significant effect on extrasynaptic Gphn clustering, and this remained unchanged with the inhibition of TrkB, Mek1, or CaMKII, respectively (Figure 25 E). In contrast, the increase in synaptic gephyrin induced by chem iLTP was prevented by inhibition of TrkB, Mek1, or CaMKII, respectively (Figure 25 F). This further emphasizes the importance of these proteins in the synaptic regulation of gephyrin during iLTP.

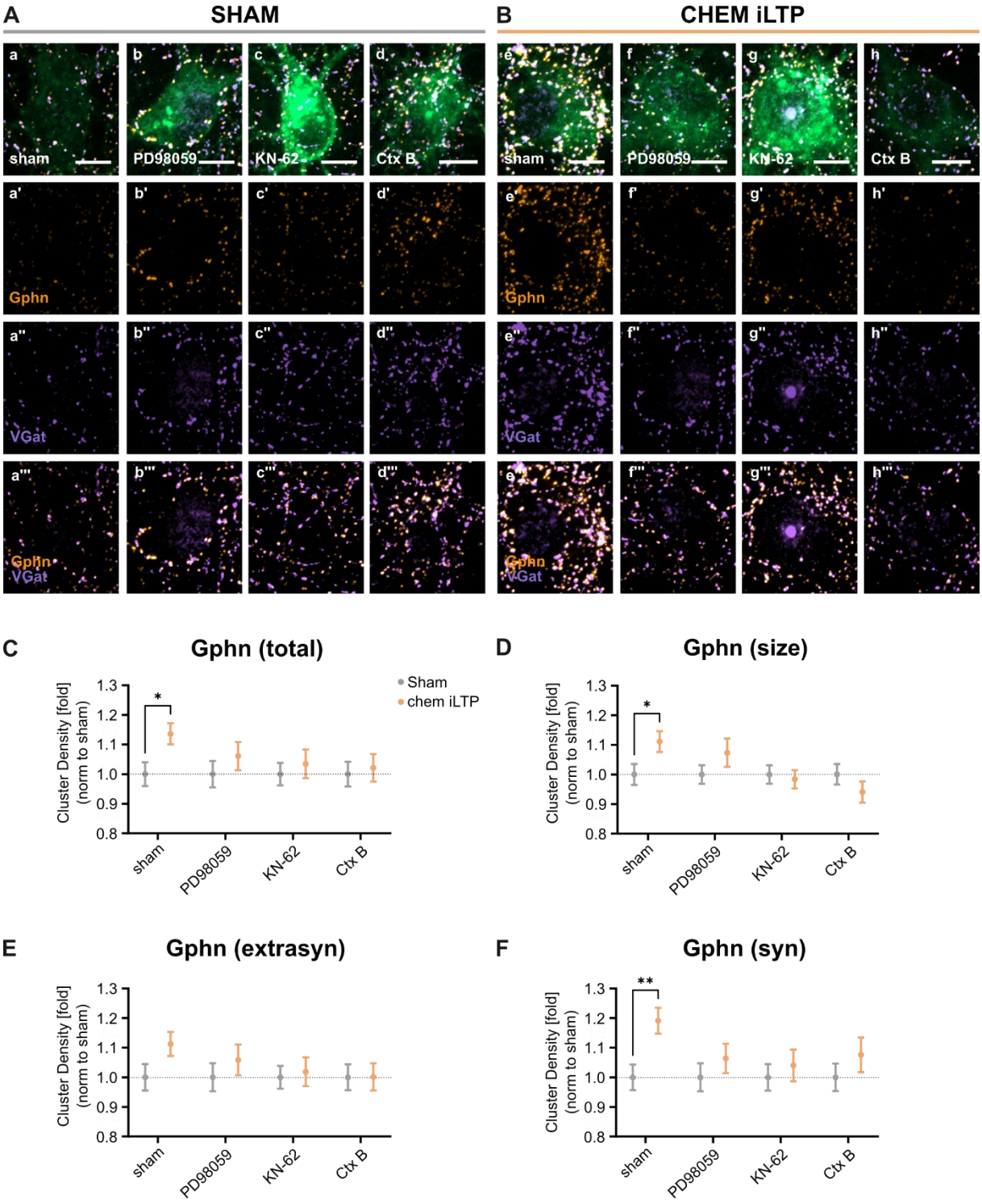

Figure 25: Inhibition of TrkB, Mek1/2 and CaMKII signaling abolishes the effects of chem iLTP on gephyrin. **A** Representative enlarged sections of primary hippocampal neuron cell bodies at DIV14, 11 days post-transduction with TrkB WT. Cells were treated with sham solution in the presence of DMSO only (sham, a), PD98059 (b), KN-62 (c), or Cyclotraxin B (Ctx B, d) and stained for gephyrin (Gphn, a'-d') and VGat (a''-d''). Colocalized markers represent GABAergic synapses (a'''-d'''). **B** According to A but for cells treated with NMDA+CNQX (chem iLTP) in the presence of DMSO only (e), PD98059 (f), KN-62 (g) or Cyclotraxin B (Ctx B, h). Scale bars: 5 µm. Full microscopic images are shown in Supplementary Figure 13. **C** Quantification of the total Gphn cluster density of EGFP positive somata, either treated with sham solution (sham, grey) or NMDA+CNQX (chem iLTP, orange). WT sham: 1.00 ± 0.04, chem iLTP =

1.14 ± 0.04; PD98059 sham: 1.00 ± 0.04, chem iLTP: 1.06 ± 0.05; KN-62 sham: 1.00 ± 0.04, chem iLTP: 1.04 ± 0.05, Cyclotraxin B: 1.00 ± 0.04, chem iLTP: 1.02 ± 0.05. **D** Quantification of mean cluster size of total Gphn. WT sham: 1.00 ± 0.04, chem iLTP = 1.11 ± 0.04; PD98059 sham: 1.00 ± 0.03, chem iLTP: 1.07 ± 0.05; KN-62 sham: 1.00 ± 0.03, chem iLTP: 0.98 ± 0.03, Cyclotraxin B: 1.00 ± 0.03, chem iLTP: 0.94 ± 0.04.**E** Quantification of extrasynaptic Gphn cluster density. WT sham: 1.00 ± 0.04, chem iLTP = 1.11 ± 0.04; PD98059 sham: 1.00 ± 0.05, chem iLTP: 1.06 ± 0.05; KN-62 sham: 1.00 ± 0.04, chem iLTP: 1.02 ± 0.05, Cyclotraxin B: 1.00 ± 0.04, chem iLTP: 1.00 ± 0.05. **F** Quantification of synaptic Gphn cluster density (colocalized Gphn + VGat marker). WT sham: 1.00 ± 0.04, chem iLTP = 1.19 ± 0.04; PD98059 sham: 1.00 ± 0.05, chem iLTP: 1.06 ± 0.05; KN-62 sham: 1.00 ± 0.05, chem iLTP: 1.04 ± 0.05, Cyclotraxin B: 1.00 ± 0.05, chem iLTP: 1.08 ± 0.06. All treated values are normalized to the respective sham-treated group. Data represent the mean ± S.E.M. with n ≥ 113 somata obtained from four independent experiments. Statistical significance was assessed by Two-way ANOVA with Tukey's multiple comparisons test (only significant comparisons between sham and the respective chem iLTP group are shown, $p < 0.05$*, $p < 0.01$**, $p < 0.001$***). Detailed statistical data is stated in Table 37**.** Figure adapted from (193).

4.8. Summarized Results II: TrkB-Dependent Gephyrin Clustering during Chem iLTP

By adapting Petrini and colleagues' protocol, it was possible to chemically induce long-term potentiation at inhibitory synapses in neuronal cultures transduced with TrkB WT and mutants. The potentiation was characterized by increased accumulation of total gephyrin in both density and size. Dissection of extra- and intrasynaptic gephyrin cluster density demonstrated the specificity of this protocol to postsynaptic inhibitory synapses.

With diminishing the kinase activity of the TrkB receptor either by overexpression of the TrkB KD mutant or by inhibiting the receptor with Ctx B, the described effects were abolished after chem iLTP, indicating the critical role of the receptor for gephyrin clustering during that process (for overview see Table 36). Whereas both signaling pathways were necessary for the chem iLTP-associated increase of total and synaptic gephyrin cluster density, only Shc-dependent pathways were essential for increasing cluster size. Additionally, inhibiting MAPK signaling and CaMKII indicates two important downstream mediators of the TrkB-dependent gephyrin clustering regulation during chem iLTP.

Table 36 Main summarized observations made during chem iLTP

CHEM ILTP				
Observation	**TrkB WT**	**TrkB SHC-**	**TrkB PLC-**	**TrkB KD**
Gphn cluster density	↑	-	-	-
Gphn cluster size	↑	-	↑	-
Gphn syn. cluster density	↑	-	-	-
Gphn extrasyn. cluster density	-	↑	↑	-
Observation	**TrkB WT Sham**	**TrkB WT +PD98059**	**TrkB WT +KN-62**	**TrkB WT +Ctx B**
Gphn cluster density	↑	-	-	-
Gphn cluster size	↑	-	-	-
Gphn syn. cluster density	↑	-	-	-
Gphn extrasyn. cluster density	-	-	-	-

5. Discussion

The primary aim of this study was to elucidate the molecular mechanisms by which TrkB regulates the clustering of inhibitory synapse scaffold protein gephyrin and, consequently, its impact on GABAergic synapses. To achieve this, the morphological and functional consequences of TrkB-dependent regulation of Gphn were investigated in primary hippocampal neurons expressing TrkB mutants with altered signaling properties.

The thesis addresses several aspects:

I. Targeting TrkB Signaling: Generation of Signaling-Deficient TrkB Mutants

To dissect TrkB-signaling-dependent effects on Gphn clustering, TrkB mutants with site-directed modifications in the key binding sites were generated, disrupting specific signaling cascades downstream of TrkB. These mutations allowed the dissection of TrkB catalytic activity and concomitant signaling pathways, facilitating a more precise analysis of their individual roles in Gphn regulation.

II. TrkB Pathway-Specific Effects on Gephyrin Clustering under Basal Conditions

Analysis of pre- and postsynaptic marker expression after overexpression of TrkB mutants in primary hippocampal neurons under basal conditions revealed that associated pathways selectively affected inhibitory synapses without altering the density of excitatory pre- and postsynaptic markers. Disrupting TrkB-Shc signaling increased Gphn accumulation, while reduced TrkB-PLCγ signaling decreased specifically synaptic Gphn, accompanied by a reduction in overall presynaptic terminals and α2-$GABA_A$Rs.

The investigation of potential mediators of TrkB-dependent Gphn regulation focused on mTOR and CaMKII signaling. Reduced TrkB-Shc signaling was accompanied by diminished mTOR activity as evidenced by reduced phosphorylated mTor and S6K, while a decrease in CaMKII autophosphorylation was observed in neurons with disrupted TrkB-PLCγ signaling.

III. Functional Implications of Altered TrkB signaling

Examination of calcium transients in neurons with modified TrkB signaling confirmed the histological findings by revealing the functional consequences of reduced morphological inhibitory synapses. Notably, interference with TrkB-PLCγ signaling increased the frequency of calcium peaks while reducing their amplitude, suggesting an increased excitability in these cells. In contrast, neurons expressing the SHC- or kinase-dead TrkB mutant showed no significant functional changes, indicating that specific TrkB pathways play distinct roles in synaptic functionality.

IV. TrkB Signaling Pathways in Chemically Induced iLTP

Lastly, the role of TrkB signaling in chemically induced inhibitory long-term potentiation (chem iLTP) was explored. Results indicated that TrkB catalytic activity is essential for the chem iLTP-associated increase in Gphn accumulation. Overexpression of SHC- and PLC- mutants demonstrated different roles of the associated pathways during chem iLTP: while both were necessary for increasing Gphn density, Gphn cluster enlargement was specifically dependent on TrkB-Shc signaling. Dissection of extra- and intrasynaptic cluster densities revealed the specific impact of chem iLTP on postsynaptic inhibitory synapses, highlighting the essential role of TrkB signaling on inhibitory synaptic plasticity. Additional experiments further confirmed the participation of TrkB and associated signaling pathways in chem iLTP. Inhibition of TrkB abolished the increase in both Gphn cluster density and size, highlighting TrkB's essential role in chem iLTP. Additionally, inhibiting MEK1/2 and CaMKII, protein kinases involved in TrkB signaling pathways, produced similar reductions, indicating that both MAPK/Erk1/2 pathway, as well as CaMKII activity, are critical to chem iLTP-induced changes in inhibitory synapse potentiation.

5.1. Targeting TrkB Signaling

Previous reports have implicated TrkB signaling in regulating the clustering, stabilization, and plasticity of the major inhibitory synaptic scaffolding protein Gphn (63, 73, 82, 181, 186). However, these studies report contrasting results depending on the experimental paradigm applied. To clarify TrkB-dependent mechanisms involved in regulating Gphn clustering, this study aimed to dissect the major TrkB signaling pathways. To this end, TrkB mutants were generated to individually investigate TrkB-Shc-dependent signaling, involving Ras-MAPK and Pi3K-Akt pathways, and TrkB-PLCγ-dependent signaling, which all include protein kinases known to play a role in regulating Gphn clustering (46, 53, 71, 73).

As previously described, mutation of the mouse TrkB-Shc binding site reduces the binding of the adaptor protein Shc, which in turn inhibits activation of Pi3K/Akt and Ras/MAPK signaling pathways (190). The study validated the impact of Y515F mutation on these pathways by measuring a decreased phosphorylation of Erk1/2, indicative of reduced Ras/MAPK pathway activation. Importantly, TrkB binding properties of PLCγ1 remained unaffected (152). In the current study, the Y515F mutation was transferred to the rat TrkB protein, and observations made during western blot analysis of TrkB transfected cells qualitatively replicated the consequences of signaling with TrkB mutation observed with the studies performed in mice. Consistent with prior research, the reduction in Erk phosphorylation was primarily observed in Erk1 (190, 203). Since TrkB autophosphorylation and PLCγ1 activation remained unaffected in SHC-, these results implicate that this TrkB mutant specifically impairs Shc-dependent signaling.

A similar approach was applied to the PLC- mutant. Previous reports have described that the Y816F mutation in mouse TrkB disrupts PLCγ1 binding while leaving Shc-dependent signaling intact (152). This study's observations were qualitatively reproduced, confirming that the PLC- mutant selectively impairs TrkB-PLCγ1-dependent signaling without altering autophosphorylation Shc-dependent pathways or TrkB autophosphorylation.

In contrast, the results observed with mutation of the TrkB-ATP binding site were unexpected. Previous work characterizing the effects of substituting the lysine responsible for ATP binding of TrkB with arginine found a complete loss of TrkB autophosphorylation reduced Shc binding, reduced Erk1/2 activation, and diminished PLCγ binding and phosphorylation, indicating a complete loss of TrkB catalytic function (99). These results were generally replicated in the KD mutant since the replacement of Lysin to Arginine at position 571 in the KD mutant completely abolished phosphorylation at Tyr706/707. However, the Erk1 phosphorylation reduction was less pronounced than the observations made in the SHC- mutant. This discrepancy may be partially explained by the inherent variability of Western blot analysis, which can be sensitive

to technical variations and, therefore, usually requires more replicates (204). Despite independent replication of these experiments (n = 3), the findings may only represent potential effects, as the sample size is too small for quantitative western blot analysis. Additionally, given that Ras/MAPK signaling is a shared pathway activated by multiple receptors (205, 206), basal activation of Erk1/2 in NIH3T3 cells might obscure TrkB mutant-specific effects, potentially also explaining the milder impact of the Y515F mutation observed in the SHC-mutant relative to previous reports. Furthermore, the reduction in autophosphorylated TrkB might alter the interaction with other proteins or induce secondary mechanisms that can increase Erk1/2 phosphorylation via secondary mechanisms (207).

To further characterize the specific effects of TrkB mutants on SHC- and PLCγ-dependent signaling, broader analyses including a larger sample size or high-throughput approaches, such as DigiWest analysis, to capture additional components of the signaling cascades would be beneficial (208). Despite the modest extent of the observed effects in Erk1/2 with KD in this study, the results demonstrate the successful abolishment of TrkB autophosphorylation with K571A and align with previously described observations in TrkB signaling interference. Together with the extensive findings from prior research, these TrkB mutants provide valuable tools for specifically targeting TrkB signaling and dissecting pathway-specific mechanisms in relevant cellular contexts.

5.2. Analysis of Synaptic Marker Expression: Differential Effects of TrkB Mutants on Gephyrin Clustering

Analysis of pre- and postsynaptic marker expression in primary hippocampal neurons in this study revealed that TrkB mutations selectively impact inhibitory synapses. The results strongly support the role of TrkB signaling in regulating Gphn clustering, with altered signaling leading to dysregulated Gphn accumulation. Additionally, they provided insights into the specific pathway-dependent mechanisms involved in this regulation.

TrkB-Shc Signaling

The increase in Gphn accumulation observed with disrupted TrkB-Shc signaling implies that the cognate signaling pathways are involved in limiting Gphn clustering under baseline conditions. Previous studies suggest potential mechanisms mediating this regulatory role, such as through mTOR-Gphn association (73, 149). Wuchter et al. showed that Bdnf-induced mTOR activation reduces the association between mTOR and Gphn and suggested this as a potential mechanism promoting its clustering. Both TrkB-Shc-dependent signaling pathways, MAPK/Erk1/2 and Pi3K/Akt, converge on Tsc1/2, thereby facilitating mTOR activity, which may, in turn, regulate Gphn release from mTOR (142, 143). While the current study observed Gphn accumulation in response to diminished TrkB-Shc signaling, it also observed decreased activation of mTOR signaling, as suggested by reduced phosphorylation of mTOR and its substrate S6K. Contradicting an mTOR-activation-dependent increase in Gphn clustering, this discrepancy raises questions about other regulatory factors that influence Gphn clustering.

Several studies, including the aforementioned work, point towards another potential mechanism that might account for the observed results of diminished TrkB-Shc signaling. This involves the interaction of Gphn with protein kinases associated with Ras/MAPK and Pi3K/Akt signaling pathways. However, with contradicting reports. Wuchter et al. reported the MAPK-signaling-dependent facilitation of Gphn clustering (73). They identified several protein kinases associated with Ras/MAPK-signaling as regulators for Gphn clustering, including MEK2. Downregulation of MEK2 signaling by transfection of primary neurons, either with a dnMEK2 or siMEK2 construct, decreased Gphn cluster densities and this effect was partially restored by cotransfection of a caMEK2 transgene (73). In contrast, Tyagarajan et al. demonstrated that Gphn cluster size and density are limited by the phosphorylation of the downstream effector sites Ser 268 (by Erk1/2) and Ser270 (by Gsk3β) in a calpain-dependent manner (53, 75). With point mutation of Gphn at Ser 268, they observed an increase in Gphn clusters, demonstrating Erk1/2 as responsible for limiting Gphn cluster size (53). Furthermore, they showed the bidirectional role of Erk1/2-dependent regulation of Gphn clustering since short-term blockade (3 h) of Erk1/2 decreased Gphn cluster density. At the same time, the long-term

pharmacological block (overnight) of Erk1/2 signaling increased the size and density of eGFP-Gphn clusters (53). Since both studies obtained these results under basal conditions and without any further stimulation of the primary neurons, the different results might be due to differential dynamics of inhibition in a time-dependent manner. Wuchter et al. analyzed Gphn clustering 7d after transfection of primary neurons with dnMEK2 and siMEK2 (73). Since Ras/MAPK-signaling is an important pathway involved in many different cellular processes (see 1.3.1), the constant downregulation allows additional mechanisms to interfere, resulting in the observed phenotype.

Consistent with the reports from Tyagarajan and colleagues, the here-induced reduction of Erk1/2 signaling with TrkB-Shc signaling interference appears to facilitate Gphn accumulation, likely due to diminished TrkB-Erk1/2 dependent phosphorylation (53).

However, given the complex regulatory network of PTMs governing Gphn, it cannot be excluded that other PTMs, induced by other protein kinases or by SUMOylation, contribute to the observed phenotype. For example, CDK5 increases Gphn clustering upon phosphorylation of Ser270 (72, 74). Furthermore, Bdnf has been shown to influence the relocation of nuclear-enriched SUMO proteins through Erk1/2 signaling, which in turn influenced SUMOylation of Gphn (209).

TrkB-PLCγ signaling

Interestingly, the morphological implications observed with the reduction of TrkB-dependent PLCγ signaling differed from those with reduced TrkB-Shc-dependent signaling disruption. Unlike the broader impact on total Gphn clusters, diminished TrkB-PLCγ signaling specifically affected Gphn clusters that were in close apposition with VGat-positive presynaptic terminals, representing inhibitory synapses at the somata of affected neurons. This aligns with a previous study using mice carrying the TrkB Y816F mutation, which observed reductions in presynaptic GAD67 and postsynaptic Gphn, linking Ca^{2+}-regulated pathways to GABAergic synapse formation (186). This hypothesis is supported by the role of TrkB-PLCγ in the IP_3-dependent release of Ca^{2+}, with mutation of the corresponding adaptation site demonstrating reduced CaMKIIα activity (125, 210). Given that Gphn is a direct substrate of CaMKII, and phosphorylation at Ser305 is critical for its trafficking to synaptic sites, together with the here observed reduction in synaptic Gphn clusters with diminished PLCγ and CaMKIIα activity, strongly suggests that TrkB regulates Gphn clustering at synaptic sites through a CaMKII-dependent mechanism (46). CaMKII-dependent Gphn clustering has been observed in response to excitatory activity and during iLTP in a calcium-dependent manner (46, 48, 71). The implications of diminished TrkB-PLCγ signaling in an activity-dependent context will be further discussed in section 5.4. Yet under basal conditions, the decreased density of inhibitory synapses coinciding with decreased autophosphorylated CaMKIIα levels indicates that

impaired CaMKII signaling may underlie the observed deficits in synaptic gephyrin clustering with diminished TrkB-PLCγ signaling.

Since Gphn clusters $GABA_AR$ receptors, it is no surprise that the knockout of Gphn is disrupting the clustering of (at least) α2- and α3-containing $GABA_AR$ clusters, without affecting their overall protein levels (62). Although an overall reduction of α2 subunits was detected with reduced TrkB-PLCγ signaling, the density of α2 subunits colocalized with gephyrin remained unchanged. This finding is consistent with previous studies reporting receptor-Gphn interactions to also occur outside of inhibitory synapses in primary neurons (211, 212). However, since TrkB-PLCγ signaling-dependent effects on gephyrin clustering observed in the current study were specific to synaptic clusters and did not affect the total gephyrin cluster density, extrasynaptic clusters may mask potential reductions in synaptic Gphn-$GABA_AR$ clusters. Notably, next to Gphn being a substrate of CaMKII, $GABA_AR$ trafficking is also regulated by CaMKII, which phosphorylates the $GABA_AR$ β3 subunit at serine 383 (Ser383), therefore potentially contributing to the observed reduction in $GABA_AR$ clusters independently of Gphn (45, 48). To determine whether TrkB-PLCγ-dependent synapse loss affects synaptic $GABA_ARs$ clustering and to investigate the role in CaMKII, further experimental investigations are warranted and should include an additional appropriate presynaptic marker, such as VGat or Synapsin, to distinguish between extra- and intrasynaptic $GABA_AR$/Gphn clusters.

TrkB Catalytic Activity

The TrkB point mutants in this study revealed the specific contributions of individual signaling pathways to TrkB-dependent regulation of Gphn clustering, while the KD mutant highlights the impact of diminished TrkB catalytic activity. Neurons expressing the KD mutant exhibited combined phenotypes like those of SHC- or PLC- mutants. Diminishing TrkB catalytic activity resulted in increased Gphn cluster size, consistent with impaired Shc-dependent signaling, while reducing the density of synaptic clusters, as observed with diminished TrkB-PLCγ signaling. However, unlike selectively diminishing PLCγ signaling, the KD mutant did not affect presynaptic clusters or $GABA_ARs$ density, suggesting that, while selectively disrupting the postsynaptic scaffold at synaptic sites, it does not eliminate complete inhibitory synapses. This suggests additional mechanisms interfering here, likely resulting from the combined signaling pathway loss, alongside the absence of TrkB catalytic activity. This deficiency may, in turn, alter additional interactions with other membrane proteins, including the TrkB isoforms (213), NMDARs (214), metabotropic glutamate receptor 2 (mGlu2) (215) or p75Ntr (114). The complexity of these interdependent mechanisms prevents a precise conclusion about the molecular mechanisms underlying the here presented findings yet underscores the importance of TrkB catalytic activity in regulating Gphn clustering.

Overall, overexpression of TrkB mutants in dissociated neurons supports current literature by highlighting the crucial role of TrkB signaling in regulating Gphn clustering and revealing pathway-specific effects, whereas Shc-dependent signaling appears essential for limiting Gphn clustering, likely through Erk1/2-Gphn interaction, PLCγ-dependent signaling governs the localization of Gphn at synaptic sites, potentially involving CaMKII activation. These findings align with previous findings *in vivo*, reporting a loss of inhibitory synapses with diminished TrkB signaling, further validating the relevance of the here used *in vitro* model (82). However, as already indicated, the precise mechanisms by which TrkB-Shc and PLCγ-signaling pathways regulate Gphn clustering require careful interpretation, and further research is needed.

5.3. Functional Consequences of Altered TrkB-dependent Gphn Clustering

To evaluate whether morphologically changes in synaptic are reflected by altered neuronal activity, calcium imaging was employed in transduced cultures, as calcium transients reliably reflect neuronal activity and signaling dynamics (199, 216). Disrupted TrkB-PLCγ signaling displayed distinct alterations in calcium transients, characterized by increased calcium transient frequency, reduced average peak amplitude, and a concomitant reduction in the AUC. In contrast, neurons with diminished TrkB-Shc signaling or autophosphorylation showed no significant alterations in calcium dynamics.

Deficits in synaptic stability or plasticity can result in an imbalance in E/I transmission, a well-documented contributor to neuropsychiatric and neurodevelopmental disorders (164, 166-169). The relative densities of excitatory and inhibitory synapses, as well as their synaptic strength can determine the E/I ratio (217). The size and molecular density of Gphn clusters strongly correlate with the density of $GABA_A$Rs or GlyRs, which in turn relates to synaptic strength (51, 53, 218). In the current study, disruption of TrkB-PLCγ signaling specifically altered the number of inhibitory synapses without affecting excitatory synapses at the soma of modified neurons, resulting in an imbalance in the excitatory and inhibitory synapses ratio that consequently increased excitatory drive, likely due to insufficient inhibitory signaling (219, 220). In fact, the disruption of Gphn has been shown to decrease the amplitude and frequency of spontaneous and miniature GABAergic synaptic currents *in vitro* and *in vivo* (218, 221, 222). Consistently, the reduction in inhibitory synapses observed with diminished TrkB-PLCγ signaling was associated with increased somatic calcium transient frequency, suggesting diminished inhibitory input at the cell bodies, resulting in increased neuronal excitability.

The decreased calcium transient amplitude in these neurons may result from frequent calcium fluctuations, which deplete intracellular calcium stores and consequently reduce the total calcium available for subsequent transients. Altered TrkB-PLCγ signaling might also affect calcium replenishment dynamics through altered interactions with transient receptor potential channels (TRCPs), which are involved in calcium refilling following store depletion (223). Additionally, disrupted TrkB-PLCγ-IP_3 signaling may also influence calcium dynamics, further contributing to the observed reduction in calcium transient amplitude (153, 224).

Whether the decrease in calcium concentration, along with reduced phosphorylation of CaMKII (as discussed in 5.2), is the cause or consequence of TrkB-PLCγ-dependent loss of inhibitory synapses remains elusive. Despite the decrease in inhibitory synapse density also observed in KD overexpressing neurons, no measurable functional consequences were detected, as shown with neurons with diminished TrkB-PLCγ signaling. Given that KD neurons exhibited

larger Gphn clusters – which can likely correlate with increased $GABA_A$Rs and, therefore, inhibitory strength (51) – this enlargement may counterbalance the effects of reduced synapse density. However, a separate analysis of intra- and extrasynaptic Gphn cluster sizes is needed to confirm this hypothesis. The similar increase in Gphn cluster size observed in SHC-expressing neurons, even in the absence of changes to synapse density, suggests that increased Gphn accumulation is more likely due to disrupted regulatory processes than a compensatory response to heightened excitatory drive. Additionally, the fact that calcium transients remained stable in KD neurons, despite the observed reduction in synapse density, further supports the idea that the decreased amplitude in calcium transients observed with diminished TrkB-PLCγ arises from increased excitability rather than a direct PLCγ influence on internal calcium fluctuations. Nevertheless, this does not rule out an initial reduction in inhibitory synapses as a consequence of impaired TrkB-PLCγ signaling.

The obtained results in this study emphasize the functional importance of TrkB-PLCγ signaling in regulating Gphn clustering, underscoring the crucial role of TrkB not only in inhibitory synapse organization but also in homeostatic maintenance of E/I balance. TrkB is known for its critical role in the delivery of excitatory scaffold proteins to postsynaptic sites (225). Although no changes were detected in somatic excitatory synapses, alterations in excitatory synaptic strength or in the E/I ratio at other compartments, such as distal dendrites, where the larger proportion of excitatory synapses is located– cannot be excluded in this study (226, 227). Both factors might contribute to the observed alterations in somatic calcium signaling, since the reduction of inhibitory synapses at dendrites can also result in hyperexcitability (228). However, the results demonstrate the involvement of TrkB in the recruitment of inhibitory scaffolding proteins, potentially through a PLCγ-Ca^{2+}-CAMKII-dependent mechanism. This interpretation is supported by the observation made in mice carrying a mutation in the TrkB-PLCγ binding site, which has documented striking deficits in Bdnf-dependent CaMKIV signaling and GABAergic stabilization (186).

To elucidate these deficits, future studies should include detailed electrophysiological recordings of postsynaptic currents, along with measurements of miniature excitatory and inhibitory postsynaptic potentials (PSPs) to assess synaptic strength. Additionally, calculating frequency ratios between excitatory and inhibitory PSPs could help to determine shifts in E/I balance more precisely (229). Combining these approaches with pharmacological manipulation targeting glutamate receptors (e.g., MK-801 and CNQX) or calcium channels of the ER (e.g., 2-APB and ryanodine) could potentially offer further insights into the underlying mechanisms driving the observed changes in synaptic and calcium dynamics.

5.4. TrkB-Dependent Gephyrin Regulation during Inhibitory Synapse Plasticity: A Mechanism of Homeostatic Regulation?

Increases in intracellular calcium and concomitant activation of Ca^{2+}-dependent proteins such as CaMKII are essential for activity-dependent LTP of synapses (230). The involvement of Ca^{2+} and CaMKII in TrkB-dependent gephyrin regulation under basal conditions suggests that TrkB signaling may similarly regulate Gphn in an activity-dependent manner, which has been already shown for eLTP (152, 210, 231).

To locally restrict neuronal activity and counterbalance rising excitation levels, neurons can activate homeostatic heterosynaptic processes (24, 46, 232). These include postsynaptic receptor lateral diffusion, allowing surface receptors to rapidly exchange between synaptic and extrasynaptic domains, a process which has been shown to be strongly influenced by Gphn (15, 19, 25). Chemical induction of iLTP in neurons overexpressing TrkB mutants demonstrated a significant role of TrkB in increasing Gphn accumulation, thereby supporting inhibitory synapse potentiation (43, 46, 48, 71). Furthermore, the mutation of TrkB revealed that its catalytic activity, as well as both Shc and PLCγ-dependent signaling pathways, are critical for Gphn accumulation during iLTP.

Chem iLTP through moderate activation of NMDARs mimics the modest raise in calcium concentration occurring in neurons subsequent to eLTP (46, 71), during eLTD (47, 48) or at regions distant from the activated synapse (32). Thus, it serves as a model for homeostatic regulation inhibitory synaptic strength subsequent to neuronal activation (43, 51, 233). After inhibition of TrkB catalytic activity, either by overexpression of the kinase-dead TrkB mutant or the pharmacological inhibition of TrkB activity by Cyclotraxin B, neurons were unable to increase overall Gphn cluster size and density, especially affecting synaptic gephyrin cluster density in response to chem iLTP. This aligns with previous studies, that already implicated a role for the TrkB ligand Bdnf in activity-dependent scaling of GABAergic synaptic strength (188, 234), suggesting now that TrkB-mediated regulation of inhibitory synaptic strength is, at least partially, mediated by the regulation of the scaffold protein gephyrin.

TrkB-PLCγ Signaling in iLTP

Previous studies have demonstrated that iLTP involves the recruitment of Gphn from extra- to intrasynaptic sites through CaMKII-mediated phosphorylation (46, 48). The presented results extend these findings by identifying TrkB as a potential upstream regulator, showing that TrkB-PLCγ signaling is essential for iLTP associated with Gphn accumulation and the increased inhibitory synapse density. A malfunction of Gphn recruitment from extra- to intrasynaptic with aberrant TrkB-PLCγ signaling might also explain the increased accumulation of Gphn clusters at extrasynaptic sites.

Moreover, the results suggest that these processes are mediated through a PLCγ-Ca^{2+}-CaMKII regulation since pharmacological inhibition of CaMKII also prevented the increase in Gphn clustering, consistent with previous reports, showing that CaMKII and PKA-mediated phosphorylation of Gphn at Ser305 and Ser 303 necessary for activity-dependent increases in Gphn cluster size and dynamics (46, 71). This suggests that calcium signaling from nearby excitatory synapses may activate CaMKII (and PKA) at inhibitory sites to enhance gephyrin clustering (163). While these findings imply a role for TrkB-PLCγ and CaMKII signaling in iLTP, a direct mechanistic link between TrkB-PLCγ and CaMKII remains to be elucidated and represents an important direction for further research. In the context of eLTP, autocrine Bdnf signaling has been identified as one mechanism for TrkB activation during spine potentiation (231). Harward and colleagues demonstrated that postsynaptic Bdnf release from stimulated dendritic spines depends on NMDAR and CaMKII activity, triggering subsequent TrkB activation that requires kinase activity and phosphorylation at Y816. Furthermore, TrkB activation was observed to occur rapidly within ~1-2 min, with TrkB activation gradually spreading to adjacent regions after 30-60 s (231). Together with the findings presented in this study, it is compelling to propose a similar mechanism responsible for TrkB-dependent homeostatic regulation at inhibitory synapses. However, further research is needed to confirm this hypothesis since it remains unclear whether moderate NMDAR stimulation alone is sufficient to induce postsynaptic Bdnf release to the extent required for effective TrkB activation.

TrkB-Shc Signaling in iLTP

Notably, this study identified TrkB Shc signaling, in addition to TrkB-PLCγ and CaMKII pathways, as a contributor to chem iLTP-induced Gphn accumulation. While TrkB-Shc signaling has been linked to limit Gphn clustering under basal conditions (discussed in 5.2) and excitatory synapse regulation (see 5.2, (139)), its involvement in activity-dependent iLTP is still under debate (71, 152, 186, 231, 235). This study, however, provides initial evidence that TrkB-Shc signaling may indeed contribute to iLTP at inhibitory synapses, likely involving Erk1/2-signaling, as suggested by MEK1 inhibition, which obtained similar results to chem iLTP with TrkB-Shc, except in the context of extrasynaptic gephyrin clustering.

Previous studies have linked Erk1/2 to activity-dependent regulation of extrasynaptic $GABA_AR$ mobility independently of Gphn. For instance, Gphn mutants, insensitive to phosphorylation at Ser268, did not show an altered structural synaptic adaptation to chronic activation (71). Regarding Gphn itself, activity-induced changes in the recruitment of Gphn to synapses relied on the complex interplay of PKA, CaMKIIα, and Gsk3β phosphorylation of Gphn (46, 48, 71).

The current study extends this understanding by demonstrating a crucial role for the Erk1/2-pathway in facilitating gephyrin scaffold organization during calcium-dependent inhibitory

synapse potentiation. Unlike previous findings by Battaglia et al., it supports the notion of Erk1/2 playing a role in regulating extrasynaptic Gphn clusters. Specifically, impaired TrkB-Shc signaling resulted in the accumulation of extrasynaptic Gphn clusters. Although resembling the phenotype observed with PLC- overexpression during chem iLTP, the possibility of additional, secondary mechanisms contributing to this outcome cannot be excluded.

Furthermore, variations in experimental paradigms may account for the contrasting results observed with Erk1/2-dependent Gphn clustering during iLTP. While the current study employed a short-term drug application, mimicking specifically the moderate calcium concentration during homeostatic processes at inhibitory synapses, Battaglia et al., used the potassium channel blocker 4-aminopyridine (4-AP), inducing prolonged activity over several hours, which allows the induction for various additional cellular adaptations (71). In the current study, both chronic reduction of TrkB-dependent Erk1/2 signaling, as well as acute inhibition of Erk1/2 signaling abolished iLTP-driven Gphn accumulation, emphasizing a contribution of (TrkB-) Erk1/2 signaling in the homeostatic regulation of activity-dependent Gphn accumulation.

This mechanism observed under chem iLTP contradicts Shc-dependent Gphn phosphorylation under baseline conditions, where Shc-dependent signaling limits Gphn accumulation. However, the supporting function of Erk1/2-signaling in Gphn clustering is in line with observations made during acute Bdnf stimulation of primary neurons, which results in an increase in Gphn clustering (54, 82). Together, the results point towards a TrkB-Erk1/2-dependent mechanism during Bdnf- and iLTP-associated Gphn clustering that is contrary to the direct Gphn phosphorylation, which usually results in calpain-dependent Gphn degradation (53). The MAPK cascade integrates numerous calcium-dependent signaling events across the cytoplasm and nucleus, playing an essential role in synaptic plasticity at excitatory synapses, particularly LTP, including NMDA-dependent and independent forms (140, 236, 237). On the one hand, it phosphorylates several synaptic proteins, thereby regulating, for example, the stabilization of scaffold protein Psd95 (238) or reducing the membrane-surface expression of the voltage-dependent K+-channel subunit Kv4.2, which results in increased excitability of the soma during eLTP (239, 240). On the other hand, activity-dependent nuclear transport of Erk1/2 targets transcription factors such as CREB and Elk1, thereby regulating gene expression during plasticity (140, 241). However, given the short timescale of the here used chem iLTP protocol, the present study rather supports a fast-acting mechanism underlying the rapid increase in Gphn clustering, such as, for instance, in the mTOR-dependent Gphn release described by Wuchter et al. (54). The mTOR-Gphn results obtained in this study were performed in the presence of acute Bdnf stimulation (54). Since Bdnf is released activity-dependent, the context in which mTOR-Gphn association has been studied could reflect a

rather activated environment (109, 110). This would not only explain why there was no involvement of mTOR signaling observed under basal conditions (see 5.2) but might represent a potential mechanism underlying the opposing effects of TrkB-Shc-dependent Gphn clustering. The reduction of Shc-signaling might result in a decreased mTOR activation and subsequently in diminished Gphn release, needed for the activity-dependent increase in Gphn clustering. Further studies are necessary to validate this hypothesis regarding mTOR activation and its association with Gphn in an activity-dependent context. Additionally, it is important to compare the cellular mechanisms involved in activity-dependent iLTP and acute Bdnf stimulation.

While TrkB is involved in multiple processes, additional mechanisms might also contribute to the observed phenotypes during NMDAR-dependent iLTP cannot be excluded, given the interaction of TrkB via fyn with NDMARs, thereby increasing their open probability or the interaction with PSD95, which facilitates TrkB signaling (115, 152, 214, 242).

Collectively several studies point to converging glutamatergic and GABAergic signaling pathways that allow activity-dependent receptor coordination for regulation and tuning of E/I balance through calcium/CaMKII-dependent mechanisms (24, 49). The presented study identified TrkB as an upstream modulator of postsynaptic, calcium-dependent iLTP by facilitating Gphn accumulation, resulting in the potentiation of inhibitory synapses. Since TrkB is mostly known for its crucial role in eLTP, this suggests a mechanism by which neuronal activity can exert homeostatic control over inhibitory synapses, potentially influencing intrinsic excitability in response to changes in activity

5.5. Conclusion and Future Perspectives

The findings presented in the current study underscore TrkB's pivotal role as a crucial regulator of GABAergic synapses through its modulation of Gphn clustering. By delineating the involved signaling pathways, the study highlights how TrkB contributes to the regulation of Gphn under basal conditions and during inhibitory synaptic plasticity, therefore expanding the view of TrkB's synaptic role.

Under basal conditions, TrkB-Shc signaling modulates inhibitory strength by fine-tuning gephyrin clustering through direct phosphorylation. However, during homeostatic regulation of GABAergic transmission, TrkB-Shc likely facilitates gephyrin accumulation through alternative mechanisms, such as mTOR signaling, rather than direct phosphorylation (see Figure 26). Given the context- and time-dependent effects of Erk1/2-mediated Gphn regulation, future studies should explore the interplay between activity and association of mTOR with Gphn following chem iLTP to elucidate its role in Erk-dependent inhibitory plasticity.

The findings also highlight the distinct role of PLCγ-dependent signaling in primary hippocampal neurons, where it facilitates the clustering of Gphn at inhibitory synapses involving CaMKII under both basal conditions and during synaptic plasticity, which contributes to the maintenance of the neuronal E/I balance. Investigating the direct mechanistic link between TrkB-PLCγ and CaMKII presents a promising avenue for future research. Furthermore, co-localization studies incorporating $GABA_ARs$, gephyrin, and presynaptic markers would provide deeper insights into how TrkB-PLCγ signaling shapes the morphology and function of GABAergic synapses.

Notably, TrkB's dual role in calcium-dependent eLTP and now iLTP positions It as a potential upstream cross-talking mediator of activity-dependent homeostatic heterosynaptic plasticity, crucial for maintaining and adjusting E/I balance. However, the precise molecular mechanisms underlying this crosstalk remain unclear. Future experiments involving the scavenging of extracellular Bdnf during chem iLTP could elucidate the role of Bdnf-TrkB signaling in these processes.

Most importantly, given the various important neuronal processes TrkB is involved in, a comprehensive transcriptional and translational analysis is needed to gain valuable insight into changes in protein synthesis related to altered TrkB signaling. Further, given the complex interplay of signaling pathways, high-throughput phospho-proteomics would provide important insight into the broader state of signaling induction beyond the primary TrkB pathways, along with a comprehensive analysis of the often-interrelated PTMs to elucidate the mechanistic adaptability of GABAergic inhibition in a TrkB related manner.

In-depth electrophysiological characterization, including detailed recordings of postsynaptic currents and measurements of miniature excitatory and inhibitory postsynaptic potentials, is needed to assess changes in synaptic strength. This would be beneficial in characterizing the functional consequences, allowing to assess changes in synaptic strength, neuronal excitability, and network activity in both inhibitory and excitatory synapses.

Although the here-developed TrkB mutants provide useful tools for dissecting pathway-specific mechanisms, their application during early neuronal development cannot exclude a potential developmental impact on the phenotypes observed. Furthermore, primary neuron cultures lack the three-dimensional, complex, and layer-specific environment of *in vivo* models. Therefore, using these tools in vivo, particularly in an adolescent or adult system, would be highly interesting in assessing the consequences of altered TrkB without including early developmental confounds. This approach could reveal whether *in vivo* results align with primary neuron observations and elucidate how disrupted iLTP affects E/I balance in different brain areas and how this is translated into behavior.

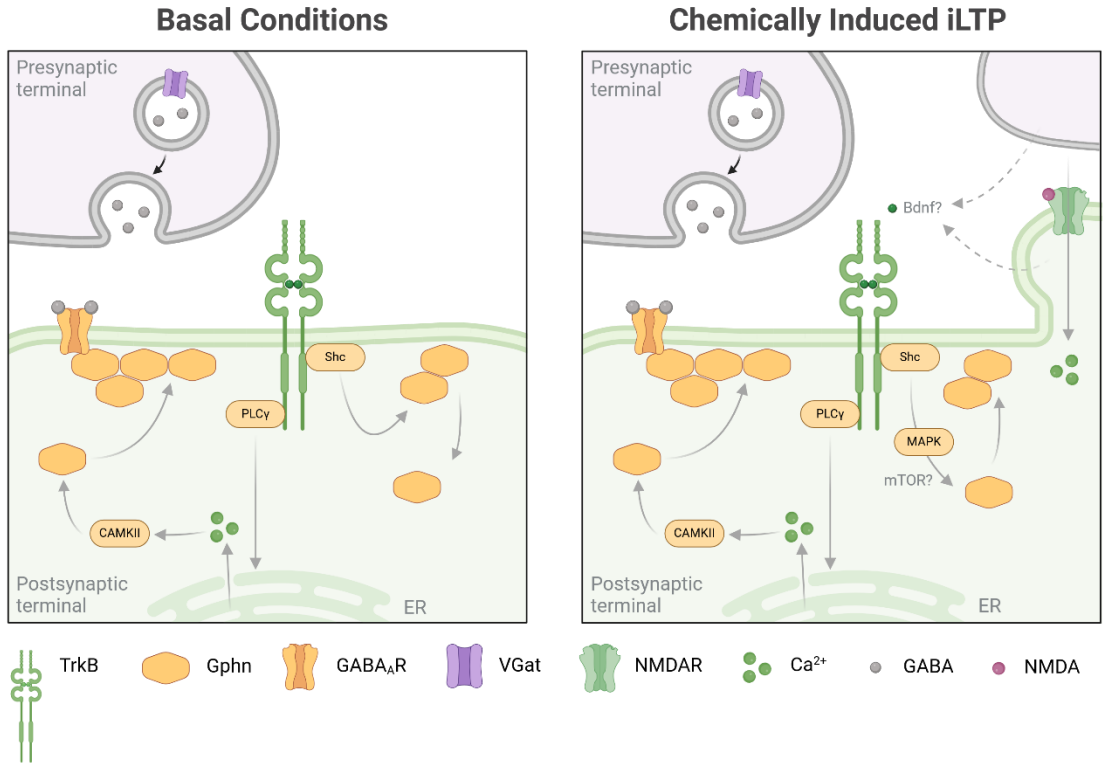

Figure 26: Working Hypothesis. During basal conditions, TrkB regulates Gphn clustering by limiting its size and density through Shc-dependent signaling. Signaling of PLCγ regulates Gphn clustering at synaptic sites through CaMKII, therefore maintaining GABAergic synapse stabilization. During calcium-dependent iLTP, trafficking of Gphn to inhibitory synapses is still TrkB-PLCγ-CaMKII dependent. In contrast, Shc-dependent signaling facilitates Gphn clustering through MAPK/Erk1/2 signaling, which could potentially involve mTOR signaling. However, the role of mTOR and Bdnf release during chem iLTP remains to be elucidated in future studies.

6. References

1. Herculano-Houzel S. The human brain in numbers: a linearly scaled-up primate brain. Front Hum Neurosci. 2009;3:31.
2. Sudhof TC. The cell biology of synapse formation. J Cell Biol. 2021;220(7).
3. Silbereis JC, Pochareddy S, Zhu Y, Li M, Sestan N. The Cellular and Molecular Landscapes of the Developing Human Central Nervous System. Neuron. 2016;89(2):248-68.
4. Connors BW, Long MA. Electrical synapses in the mammalian brain. Annu Rev Neurosci. 2004;27:393-418.
5. Hammond C, Esclapez M. The chemical synapses. Cellular and Molecular Neurophysiology:. 2015:121-44.
6. Halassa MM, Fellin T, Haydon PG. The tripartite synapse: roles for gliotransmission in health and disease. Trends Mol Med. 2007;13(2):54-63.
7. Berry KP, Nedivi E. Spine Dynamics: Are They All the Same? Neuron. 2017;96(1):43-55.
8. Geiger JR, Melcher T, Koh DS, Sakmann B, Seeburg PH, Jonas P, et al. Relative abundance of subunit mRNAs determines gating and Ca2+ permeability of AMPA receptors in principal neurons and interneurons in rat CNS. Neuron. 1995;15(1):193-204.
9. Hanada T. Ionotropic Glutamate Receptors in Epilepsy: A Review Focusing on AMPA and NMDA Receptors. Biomolecules. 2020;10(3).
10. Paoletti P. Molecular basis of NMDA receptor functional diversity. Eur J Neurosci. 2011;33(8):1351-65.
11. Keith D, El-Husseini A. Excitation Control: Balancing PSD-95 Function at the Synapse. Front Mol Neurosci. 2008;1:4.
12. Lee HJ, Zheng JJ. PDZ domains and their binding partners: structure, specificity, and modification. Cell Commun Signal. 2010;8:8.
13. Buddhala C, Hsu CC, Wu JY. A novel mechanism for GABA synthesis and packaging into synaptic vesicles. Neurochem Int. 2009;55(1-3):9-12.
14. Groeneweg FL, Trattnig C, Kuhse J, Nawrotzki RA, Kirsch J. Gephyrin: a key regulatory protein of inhibitory synapses and beyond. Histochem Cell Biol. 2018;150(5):489-508.
15. Kasaragod VB, Schindelin H. Structure of Heteropentameric GABA(A) Receptors and Receptor-Anchoring Properties of Gephyrin. Front Mol Neurosci. 2019;12:191.
16. Fritschy JM, Harvey RJ, Schwarz G. Gephyrin: where do we stand, where do we go? Trends Neurosci. 2008;31(5):257-64.
17. Zhou L, Kiss E, Demmig R, Kirsch J, Nawrotzki RA, Kuhse J. Binding of gephyrin to microtubules is regulated by its phosphorylation at Ser270. Histochem Cell Biol. 2021;156(1):5-18.
18. Pizzarelli R, Griguoli M, Zacchi P, Petrini EM, Barberis A, Cattaneo A, et al. Tuning GABAergic Inhibition: Gephyrin Molecular Organization and Functions. Neuroscience. 2020;439:125-36.
19. Choquet D, Triller A. The dynamic synapse. Neuron. 2013;80(3):691-703.
20. Abraham WC, Jones OD, Glanzman DL. Is plasticity of synapses the mechanism of long-term memory storage? NPJ Sci Learn. 2019;4:9.
21. Schmidt MV, Abraham WC, Maroun M, Stork O, Richter-Levin G. Stress-induced metaplasticity: from synapses to behavior. Neuroscience. 2013;250:112-20.
22. Citri A, Malenka RC. Synaptic plasticity: multiple forms, functions, and mechanisms. Neuropsychopharmacology. 2008;33(1):18-41.
23. Galanis C, Vlachos A. Hebbian and Homeostatic Synaptic Plasticity-Do Alterations of One Reflect Enhancement of the Other? Front Cell Neurosci. 2020;14:50.
24. Chapman CA, Nuwer JL, Jacob TC. The Yin and Yang of GABAergic and Glutamatergic Synaptic Plasticity: Opposites in Balance by Crosstalking Mechanisms. Front Synaptic Neurosci. 2022;14:911020.
25. Petrini EM, Barberis A. Diffusion dynamics of synaptic molecules during inhibitory postsynaptic plasticity. Front Cell Neurosci. 2014;8:300.
26. Makino H, Malinow R. AMPA receptor incorporation into synapses during LTP: the role of lateral movement and exocytosis. Neuron. 2009;64(3):381-90.

27. Turrigiano GG, Nelson SB. Homeostatic plasticity in the developing nervous system. Nat Rev Neurosci. 2004;5(2):97-107.
28. Udakis M, Pedrosa V, Chamberlain SEL, Clopath C, Mellor JR. Interneuron-specific plasticity at parvalbumin and somatostatin inhibitory synapses onto CA1 pyramidal neurons shapes hippocampal output. Nat Commun. 2020;11(1):4395.
29. Castillo PE, Chiu CQ, Carroll RC. Long-term plasticity at inhibitory synapses. Curr Opin Neurobiol. 2011;21(2):328-38.
30. Malenka RC, Bear MF. LTP and LTD: an embarrassment of riches. Neuron. 2004;44(1):5-21.
31. Chiu CQ, Barberis A, Higley MJ. Preserving the balance: diverse forms of long-term GABAergic synaptic plasticity. Nat Rev Neurosci. 2019;20(5):272-81.
32. Ravasenga T, Ruben M, Regio V, Polenghi A, Petrini EM, Barberis A. Spatial regulation of coordinated excitatory and inhibitory synaptic plasticity at dendritic synapses. Cell Rep. 2022;38(6):110347.
33. Tong R, Chater TE, Emptage NJ, Goda Y. Heterosynaptic cross-talk of pre- and postsynaptic strengths along segments of dendrites. Cell Rep. 2021;34(4):108693.
34. Jenks KR, Tsimring K, Ip JPK, Zepeda JC, Sur M. Heterosynaptic Plasticity and the Experience-Dependent Refinement of Developing Neuronal Circuits. Front Neural Circuits. 2021;15:803401.
35. Wang Q, Yin P, Yu B, Zhao Z, Richter-Levin G, Yu L, et al. Down-regulation of dorsal striatal alphaCaMKII causes striatum-related cognitive and synaptic disorders. Exp Neurol. 2017;298(Pt A):112-21.
36. Yang SN, Tang YG, Zucker RS. Selective induction of LTP and LTD by postsynaptic [Ca2+]i elevation. J Neurophysiol. 1999;81(2):781-7.
37. Yasuda R, Hayashi Y, Hell JW. CaMKII: a central molecular organizer of synaptic plasticity, learning and memory. Nat Rev Neurosci. 2022;23(11):666-82.
38. Lisman J, Schulman H, Cline H. The molecular basis of CaMKII function in synaptic and behavioural memory. Nat Rev Neurosci. 2002;3(3):175-90.
39. Lisman J, Yasuda R, Raghavachari S. Mechanisms of CaMKII action in long-term potentiation. Nat Rev Neurosci. 2012;13(3):169-82.
40. Zeng Y, Zhao D, Xie CW. Neurotrophins enhance CaMKII activity and rescue amyloid-beta-induced deficits in hippocampal synaptic plasticity. J Alzheimers Dis. 2010;21(3):823-31.
41. Morales-Weil K, Moreno M, Ahumada J, Arriagada J, Fuentealba P, Bonansco C, et al. Priming of GABAergic Long-term Potentiation by Muscarinic Receptors. Neuroscience. 2020;428:242-51.
42. Marsden KC, Beattie JB, Friedenthal J, Carroll RC. NMDA receptor activation potentiates inhibitory transmission through GABA receptor-associated protein-dependent exocytosis of GABA(A) receptors. J Neurosci. 2007;27(52):14326-37.
43. Bannai H, Niwa F, Sherwood MW, Shrivastava AN, Arizono M, Miyamoto A, et al. Bidirectional Control of Synaptic GABAAR Clustering by Glutamate and Calcium. Cell Rep. 2015;13(12):2768-80.
44. Saliba RS, Kretschmannova K, Moss SJ. Activity-dependent phosphorylation of GABAA receptors regulates receptor insertion and tonic current. EMBO J. 2012;31(13):2937-51.
45. Houston CM, He Q, Smart TG. CaMKII phosphorylation of the GABA(A) receptor: receptor subtype- and synapse-specific modulation. J Physiol. 2009;587(Pt 10):2115-25.
46. Flores CE, Nikonenko I, Mendez P, Fritschy JM, Tyagarajan SK, Muller D. Activity-dependent inhibitory synapse remodeling through gephyrin phosphorylation. Proc Natl Acad Sci U S A. 2015;112(1):E65-72.
47. Marsden KC, Shemesh A, Bayer KU, Carroll RC. Selective translocation of Ca2+/calmodulin protein kinase IIalpha (CaMKIIalpha) to inhibitory synapses. Proc Natl Acad Sci U S A. 2010;107(47):20559-64.
48. Petrini EM, Ravasenga T, Hausrat TJ, Iurilli G, Olcese U, Racine V, et al. Synaptic recruitment of gephyrin regulates surface GABAA receptor dynamics for the expression of inhibitory LTP. Nat Commun. 2014;5:3921.
49. Cook SG, Buonarati OR, Coultrap SJ, Bayer KU. CaMKII holoenzyme mechanisms that govern the LTP versus LTD decision. Sci Adv. 2021;7(16).

50. Bai G, Wang Y, Zhang M. Gephyrin-mediated formation of inhibitory postsynaptic density sheet via phase separation. Cell Res. 2021;31(3):312-25.
51. Alvarez FJ. Gephyrin and the regulation of synaptic strength and dynamics at glycinergic inhibitory synapses. Brain Res Bull. 2017;129:50-65.
52. Tyagarajan SK, Fritschy JM. Gephyrin: a master regulator of neuronal function? Nat Rev Neurosci. 2014;15(3):141-56.
53. Tyagarajan SK, Ghosh H, Yevenes GE, Imanishi SY, Zeilhofer HU, Gerrits B, et al. Extracellular signal-regulated kinase and glycogen synthase kinase 3beta regulate gephyrin postsynaptic aggregation and GABAergic synaptic function in a calpain-dependent mechanism. J Biol Chem. 2013;288(14):9634-47.
54. Wuchter J. Rezeptortyrosinkinasen regulieren die Oberflächenaggregation des neuronalen Gerüstproteins Gephyrin. Universitätsbibliothek Tübingen: Universität Tübingen; 2012.
55. Pfeiffer F, Graham D, Betz H. Purification by affinity chromatography of the glycine receptor of rat spinal cord. J Biol Chem. 1982;257(16):9389-93.
56. Kirsch J, Langosch D, Prior P, Littauer UZ, Schmitt B, Betz H. The 93-kDa glycine receptor-associated protein binds to tubulin. J Biol Chem. 1991;266(33):22242-5.
57. Kasaragod VB, Schindelin H. Structure-Function Relationships of Glycine and GABA(A) Receptors and Their Interplay With the Scaffolding Protein Gephyrin. Front Mol Neurosci. 2018;11:317.
58. Crosby KC, Gookin SE, Garcia JD, Hahm KM, Dell'Acqua ML, Smith KR. Nanoscale Subsynaptic Domains Underlie the Organization of the Inhibitory Synapse. Cell Rep. 2019;26(12):3284-97 e3.
59. Specht CG, Izeddin I, Rodriguez PC, El Beheiry M, Rostaing P, Darzacq X, et al. Quantitative nanoscopy of inhibitory synapses: counting gephyrin molecules and receptor binding sites. Neuron. 2013;79(2):308-21.
60. Maric HM, Kasaragod VB, Hausrat TJ, Kneussel M, Tretter V, Stromgaard K, et al. Molecular basis of the alternative recruitment of GABA(A) versus glycine receptors through gephyrin. Nat Commun. 2014;5:5767.
61. Uezu A, Kanak DJ, Bradshaw TW, Soderblom EJ, Catavero CM, Burette AC, et al. Identification of an elaborate complex mediating postsynaptic inhibition. Science. 2016;353(6304):1123-9.
62. Tretter V, Jacob TC, Mukherjee J, Fritschy JM, Pangalos MN, Moss SJ. The clustering of GABA(A) receptor subtypes at inhibitory synapses is facilitated via the direct binding of receptor alpha 2 subunits to gephyrin. J Neurosci. 2008;28(6):1356-65.
63. Mou L, Dias BG, Gosnell H, Ressler KJ. Gephyrin plays a key role in BDNF-dependent regulation of amygdala surface GABAARs. Neuroscience. 2013;255:33-44.
64. Lorenz-Guertin JM, Jacob TC. GABA type a receptor trafficking and the architecture of synaptic inhibition. Dev Neurobiol. 2018;78(3):238-70.
65. Hannan S, Minere M, Harris J, Izquierdo P, Thomas P, Tench B, et al. GABA(A)R isoform and subunit structural motifs determine synaptic and extrasynaptic receptor localisation. Neuropharmacology. 2020;169:107540.
66. Mukherjee J, Kretschmannova K, Gouzer G, Maric HM, Ramsden S, Tretter V, et al. The residence time of GABA(A)Rs at inhibitory synapses is determined by direct binding of the receptor alpha1 subunit to gephyrin. J Neurosci. 2011;31(41):14677-87.
67. Kowalczyk S, Winkelmann A, Smolinsky B, Forstera B, Neundorf I, Schwarz G, et al. Direct binding of GABAA receptor beta2 and beta3 subunits to gephyrin. Eur J Neurosci. 2013;37(4):544-54.
68. Maynard SA, Triller A. Inhibitory Receptor Diffusion Dynamics. Front Mol Neurosci. 2019;12:313.
69. Ghosh H, Auguadri L, Battaglia S, Simone Thirouin Z, Zemoura K, Messner S, et al. Several posttranslational modifications act in concert to regulate gephyrin scaffolding and GABAergic transmission. Nat Commun. 2016;7:13365.
70. Ubersax JA, Ferrell JE, Jr. Mechanisms of specificity in protein phosphorylation. Nat Rev Mol Cell Biol. 2007;8(7):530-41.

71. Battaglia S, Renner M, Russeau M, Come E, Tyagarajan SK, Levi S. Activity-Dependent Inhibitory Synapse Scaling Is Determined by Gephyrin Phosphorylation and Subsequent Regulation of GABA(A) Receptor Diffusion. eNeuro. 2018;5(1).
72. Kuhse J, Kalbouneh H, Schlicksupp A, Mukusch S, Nawrotzki R, Kirsch J. Phosphorylation of gephyrin in hippocampal neurons by cyclin-dependent kinase CDK5 at Ser-270 is dependent on collybistin. J Biol Chem. 2012;287(37):30952-66.
73. Wuchter J, Beuter S, Treindl F, Herrmann T, Zeck G, Templin MF, et al. A comprehensive small interfering RNA screen identifies signaling pathways required for gephyrin clustering. J Neurosci. 2012;32(42):14821-34.
74. Kalbouneh H, Schlicksupp A, Kirsch J, Kuhse J. Cyclin-dependent kinase 5 is involved in the phosphorylation of gephyrin and clustering of GABAA receptors at inhibitory synapses of hippocampal neurons. PLoS One. 2014;9(8):e104256.
75. Tyagarajan SK, Ghosh H, Yevenes GE, Nikonenko I, Ebeling C, Schwerdel C, et al. Regulation of GABAergic synapse formation and plasticity by GSK3beta-dependent phosphorylation of gephyrin. Proc Natl Acad Sci U S A. 2011;108(1):379-84.
76. Bannai H, Levi S, Schweizer C, Inoue T, Launey T, Racine V, et al. Activity-dependent tuning of inhibitory neurotransmission based on GABAAR diffusion dynamics. Neuron. 2009;62(5):670-82.
77. Welle TM, Rajgor D, Kareemo DJ, Garcia JD, Zych SM, Wolfe SE, et al. miRNA-mediated control of gephyrin synthesis drives sustained inhibitory synaptic plasticity. EMBO Rep. 2024.
78. Pennacchietti F, Vascon S, Nieus T, Rosillo C, Das S, Tyagarajan SK, et al. Nanoscale Molecular Reorganization of the Inhibitory Postsynaptic Density Is a Determinant of GABAergic Synaptic Potentiation. J Neurosci. 2017;37(7):1747-56.
79. Lemmon MA, Schlessinger J. Cell signaling by receptor tyrosine kinases. Cell. 2010;141(7):1117-34.
80. Minichiello L. TrkB signalling pathways in LTP and learning. Nat Rev Neurosci. 2009;10(12):850-60.
81. Trenker R, Jura N. Receptor tyrosine kinase activation: From the ligand perspective. Curr Opin Cell Biol. 2020;63:174-85.
82. Beuter S. Rezeptortyrosinkinasen regulieren die Interneuronkonnektivität in spezifischen Zellkompartimenten von Körnerzellen [Dissertation]. Universitätsbibliothek Tübingen: Eberhard Karls Universität Tübingen; 2017.
83. Saha R, Wüstner L-S, Chakraborty D, Anunu R, Mandel S, Hazra JD, et al. Intra-BLA alteration of interneurons' modulation of activity in rats, reveals a dissociation between effects on anxiety symptoms and extinction learning. Neurobiology of Stress. 2024;33:100681.
84. Jeckel P, Kriebel M, Volkmer H. Autism Spectrum Disorder Risk Factor Met Regulates the Organization of Inhibitory Synapses. Front Mol Neurosci. 2021;14:659856.
85. Huang EJ, Reichardt LF. Neurotrophins: roles in neuronal development and function. Annu Rev Neurosci. 2001;24:677-736.
86. Li Y, Wei C, Wang W, Li Q, Wang ZC. Tropomyosin receptor kinase B (TrkB) signalling: targeted therapy in neurogenic tumours. J Pathol Clin Res. 2023;9(2):89-99.
87. Barbacid M. Structural and functional properties of the TRK family of neurotrophin receptors. Ann N Y Acad Sci. 1995;766:442-58.
88. Demir IE, Tieftrunk E, Schorn S, Friess H, Ceyhan GO. Nerve growth factor & TrkA as novel therapeutic targets in cancer. Biochim Biophys Acta. 2016;1866(1):37-50.
89. Barbacid M. The Trk family of neurotrophin receptors. J Neurobiol. 1994;25(11):1386-403.
90. Berkemeier LR, Winslow JW, Kaplan DR, Nikolics K, Goeddel DV, Rosenthal A. Neurotrophin-5: a novel neurotrophic factor that activates trk and trkB. Neuron. 1991;7(5):857-66.
91. Klein R, Nanduri V, Jing SA, Lamballe F, Tapley P, Bryant S, et al. The trkB tyrosine protein kinase is a receptor for brain-derived neurotrophic factor and neurotrophin-3. Cell. 1991;66(2):395-403.
92. Stoilov P, Castren E, Stamm S. Analysis of the human TrkB gene genomic organization reveals novel TrkB isoforms, unusual gene length, and splicing mechanism. Biochem Biophys Res Commun. 2002;290(3):1054-65.

93. Luberg K, Wong J, Weickert CS, Timmusk T. Human TrkB gene: novel alternative transcripts, protein isoforms and expression pattern in the prefrontal cerebral cortex during postnatal development. J Neurochem. 2010;113(4):952-64.
94. Fenner BM. Truncated TrkB: beyond a dominant negative receptor. Cytokine Growth Factor Rev. 2012;23(1-2):15-24.
95. Wang Y, Liang J, Xu B, Yang J, Wu Z, Cheng L. TrkB/BDNF signaling pathway and its small molecular agonists in CNS injury. Life Sci. 2024;336:122282.
96. Haapasalo A, Sipola I, Larsson K, Akerman KE, Stoilov P, Stamm S, et al. Regulation of TRKB surface expression by brain-derived neurotrophic factor and truncated TRKB isoforms. J Biol Chem. 2002;277(45):43160-7.
97. Jing S, Tapley P, Barbacid M. Nerve growth factor mediates signal transduction through trk homodimer receptors. Neuron. 1992;9(6):1067-79.
98. Middlemas DS, Meisenhelder J, Hunter T. Identification of TrkB autophosphorylation sites and evidence that phospholipase C-gamma 1 is a substrate of the TrkB receptor. J Biol Chem. 1994;269(7):5458-66.
99. McCarty JH, Feinstein SC. Activation loop tyrosines contribute varying roles to TrkB autophosphorylation and signal transduction. Oncogene. 1998;16(13):1691-700.
100. Bertrand T, Kothe M, Liu J, Dupuy A, Rak A, Berne PF, et al. The crystal structures of TrkA and TrkB suggest key regions for achieving selective inhibition. J Mol Biol. 2012;423(3):439-53.
101. Hubbard SR, Till JH. Protein tyrosine kinase structure and function. Annu Rev Biochem. 2000;69:373-98.
102. Leal G, Bramham CR, Duarte CB. BDNF and Hippocampal Synaptic Plasticity. Vitam Horm. 2017;104:153-95.
103. Numakawa T, Suzuki S, Kumamaru E, Adachi N, Richards M, Kunugi H. BDNF function and intracellular signaling in neurons. Histol Histopathol. 2010;25(2):237-58.
104. Poo MM. Neurotrophins as synaptic modulators. Nat Rev Neurosci. 2001;2(1):24-32.
105. Hofer M, Pagliusi SR, Hohn A, Leibrock J, Barde YA. Regional distribution of brain-derived neurotrophic factor mRNA in the adult mouse brain. EMBO J. 1990;9(8):2459-64.
106. Timmusk T, Palm K, Metsis M, Reintam T, Paalme V, Saarma M, et al. Multiple promoters direct tissue-specific expression of the rat BDNF gene. Neuron. 1993;10(3):475-89.
107. Chen WG, West AE, Tao X, Corfas G, Szentirmay MN, Sawadogo M, et al. Upstream stimulatory factors are mediators of Ca2+-responsive transcription in neurons. J Neurosci. 2003;23(7):2572-81.
108. Falkenberg T, Lindefors N, Camilli F, Metsis M, Ungerstedt U. Glutamate release correlates with brain-derived neurotrophic factor and trkB mRNA expression in the CA1 region of rat hippocampus. Brain Res Mol Brain Res. 1996;42(2):317-27.
109. Pang PT, Teng HK, Zaitsev E, Woo NT, Sakata K, Zhen S, et al. Cleavage of proBDNF by tPA/plasmin is essential for long-term hippocampal plasticity. Science. 2004;306(5695):487-91.
110. Foltran RB, Diaz SL. BDNF isoforms: a round trip ticket between neurogenesis and serotonin? J Neurochem. 2016;138(2):204-21.
111. Miranda M, Morici JF, Zanoni MB, Bekinschtein P. Brain-Derived Neurotrophic Factor: A Key Molecule for Memory in the Healthy and the Pathological Brain. Front Cell Neurosci. 2019;13:363.
112. Niculescu D, Michaelsen-Preusse K, Guner U, van Dorland R, Wierenga CJ, Lohmann C. A BDNF-Mediated Push-Pull Plasticity Mechanism for Synaptic Clustering. Cell Rep. 2018;24(8):2063-74.
113. Bibel M, Hoppe E, Barde YA. Biochemical and functional interactions between the neurotrophin receptors trk and p75NTR. EMBO J. 1999;18(3):616-22.
114. Zanin JP, Montroull LE, Volosin M, Friedman WJ. The p75 Neurotrophin Receptor Facilitates TrkB Signaling and Function in Rat Hippocampal Neurons. Front Cell Neurosci. 2019;13:485.
115. Fred SM, Moliner R, Antila H, Engelhardt KA, Schluter OM, Casarotto PC, et al. TRKB interaction with PSD95 is associated with latency of fluoxetine and 2R,6R-hydroxynorketamine. Eur J Neurosci. 2023;57(8):1215-24.

116. Eide FF, Vining ER, Eide BL, Zang K, Wang XY, Reichardt LF. Naturally occurring truncated trkB receptors have dominant inhibitory effects on brain-derived neurotrophic factor signaling. J Neurosci. 1996;16(10):3123-9.
117. Huang P, Liu A, Song Y, Hope JM, Cui B, Duan L. Optical Activation of TrkB Signaling. J Mol Biol. 2020;432(13):3761-70.
118. Wang CS, Kavalali ET, Monteggia LM. BDNF signaling in context: From synaptic regulation to psychiatric disorders. Cell. 2022;185(1):62-76.
119. Mou L, Heldt SA, Ressler KJ. Rapid brain-derived neurotrophic factor-dependent sequestration of amygdala and hippocampal GABA(A) receptors via different tyrosine receptor kinase B-mediated phosphorylation pathways. Neuroscience. 2011;176:72-85.
120. Gottmann K, Mittmann T, Lessmann V. BDNF signaling in the formation, maturation and plasticity of glutamatergic and GABAergic synapses. Exp Brain Res. 2009;199(3-4):203-34.
121. Qi C, Chen A, Mao H, Hu E, Ge J, Ma G, et al. Excitatory and Inhibitory Synaptic Imbalance Caused by Brain-Derived Neurotrophic Factor Deficits During Development in a Valproic Acid Mouse Model of Autism. Front Mol Neurosci. 2022;15:860275.
122. Park H, Poo MM. Neurotrophin regulation of neural circuit development and function. Nat Rev Neurosci. 2013;14(1):7-23.
123. Wu CH, Chen CC, Hung TH, Chuang YC, Chao M, Shyue SK, et al. Activation of TrkB/Akt signaling by a TrkB receptor agonist improves long-term histological and functional outcomes in experimental intracerebral hemorrhage. J Biomed Sci. 2019;26(1):53.
124. Kavanaugh WM, Williams LT. An alternative to SH2 domains for binding tyrosine-phosphorylated proteins. Science. 1994;266(5192):1862-5.
125. Reichardt LF. Neurotrophin-regulated signalling pathways. Philos Trans R Soc Lond B Biol Sci. 2006;361(1473):1545-64.
126. Asadi M, Taghizadeh S, Kaviani E, Vakili O, Taheri-Anganeh M, Tahamtan M, et al. Caspase-3: Structure, function, and biotechnological aspects. Biotechnol Appl Biochem. 2022;69(4):1633-45.
127. Atwal JK, Massie B, Miller FD, Kaplan DR. The TrkB-Shc site signals neuronal survival and local axon growth via MEK and P13-kinase. Neuron. 2000;27(2):265-77.
128. Tecuatl C, Herrrera-Lopez G, Martin-Avila A, Yin B, Weber S, Barrionuevo G, et al. TrkB-mediated activation of the phosphatidylinositol-3-kinase/Akt cascade reduces the damage inflicted by oxygen-glucose deprivation in area CA3 of the rat hippocampus. Eur J Neurosci. 2018;47(9):1096-109.
129. Miller FD, Kaplan DR. Neurotrophin signalling pathways regulating neuronal apoptosis. Cell Mol Life Sci. 2001;58(8):1045-53.
130. Sarbassov DD, Ali SM, Sabatini DM. Growing roles for the mTOR pathway. Curr Opin Cell Biol. 2005;17(6):596-603.
131. Peineau S, Bradley C, Taghibiglou C, Doherty A, Bortolotto ZA, Wang YT, et al. The role of GSK-3 in synaptic plasticity. Br J Pharmacol. 2008;153 Suppl 1(Suppl 1):S428-37.
132. Moreno-Jimenez EP, Flor-Garcia M, Hernandez-Vivanco A, Terreros-Roncal J, Rodriguez-Moreno CB, Toni N, et al. GSK-3beta orchestrates the inhibitory innervation of adult-born dentate granule cells in vivo. Cell Mol Life Sci. 2023;80(8):225.
133. Yoshii A, Constantine-Paton M. Postsynaptic BDNF-TrkB signaling in synapse maturation, plasticity, and disease. Dev Neurobiol. 2010;70(5):304-22.
134. Wang JQ, Mao L. The ERK Pathway: Molecular Mechanisms and Treatment of Depression. Mol Neurobiol. 2019;56(9):6197-205.
135. Mao LM, Wang JQ. Synaptically Localized Mitogen-Activated Protein Kinases: Local Substrates and Regulation. Mol Neurobiol. 2016;53(9):6309-15.
136. Finkbeiner S, Tavazoie SF, Maloratsky A, Jacobs KM, Harris KM, Greenberg ME. CREB: a major mediator of neuronal neurotrophin responses. Neuron. 1997;19(5):1031-47.
137. Wang JQ, Fibuch EE, Mao L. Regulation of mitogen-activated protein kinases by glutamate receptors. J Neurochem. 2007;100(1):1-11.

138. Giachello CN, Fiumara F, Giacomini C, Corradi A, Milanese C, Ghirardi M, et al. MAPK/Erk-dependent phosphorylation of synapsin mediates formation of functional synapses and short-term homosynaptic plasticity. J Cell Sci. 2010;123(Pt 6):881-93.
139. Yoshii A, Constantine-Paton M. Postsynaptic localization of PSD-95 is regulated by all three pathways downstream of TrkB signaling. Front Synaptic Neurosci. 2014;6:6.
140. Thomas GM, Huganir RL. MAPK cascade signalling and synaptic plasticity. Nat Rev Neurosci. 2004;5(3):173-83.
141. Brady ML, Pilli J, Lorenz-Guertin JM, Das S, Moon CE, Graff N, et al. Depolarizing, inhibitory GABA type A receptor activity regulates GABAergic synapse plasticity via ERK and BDNF signaling. Neuropharmacology. 2018;128:324-39.
142. Proud CG. Phosphorylation and Signal Transduction Pathways in Translational Control. Cold Spring Harb Perspect Biol. 2019;11(7).
143. Inoki K, Li Y, Zhu T, Wu J, Guan KL. TSC2 is phosphorylated and inhibited by Akt and suppresses mTOR signalling. Nat Cell Biol. 2002;4(9):648-57.
144. Panwar V, Singh A, Bhatt M, Tonk RK, Azizov S, Raza AS, et al. Multifaceted role of mTOR (mammalian target of rapamycin) signaling pathway in human health and disease. Signal Transduct Target Ther. 2023;8(1):375.
145. Lipton JO, Sahin M. The neurology of mTOR. Neuron. 2014;84(2):275-91.
146. Huang H, Jing B, Zhu F, Jiang W, Tang P, Shi L, et al. Disruption of neuronal RHEB signaling impairs oligodendrocyte differentiation and myelination through mTORC1-DLK1 axis. Cell Rep. 2023;42(7):112801.
147. Raab-Graham KF, Haddick PC, Jan YN, Jan LY. Activity- and mTOR-dependent suppression of Kv1.1 channel mRNA translation in dendrites. Science. 2006;314(5796):144-8.
148. Li N, Lee B, Liu RJ, Banasr M, Dwyer JM, Iwata M, et al. mTOR-dependent synapse formation underlies the rapid antidepressant effects of NMDA antagonists. Science. 2010;329(5994):959-64.
149. Sabatini DM, Barrow RK, Blackshaw S, Burnett PE, Lai MM, Field ME, et al. Interaction of RAFT1 with gephyrin required for rapamycin-sensitive signaling. Science. 1999;284(5417):1161-4.
150. Moya-Alvarado G, Valero-Pena X, Aguirre-Soto A, Bustos FJ, Lazo OM, Bronfman FC. PLC-gamma-Ca(2+) pathway regulates axonal TrkB endocytosis and is required for long-distance propagation of BDNF signaling. Front Mol Neurosci. 2024;17:1009404.
151. Sciarretta C, Fritzsch B, Beisel K, Rocha-Sanchez SM, Buniello A, Horn JM, et al. PLCgamma-activated signalling is essential for TrkB mediated sensory neuron structural plasticity. BMC Dev Biol. 2010;10:103.
152. Minichiello L, Calella AM, Medina DL, Bonhoeffer T, Klein R, Korte M. Mechanism of TrkB-mediated hippocampal long-term potentiation. Neuron. 2002;36(1):121-37.
153. Li Y, Jia YC, Cui K, Li N, Zheng ZY, Wang YZ, et al. Essential role of TRPC channels in the guidance of nerve growth cones by brain-derived neurotrophic factor. Nature. 2005;434(7035):894-8.
154. Leal G, Afonso PM, Salazar IL, Duarte CB. Regulation of hippocampal synaptic plasticity by BDNF. Brain Res. 2015;1621:82-101.
155. Herring BE, Nicoll RA. Long-Term Potentiation: From CaMKII to AMPA Receptor Trafficking. Annu Rev Physiol. 2016;78:351-65.
156. Miranda-Lourenco C, Ribeiro-Rodrigues L, Fonseca-Gomes J, Tanqueiro SR, Belo RF, Ferreira CB, et al. Challenges of BDNF-based therapies: From common to rare diseases. Pharmacol Res. 2020;162:105281.
157. Notaras M, van den Buuse M. Neurobiology of BDNF in fear memory, sensitivity to stress, and stress-related disorders. Mol Psychiatry. 2020;25(10):2251-74.
158. Miao Z, Wang Y, Sun Z. The Relationships Between Stress, Mental Disorders, and Epigenetic Regulation of BDNF. Int J Mol Sci. 2020;21(4).
159. Arora I, Mal P, Arora P, Paul A, Kumar M. GABAergic implications in anxiety and related disorders. Biochem Biophys Res Commun. 2024;724:150218.
160. Bi D, Wen L, Wu Z, Shen Y. GABAergic dysfunction in excitatory and inhibitory (E/I) imbalance drives the pathogenesis of Alzheimer's disease. Alzheimers Dement. 2020;16(9):1312-29.

161. Duman RS, Aghajanian GK. Synaptic dysfunction in depression: potential therapeutic targets. Science. 2012;338(6103):68-72.
162. Duman RS, Sanacora G, Krystal JH. Altered Connectivity in Depression: GABA and Glutamate Neurotransmitter Deficits and Reversal by Novel Treatments. Neuron. 2019;102(1):75-90.
163. Gao R, Penzes P. Common mechanisms of excitatory and inhibitory imbalance in schizophrenia and autism spectrum disorders. Curr Mol Med. 2015;15(2):146-67.
164. Mele M, Costa RO, Duarte CB. Alterations in GABA(A)-Receptor Trafficking and Synaptic Dysfunction in Brain Disorders. Front Cell Neurosci. 2019;13:77.
165. Smith-Dijak AI, Sepers MD, Raymond LA. Alterations in synaptic function and plasticity in Huntington disease. J Neurochem. 2019;150(4):346-65.
166. Luscher B, Shen Q, Sahir N. The GABAergic deficit hypothesis of major depressive disorder. Mol Psychiatry. 2011;16(4):383-406.
167. Fatemi SH, Reutiman TJ, Folsom TD, Thuras PD. GABA(A) receptor downregulation in brains of subjects with autism. J Autism Dev Disord. 2009;39(2):223-30.
168. Fung SJ, Fillman SG, Webster MJ, Shannon Weickert C. Schizophrenia and bipolar disorder show both common and distinct changes in cortical interneuron markers. Schizophr Res. 2014;155(1-3):26-30.
169. Selten M, van Bokhoven H, Nadif Kasri N. Inhibitory control of the excitatory/inhibitory balance in psychiatric disorders. F1000Res. 2018;7:23.
170. Casarotto PC, Girych M, Fred SM, Kovaleva V, Moliner R, Enkavi G, et al. Antidepressant drugs act by directly binding to TRKB neurotrophin receptors. Cell. 2021;184(5):1299-313 e19.
171. Enkavi G, Girych M, Moliner R, Vattulainen I, Castren E. TrkB transmembrane domain: bridging structural understanding with therapeutic strategy. Trends Biochem Sci. 2024;49(5):445-56.
172. Jiang CC, Lin LS, Long S, Ke XY, Fukunaga K, Lu YM, et al. Signalling pathways in autism spectrum disorder: mechanisms and therapeutic implications. Signal Transduct Target Ther. 2022;7(1):229.
173. Jope RS, Roh MS. Glycogen synthase kinase-3 (GSK3) in psychiatric diseases and therapeutic interventions. Curr Drug Targets. 2006;7(11):1421-34.
174. Rosina E, Battan B, Siracusano M, Di Criscio L, Hollis F, Pacini L, et al. Disruption of mTOR and MAPK pathways correlates with severity in idiopathic autism. Transl Psychiatry. 2019;9(1):50.
175. Stertz L, Di Re J, Pei G, Fries GR, Mendez E, Li S, et al. Convergent genomic and pharmacological evidence of PI3K/GSK3 signaling alterations in neurons from schizophrenia patients. Neuropsychopharmacology. 2021;46(3):673-82.
176. An S, Wang J, Zhang X, Duan Y, Xu Y, Lv J, et al. alphaCaMKII in the lateral amygdala mediates PTSD-Like behaviors and NMDAR-Dependent LTD. Neurobiol Stress. 2021;15:100359.
177. Iroegbu JD, Ijomone OK, Femi-Akinlosotu OM, Ijomone OM. ERK/MAPK signalling in the developing brain: Perturbations and consequences. Neurosci Biobehav Rev. 2021;131:792-805.
178. Colucci-D'Amato L, Speranza L, Volpicelli F. Neurotrophic Factor BDNF, Physiological Functions and Therapeutic Potential in Depression, Neurodegeneration and Brain Cancer. Int J Mol Sci. 2020;21(20).
179. Elmariah SB, Crumling MA, Parsons TD, Balice-Gordon RJ. Postsynaptic TrkB-mediated signaling modulates excitatory and inhibitory neurotransmitter receptor clustering at hippocampal synapses. J Neurosci. 2004;24(10):2380-93.
180. Guilloux JP, Douillard-Guilloux G, Kota R, Wang X, Gardier AM, Martinowich K, et al. Molecular evidence for BDNF- and GABA-related dysfunctions in the amygdala of female subjects with major depression. Mol Psychiatry. 2012;17(11):1130-42.
181. Gonzalez MI. Brain-derived neurotrophic factor promotes gephyrin protein expression and GABAA receptor clustering in immature cultured hippocampal cells. Neurochem Int. 2014;72:14-21.
182. Beuter S, Ardi Z, Horovitz O, Wuchter J, Keller S, Saha R, et al. Receptor tyrosine kinase EphA7 is required for interneuron connectivity at specific subcellular compartments of granule cells. Sci Rep. 2016;6:29710.
183. Freund TF, Buzsaki G. Interneurons of the hippocampus. Hippocampus. 1996;6(4):347-470.

184. Scharfman HE. The enigmatic mossy cell of the dentate gyrus. Nat Rev Neurosci. 2016;17(9):562-75.
185. Tzilivaki A, Tukker JJ, Maier N, Poirazi P, Sammons RP, Schmitz D. Hippocampal GABAergic interneurons and memory. Neuron. 2023;111(20):3154-75.
186. Chen AI, Nguyen CN, Copenhagen DR, Badurek S, Minichiello L, Ranscht B, et al. TrkB (tropomyosin-related kinase B) controls the assembly and maintenance of GABAergic synapses in the cerebellar cortex. J Neurosci. 2011;31(8):2769-80.
187. Seil FJ, Drake-Baumann R. TrkB receptor ligands promote activity-dependent inhibitory synaptogenesis. J Neurosci. 2000;20(14):5367-73.
188. Swanwick CC, Murthy NR, Kapur J. Activity-dependent scaling of GABAergic synapse strength is regulated by brain-derived neurotrophic factor. Mol Cell Neurosci. 2006;31(3):481-92.
189. Kriebel M, Ebel J, Battke F, Griesbach S, Volkmer H. Interference With Complex IV as a Model of Age-Related Decline in Synaptic Connectivity. Front Mol Neurosci. 2020;13:43.
190. Minichiello L, Casagranda F, Tatche RS, Stucky CL, Postigo A, Lewin GR, et al. Point mutation in trkB causes loss of NT4-dependent neurons without major effects on diverse BDNF responses. Neuron. 1998;21(2):335-45.
191. Higashimoto T, Urbinati F, Perumbeti A, Jiang G, Zarzuela A, Chang LJ, et al. The woodchuck hepatitis virus post-transcriptional regulatory element reduces readthrough transcription from retroviral vectors. Gene Ther. 2007;14(17):1298-304.
192. Zufferey R, Donello JE, Trono D, Hope TJ. Woodchuck hepatitis virus posttranscriptional regulatory element enhances expression of transgenes delivered by retroviral vectors. J Virol. 1999;73(4):2886-92.
193. Wustner LS, Beuter S, Kriebel M, Volkmer H. Dissection of signaling pathways regulating TrkB-dependent gephyrin clustering. Front Mol Neurosci. 2024;17:1480820.
194. Keaveney MK, Rahsepar B, Tseng HA, Fernandez FR, Mount RA, Ta T, et al. CaMKIIalpha-Positive Interneurons Identified via a microRNA-Based Viral Gene Targeting Strategy. J Neurosci. 2020;40(50):9576-88.
195. Veres JM, Andrasi T, Nagy-Pal P, Hajos N. CaMKIIalpha Promoter-Controlled Circuit Manipulations Target Both Pyramidal Cells and Inhibitory Interneurons in Cortical Networks. eNeuro. 2023;10(4).
196. Johnstone A, Mobley W. Local TrkB signaling: themes in development and neural plasticity. Cell Tissue Res. 2020;382(1):101-11.
197. Bloodgood BL, Sharma N, Browne HA, Trepman AZ, Greenberg ME. The activity-dependent transcription factor NPAS4 regulates domain-specific inhibition. Nature. 2013;503(7474):121-5.
198. Lin PY, Kavalali ET, Monteggia LM. Genetic Dissection of Presynaptic and Postsynaptic BDNF-TrkB Signaling in Synaptic Efficacy of CA3-CA1 Synapses. Cell Rep. 2018;24(6):1550-61.
199. Ali F, Kwan AC. Interpreting in vivo calcium signals from neuronal cell bodies, axons, and dendrites: a review. Neurophotonics. 2020;7(1):011402.
200. Nave BT, Ouwens M, Withers DJ, Alessi DR, Shepherd PR. Mammalian target of rapamycin is a direct target for protein kinase B: identification of a convergence point for opposing effects of insulin and amino-acid deficiency on protein translation. Biochem J. 1999;344 Pt 2(Pt 2):427-31.
201. Weng QP, Kozlowski M, Belham C, Zhang A, Comb MJ, Avruch J. Regulation of the p70 S6 kinase by phosphorylation in vivo. Analysis using site-specific anti-phosphopeptide antibodies. J Biol Chem. 1998;273(26):16621-9.
202. Miller SG, Patton BL, Kennedy MB. Sequences of autophosphorylation sites in neuronal type II CaM kinase that control Ca2(+)-independent activity. Neuron. 1988;1(7):593-604.
203. Zacchi P, Antonelli R, Cherubini E. Gephyrin phosphorylation in the functional organization and plasticity of GABAergic synapses. Front Cell Neurosci. 2014;8:103.
204. Pillai-Kastoori L, Schutz-Geschwender AR, Harford JA. A systematic approach to quantitative Western blot analysis. Anal Biochem. 2020;593:113608.
205. Pearson G, Robinson F, Beers Gibson T, Xu BE, Karandikar M, Berman K, et al. Mitogen-activated protein (MAP) kinase pathways: regulation and physiological functions. Endocr Rev. 2001;22(2):153-83.

206. Wortzel I, Seger R. The ERK Cascade: Distinct Functions within Various Subcellular Organelles. Genes Cancer. 2011;2(3):195-209.
207. Lee FS, Rajagopal R, Chao MV. Distinctive features of Trk neurotrophin receptor transactivation by G protein-coupled receptors. Cytokine Growth Factor Rev. 2002;13(1):11-7.
208. Treindl F, Ruprecht B, Beiter Y, Schultz S, Dottinger A, Staebler A, et al. A bead-based western for high-throughput cellular signal transduction analyses. Nat Commun. 2016;7:12852.
209. Thirouin ZS, Figueiredo M, Hleihil M, Gill R, Bosshard G, McKinney RA, et al. Trophic factor BDNF inhibits GABAergic signaling by facilitating dendritic enrichment of SUMO E3 ligase PIAS3 and altering gephyrin scaffold. J Biol Chem. 2022;298(5):101840.
210. Musumeci G, Sciarretta C, Rodriguez-Moreno A, Al Banchaabouchi M, Negrete-Diaz V, Costanzi M, et al. TrkB modulates fear learning and amygdalar synaptic plasticity by specific docking sites. J Neurosci. 2009;29(32):10131-43.
211. Danglot L, Triller A, Bessis A. Association of gephyrin with synaptic and extrasynaptic GABAA receptors varies during development in cultured hippocampal neurons. Mol Cell Neurosci. 2003;23(2):264-78.
212. Ehrensperger MV, Hanus C, Vannier C, Triller A, Dahan M. Multiple association states between glycine receptors and gephyrin identified by SPT analysis. Biophys J. 2007;92(10):3706-18.
213. Tessarollo L, Yanpallewar S. TrkB Truncated Isoform Receptors as Transducers and Determinants of BDNF Functions. Front Neurosci. 2022;16:847572.
214. Yamada K, Nabeshima T. Interaction of BDNF/TrkB signaling with NMDA receptor in learning and memory. Drug News Perspect. 2004;17(7):435-8.
215. Philibert CE, Disdier C, Lafon PA, Bouyssou A, Oosterlaken M, Galant S, et al. TrkB receptor interacts with mGlu(2) receptor and mediates antipsychotic-like effects of mGlu(2) receptor activation in the mouse. Sci Adv. 2024;10(4):eadg1679.
216. Grienberger C, Konnerth A. Imaging calcium in neurons. Neuron. 2012;73(5):862-85.
217. le Feber J, Dummer A, Hassink GC, van Putten M, Hofmeijer J. Evolution of Excitation-Inhibition Ratio in Cortical Cultures Exposed to Hypoxia. Front Cell Neurosci. 2018;12:183.
218. Yu W, Jiang M, Miralles CP, Li RW, Chen G, de Blas AL. Gephyrin clustering is required for the stability of GABAergic synapses. Mol Cell Neurosci. 2007;36(4):484-500.
219. Huiskamp M, Kiljan S, Kulik S, Witte ME, Jonkman LE, Gjm Bol J, et al. Inhibitory synaptic loss drives network changes in multiple sclerosis: An ex vivo to in silico translational study. Mult Scler. 2022;28(13):2010-9.
220. Bateup HS, Johnson CA, Denefrio CL, Saulnier JL, Kornacker K, Sabatini BL. Excitatory/inhibitory synaptic imbalance leads to hippocampal hyperexcitability in mouse models of tuberous sclerosis. Neuron. 2013;78(3):510-22.
221. Marchionni I, Kasap Z, Mozrzymas JW, Sieghart W, Cherubini E, Zacchi P. New insights on the role of gephyrin in regulating both phasic and tonic GABAergic inhibition in rat hippocampal neurons in culture. Neuroscience. 2009;164(2):552-62.
222. Gross GG, Straub C, Perez-Sanchez J, Dempsey WP, Junge JA, Roberts RW, et al. An E3-ligase-based method for ablating inhibitory synapses. Nat Methods. 2016;13(8):673-8.
223. Secondo A, Bagetta G, Amantea D. On the Role of Store-Operated Calcium Entry in Acute and Chronic Neurodegenerative Diseases. Front Mol Neurosci. 2018;11:87.
224. Nakata H, Nakamura S. Brain-derived neurotrophic factor regulates AMPA receptor trafficking to post-synaptic densities via IP3R and TRPC calcium signaling. FEBS Lett. 2007;581(10):2047-54.
225. Yoshii A, Murata Y, Kim J, Zhang C, Shokat KM, Constantine-Paton M. TrkB and protein kinase Mzeta regulate synaptic localization of PSD-95 in developing cortex. J Neurosci. 2011;31(33):11894-904.
226. Megias M, Emri Z, Freund TF, Gulyas AI. Total number and distribution of inhibitory and excitatory synapses on hippocampal CA1 pyramidal cells. Neuroscience. 2001;102(3):527-40.
227. Spruston N. Pyramidal neurons: dendritic structure and synaptic integration. Nat Rev Neurosci. 2008;9(3):206-21.

228. Rui Y, Myers KR, Yu K, Wise A, De Blas AL, Hartzell HC, et al. Activity-dependent regulation of dendritic growth and maintenance by glycogen synthase kinase 3beta. Nat Commun. 2013;4:2628.
229. Bassetti D, Luhmann HJ, Kirischuk S. Presynaptic GABA(B) receptor-mediated network excitation in the medial prefrontal cortex of Tsc2(+/-) mice. Pflugers Arch. 2021;473(8):1261-71.
230. Silva AJ, Stevens CF, Tonegawa S, Wang Y. Deficient hippocampal long-term potentiation in alpha-calcium-calmodulin kinase II mutant mice. Science. 1992;257(5067):201-6.
231. Harward SC, Hedrick NG, Hall CE, Parra-Bueno P, Milner TA, Pan E, et al. Autocrine BDNF-TrkB signalling within a single dendritic spine. Nature. 2016;538(7623):99-103.
232. Lushnikova I, Skibo G, Muller D, Nikonenko I. Excitatory synaptic activity is associated with a rapid structural plasticity of inhibitory synapses on hippocampal CA1 pyramidal cells. Neuropharmacology. 2011;60(5):757-64.
233. Chiu CQ, Martenson JS, Yamazaki M, Natsume R, Sakimura K, Tomita S, et al. Input-Specific NMDAR-Dependent Potentiation of Dendritic GABAergic Inhibition. Neuron. 2018;97(2):368-77 e3.
234. Bolton MM, Pittman AJ, Lo DC. Brain-derived neurotrophic factor differentially regulates excitatory and inhibitory synaptic transmission in hippocampal cultures. J Neurosci. 2000;20(9):3221-32.
235. Korte M, Minichiello L, Klein R, Bonhoeffer T. Shc-binding site in the TrkB receptor is not required for hippocampal long-term potentiation. Neuropharmacology. 2000;39(5):717-24.
236. Kanterewicz BI, Urban NN, McMahon DB, Norman ED, Giffen LJ, Favata MF, et al. The extracellular signal-regulated kinase cascade is required for NMDA receptor-independent LTP in area CA1 but not area CA3 of the hippocampus. J Neurosci. 2000;20(9):3057-66.
237. Miningou N, Blackwell KT. The road to ERK activation: Do neurons take alternate routes? Cell Signal. 2020;68:109541.
238. Sabio G, Reuver S, Feijoo C, Hasegawa M, Thomas GM, Centeno F, et al. Stress- and mitogen-induced phosphorylation of the synapse-associated protein SAP90/PSD-95 by activation of SAPK3/p38gamma and ERK1/ERK2. Biochem J. 2004;380(Pt 1):19-30.
239. Adams JP, Anderson AE, Varga AW, Dineley KT, Cook RG, Pfaffinger PJ, et al. The A-type potassium channel Kv4.2 is a substrate for the mitogen-activated protein kinase ERK. J Neurochem. 2000;75(6):2277-87.
240. Kim J, Jung SC, Clemens AM, Petralia RS, Hoffman DA. Regulation of dendritic excitability by activity-dependent trafficking of the A-type K+ channel subunit Kv4.2 in hippocampal neurons. Neuron. 2007;54(6):933-47.
241. Ying SW, Futter M, Rosenblum K, Webber MJ, Hunt SP, Bliss TV, et al. Brain-derived neurotrophic factor induces long-term potentiation in intact adult hippocampus: requirement for ERK activation coupled to CREB and upregulation of Arc synthesis. J Neurosci. 2002;22(5):1532-40.
242. Levine ES, Crozier RA, Black IB, Plummer MR. Brain-derived neurotrophic factor modulates hippocampal synaptic transmission by increasing N-methyl-D-aspartic acid receptor activity. Proc Natl Acad Sci U S A. 1998;95(17):10235-9.

7. Appendix

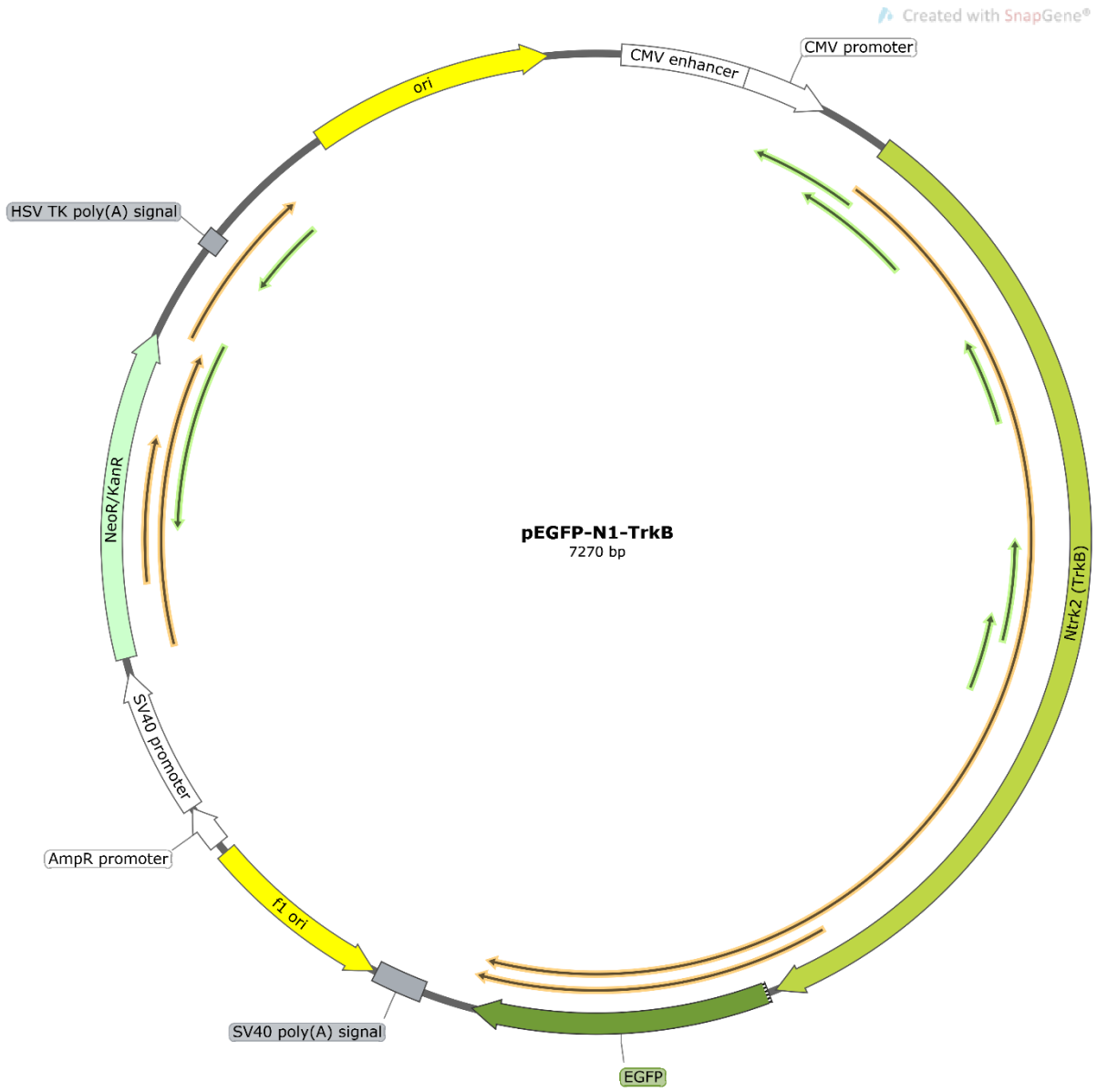

Supplementary Figure 1: pEGFP-N1-TrkB expression vector. Map of the pEGPF-N1-TrkB expression vector (a gift from Rosalind Segal (Addgene plasmid # 32500; http://n2t.net/addgene:32500; RRID: Addgene_32500)), containing the coding sequence of the rat *Ntrk2* (TrkB) gene fused to an EGFP at the C-terminus. Expression of the transgene is driven by an upstream CMV promotor equipped with a 5' CMV enhancer. *Map created with SnapGene Viewer 5.3.1.*

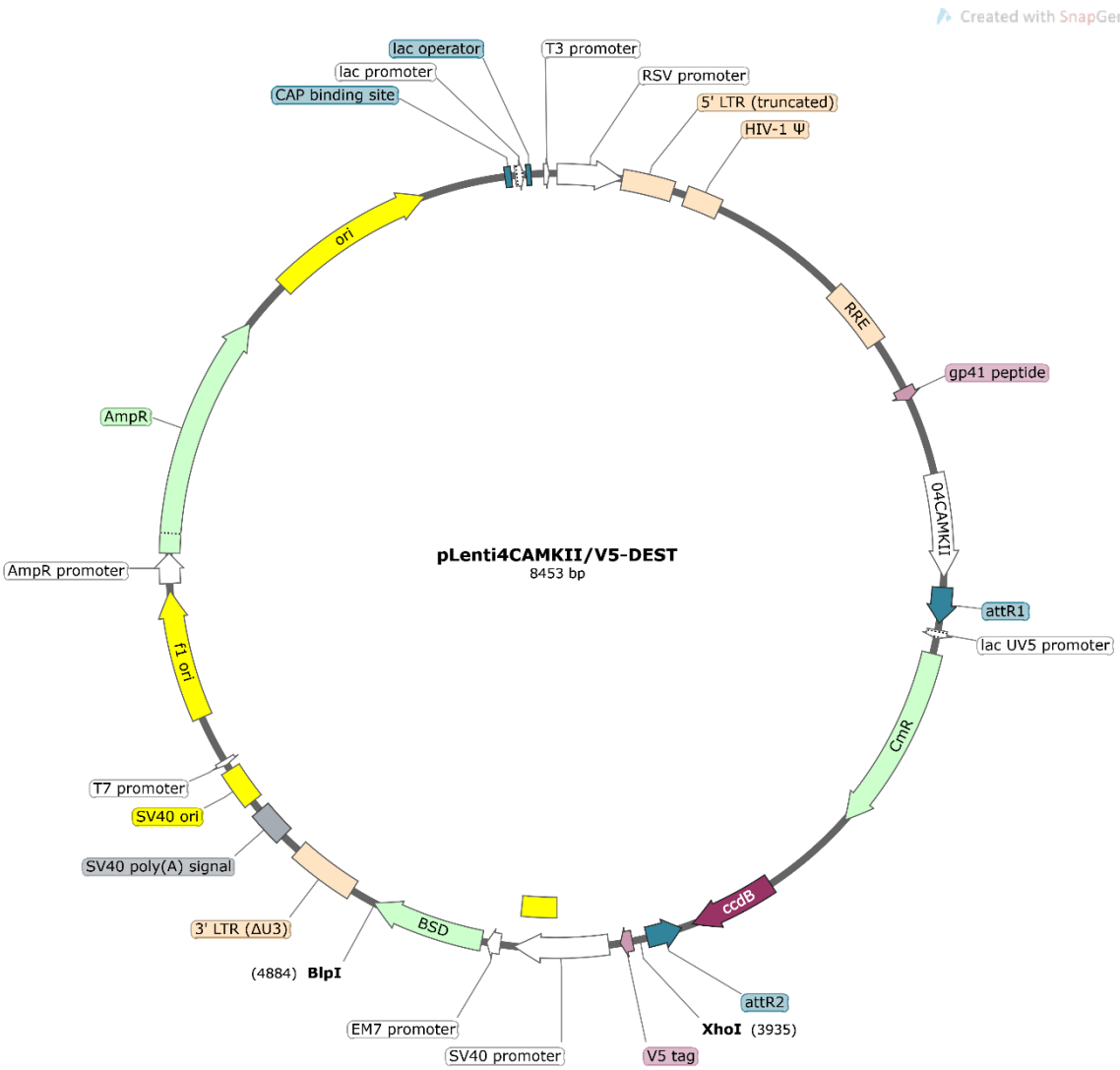

Supplementary Figure 2: Map of the pLenti4CAMKII/V5-DEST vector. Modified pLenti5/V5-DEST® vector, kindly provided by Martin Kriebel. The original CMV promotor was replaced with a functional α-CaMKII promotor fragment to restrict expression of the downstream transgene to excitatory neurons. *Map generated with SnapGene Viewer 5.3.1.*

Supplementary Figure 3:Map of the lentiviral transfer vector pLenti4CAMKII/ /WPRE. This vector allows for transgene insertion via Gateway® recombination at the corresponding attachment sites (attR1, attR2). Transgene expression is driven by an upstream CaMKII. To enhance expression, a WHV posttranscriptional Regulatory element (WPRE) was inserted downstream of the Gateway-attachment site attR2. *Map generated with SnapGene Viewer 5.3.1.*

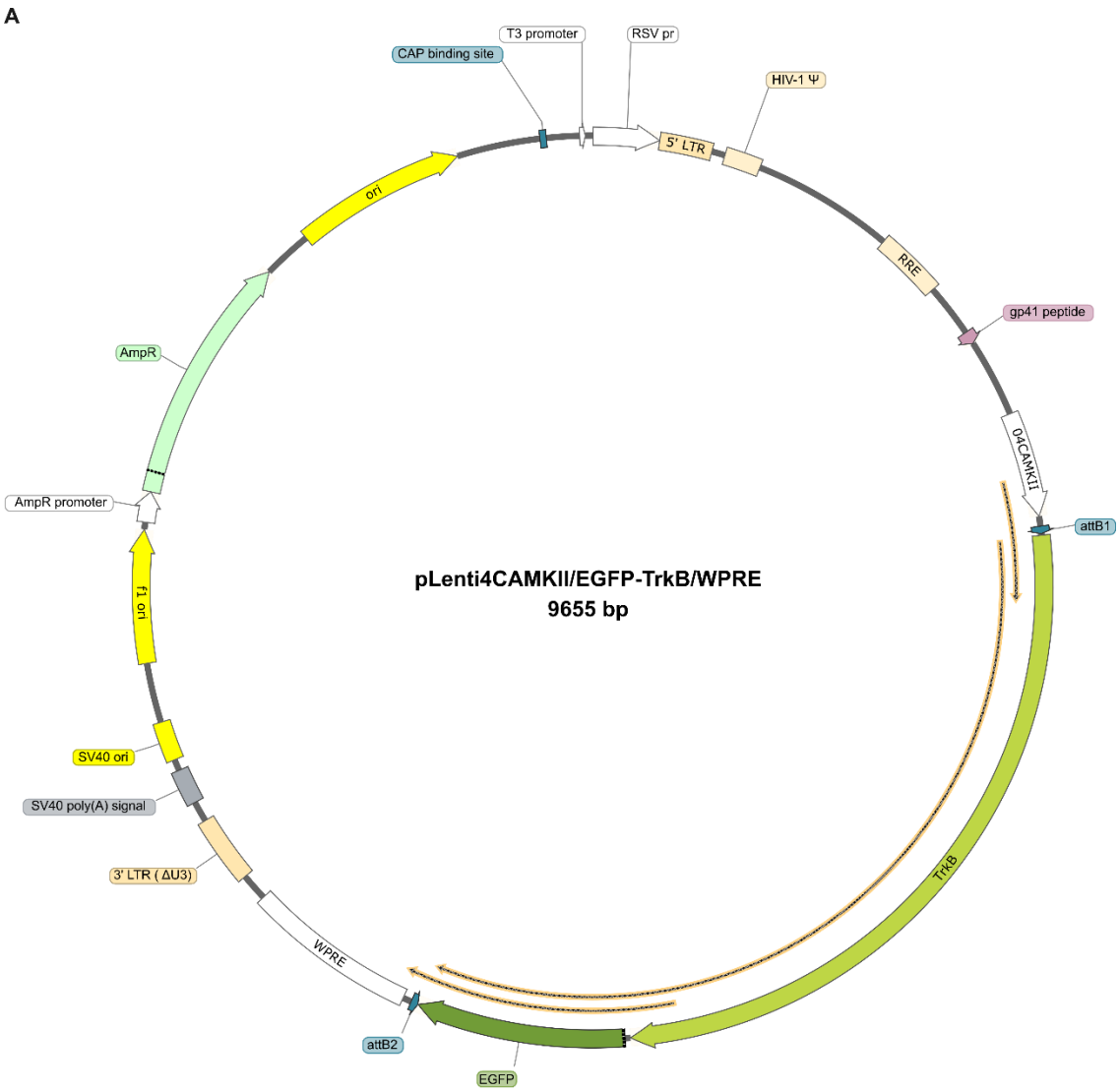

Supplementary Figure 4: Map of the TrkB variant expression vector pLenti4CAMKII/EGFP-TrkB/WPRE. Representative map of pLenti4CAMKII/EGFP-TrkB/WPRE, which resulted from the recombination of EGFP-N1-TrkB (WT) transgene with the transfer vector pLenti4CAMKII/ /WPRE via Gateway® recombination. *Map created with SnapGene Viewer 5.3.1.*

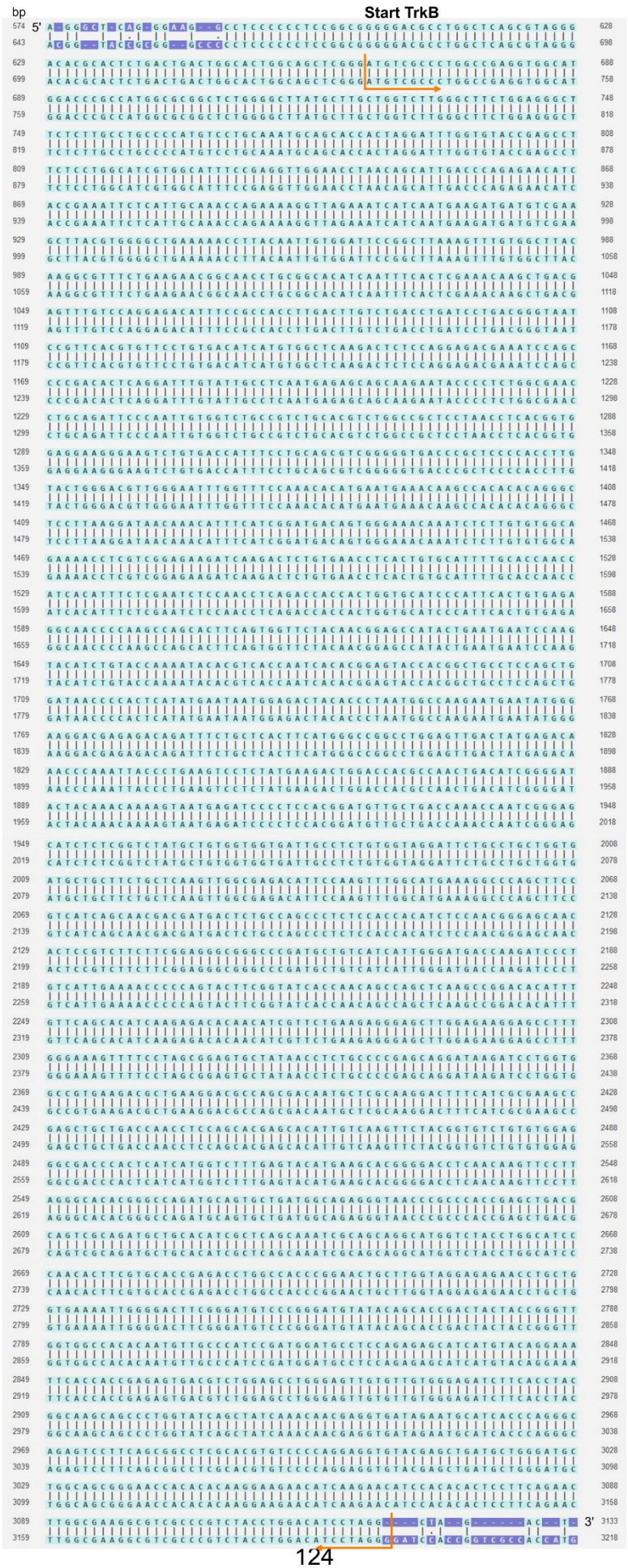
bp
Start TrkB
5'
3'

Supplementary Figure 5: Sequence alignment of rat *TrkB* cds with TrkB cds in pEGFP-N1-TrkB. Alignment of the complete *TrkB* cds from NCBI reference sequence M55291.1 (top sequence) and *TrkB* cds encoded in the pEGFP-N1-TrkB plasmid (bottom sequence). Orange arrows indicate the start and stop sequences of the respective *TrkB* sequences. Non-identical base pairs (bp) are highlighted in lilac, indicating sequence variations between both *TrkB* cds. *Bp: basepair numbers; Sequence alignment was performed with the alignment tool of Vectorbuilder.com.*

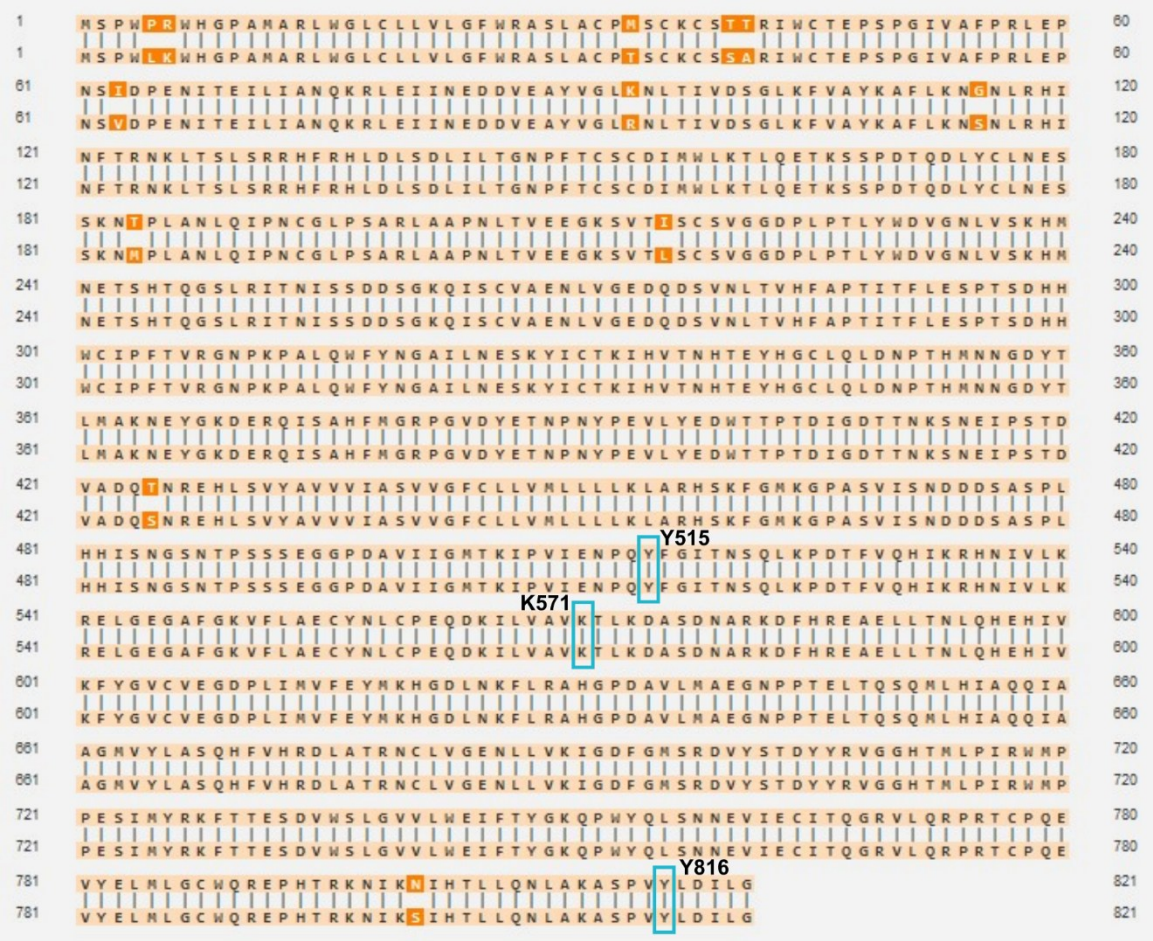

Supplementary Figure 6: Comparison of *Rattus norvegicus* and *Mus musculus* TrkB aa sequence showed preserved binding sites at Y515, K571, and Y816. Alignment of protein sequence from rat full length TrkB (M55291.1, top sequence) with mouse TrkB protein sequence (NM_001025074.3, bottom sequence) demonstrated the conservation of critical binding sites. Residues described as being responsible for the binding of Shc (Y515), ATP (K571), and PLCγ (Y816) in mouse TrkB are preserved in the rat TrkB ortholog (sites indicated by blue rectangles). Non-identical amino acids are highlighted in dark orange, indicating sequence variations between both TrkB proteins. The numbers indicate the position of the amino acids. *Sequence alignment was performed with the alignment tool of Vectorbuilder.com.*

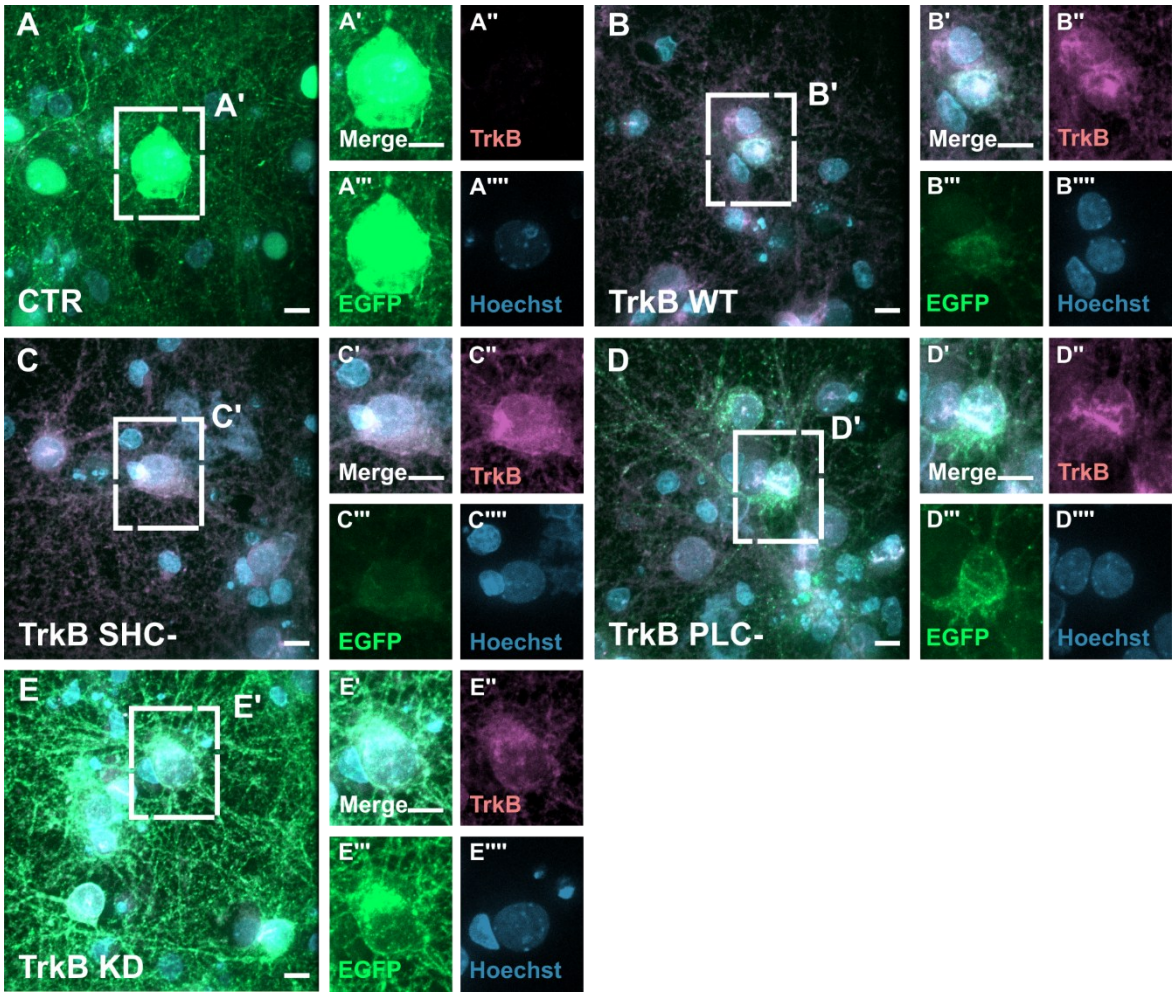

Supplementary Figure 7: Overview microscopic images corresponding to Figure 14. A Representative image of primary hippocampal neurons at DIV14, 11 days post-transduction with an EGFP-control virus (CTR). The dashed rectangle indicates the section depicted in A' and Figure 14 and including the corresponding expression of TrkB (A'), EGFP (A''), and Hoechst (A'''). **B-E** As described in A, but for TrkB WT (B), SHC- (C), PLC- (D), and KD (E). Scale bars: 5 µm. Figure adapted from (193).

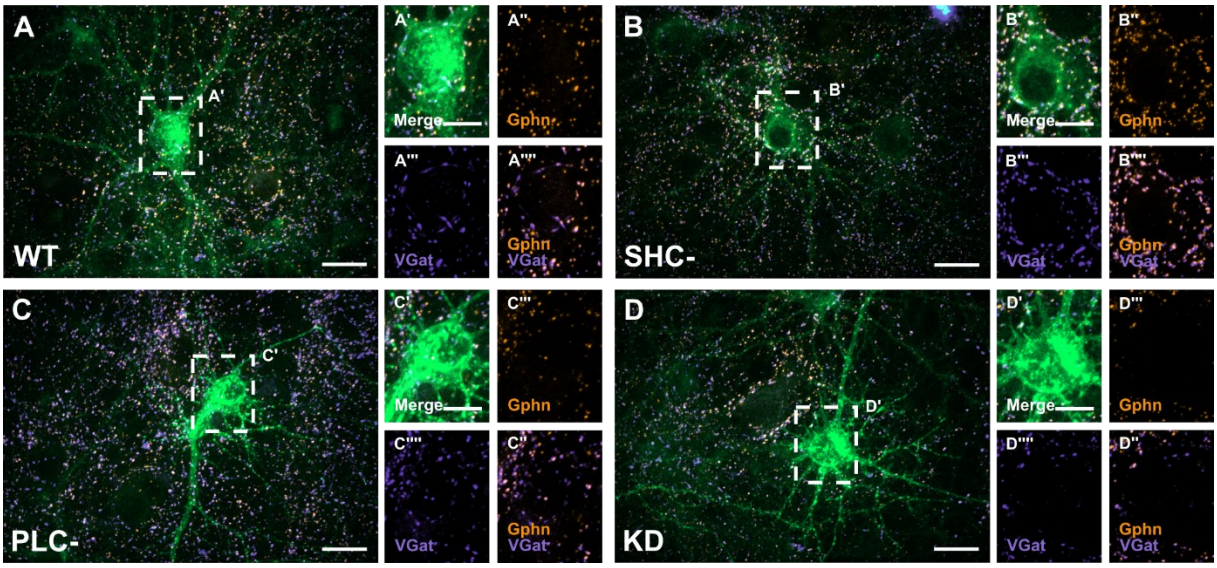

Supplementary Figure 8: Overview microscopic images corresponding to Figure 16. A Representative image of primary hippocampal neurons at DIV14, 11 days post-transduction with TrkB WT. The dashed rectangle indicates the enlarged section depicted in A' and Figure 16, stained for Gephyrin (Gphn, A'') and VGat (A''') which frequently colocalize (A''''). **B-D** According to A but for SHC- (B), PLC- (C) and KD (D) mutants. Scale bars: 10 µm (A-D) and 5 µm (A'-D''''). Figure adapted from (193).

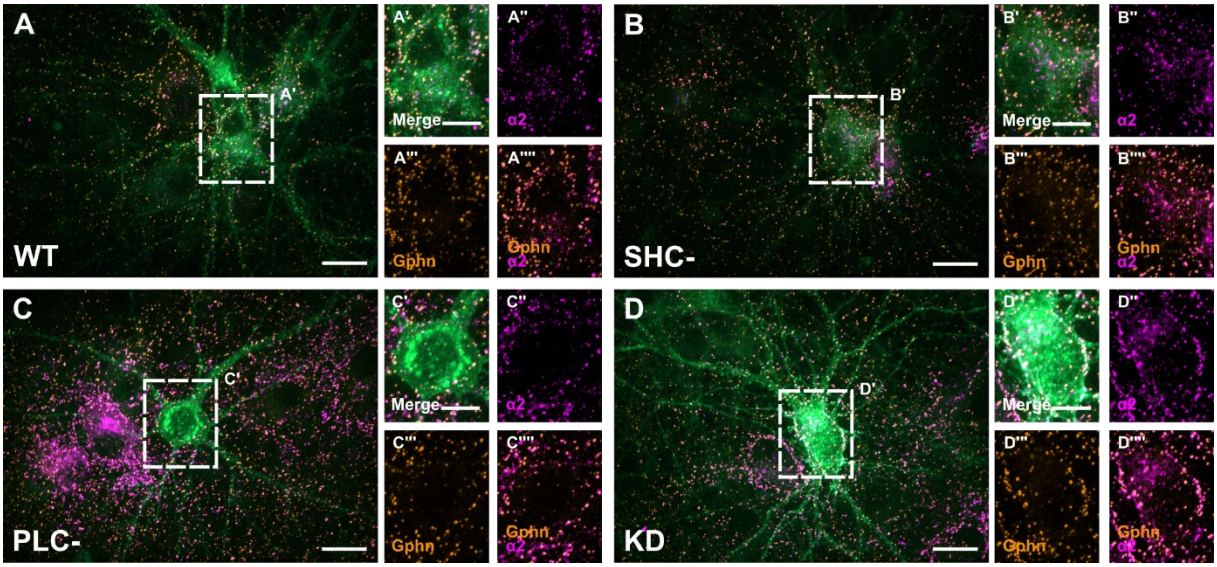

Supplementary Figure 9: Overview microscopic images corresponding to Figure 17. A Representative image of primary hippocampal neurons at DIV14, 11 days post-transduction with TrkB WT. The dashed rectangle indicates the enlarged section depicted in A' and in Figure 17, stained for α2 (A'') and Gphn (A''') which frequently colocalize (A'''). **B-D** According to A but for SHC- (B), PLC- (C) and KD (D) mutants. Scale bars: 10 µm (A-D) and 5 µm (A'-D'''').

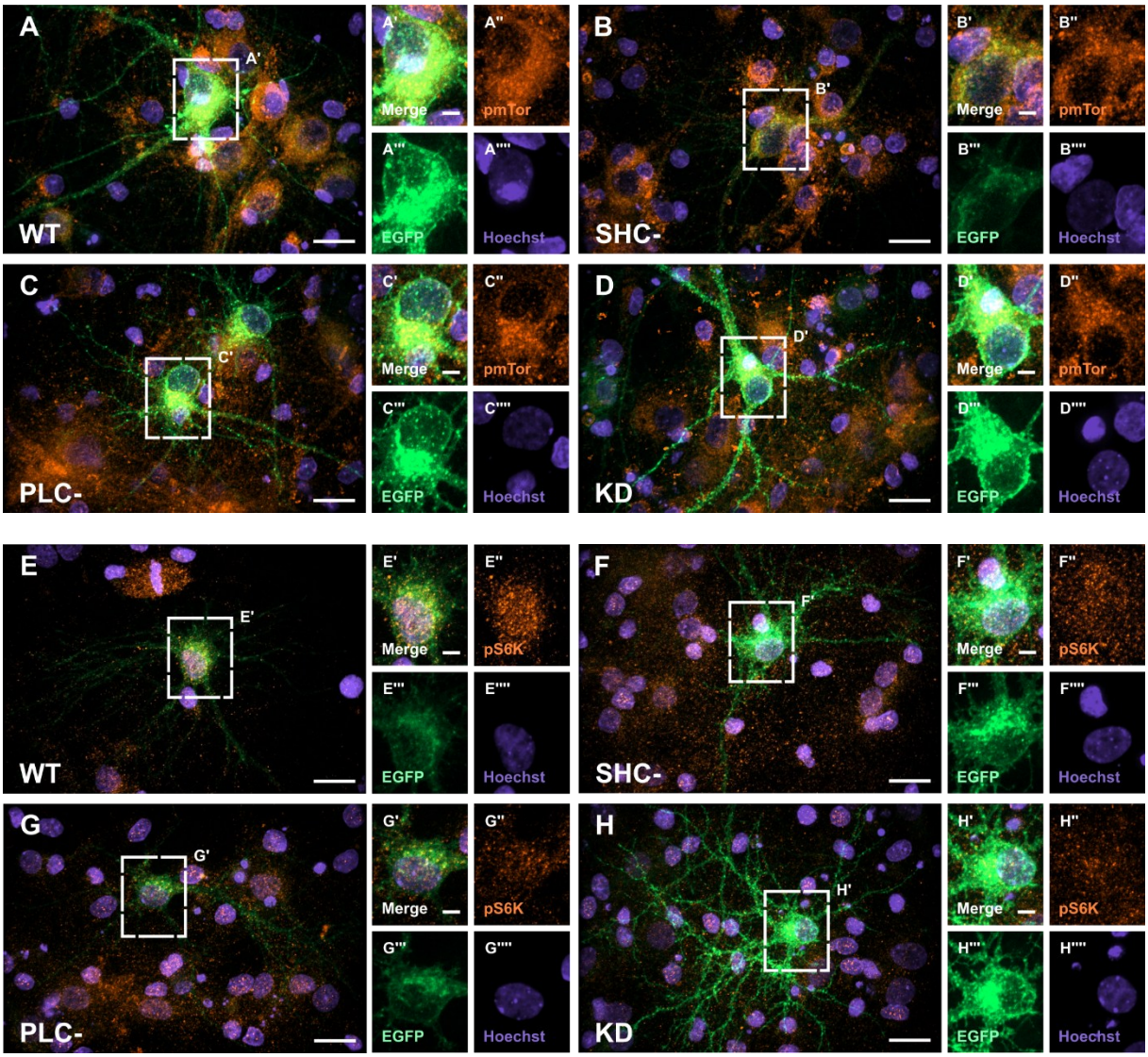

Supplementary Figure 10: Overview microscopic images corresponding to Figure 21. A Representative image of primary hippocampal neurons at DIV14, 11 days post-transduction with TrkB WT. The dashed rectangle indicates the enlarged section depicted in A' and Figure 21, including the corresponding expression of pmTOR (A''), EGFP (A'''), and Hoechst (A''''). **B-D** According to A but for SHC- (B), PLC- (C) and KD (D) mutants. **E** Representative image of primary hippocampal neurons at DIV14, 11 days post-transduction with TrkB WT. The dashed rectangle indicates the enlarged section depicted in E' and Figure 21 including the corresponding expression of pS6K (E''), EGFP (E'''), and Hoechst (E''''). **F-H** According to E, but for SHC- (F), PLC- (G), and KD (H) mutants. Scale bars: 10 µm (A-H) and 5 µm (A'-H'''').

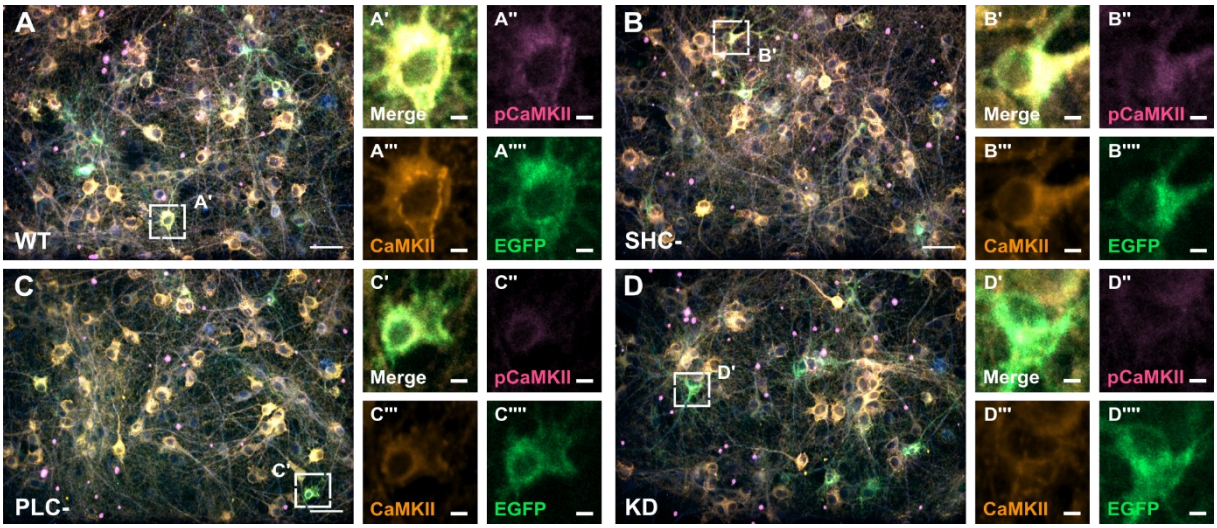

Supplementary Figure 11: Overview microscopic images corresponding to Figure 22. A Representative images of primary hippocampal neurons at DIV14, 11 days post-transduction with TrkB WT. The dashed rectangle indicates the enlarged section depicted in A' and Figure 22, including the corresponding expression of pCaMKII (A''), total CaMKII (A'''), and EGFP (A''''). **B-D** According to A but for SHC- (B), PLC- (C) and KD (D) mutants. Scale bars: 10 µm (A,B,C,D) and 2.5 µm (A'-D'''').

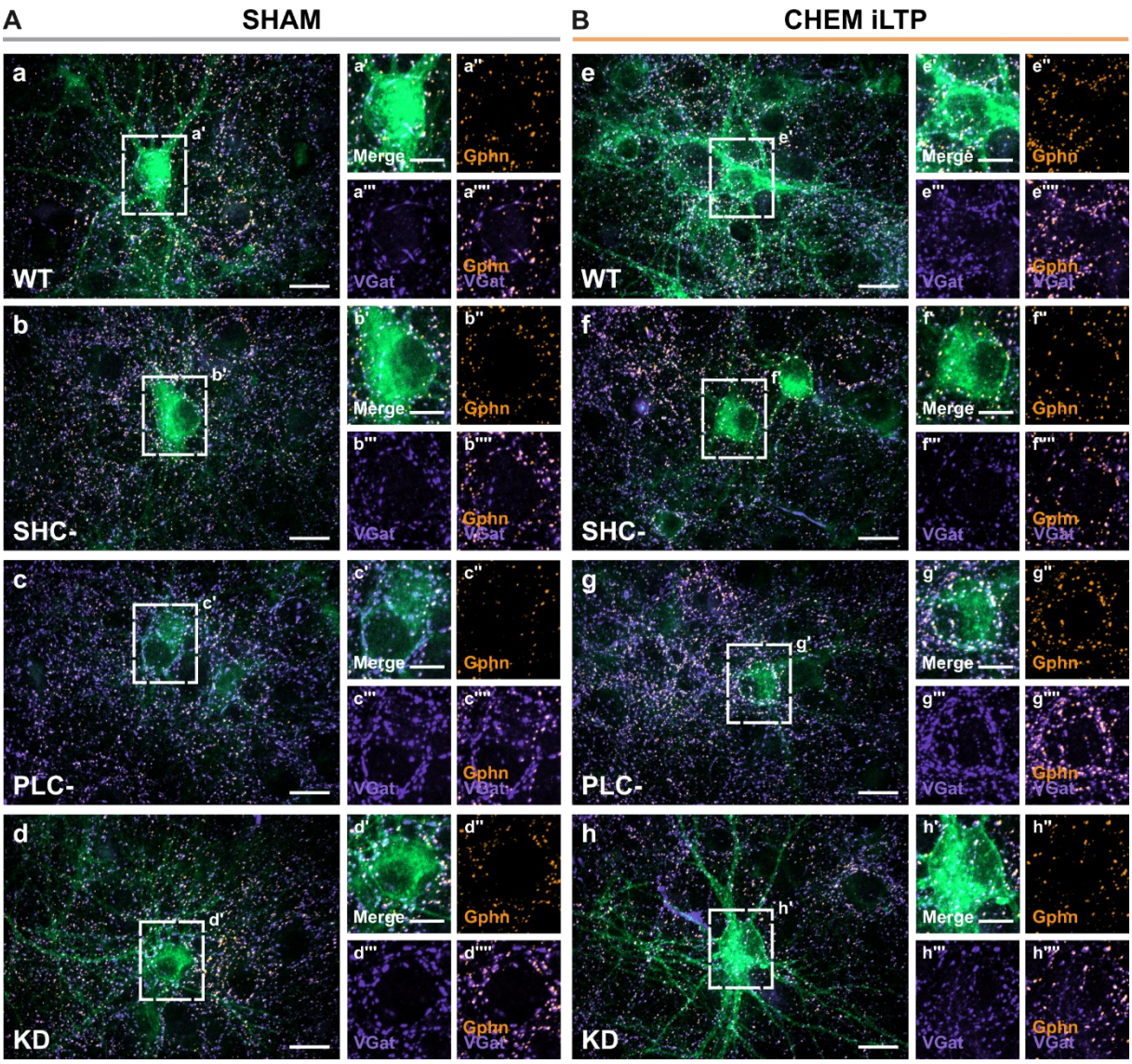

Supplementary Figure 12: Overview microscopic images corresponding to Figure 24. Representative images of primary hippocampal neurons at DIV14, 11 days post-transduction with TrkB mutants. **A** Neurons treated with DMSO control solution (sham). **B** Neurons treated with NMDA+CNQX (chem iLTP). **a,e** Neurons overexpressing TrkB WT were stained for synaptic markers as indicated. The dashed rectangle indicates the enlarged sections depicted in a' and e' and Figure 24. **b-h** According to a,e but for neurons expressing SHC- (b, f), PLC- (c, g) and KD (d, h). Scale bars: 10 µm (a-h) and 5 µm (a'-h''''). Figure adapted from (193).

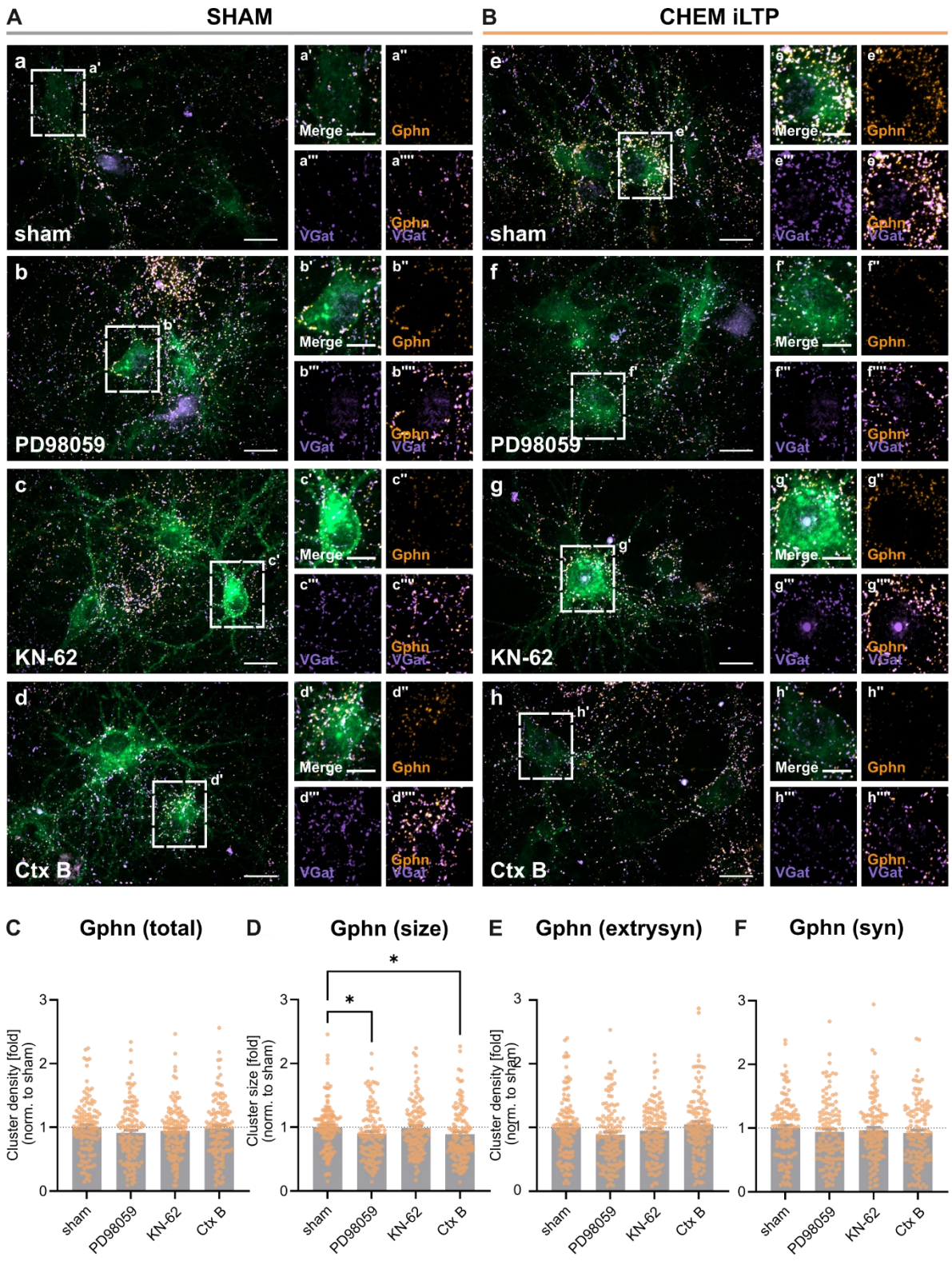

Supplementary Figure 13: Overview microscopic images corresponding to Figure 25. Representative images of primary hippocampal neurons at DIV14, 11 days post-transduction with TrkB WT. **A** Neurons treated with DMSO control solution (sham) **B** Neurons treated with NMDA+CNQX (chem iLTP). **a,e** Neurons were treated with a DMSO control during the treatment and were stained for synaptic markers as indicated. The dashed rectangle indicates the enlarged sections depicted in a' and e' and Figure 25. **b-h** According to a,e but for neurons treated with 50 µM PD98059 (b, f), 3 µM KN-62 (c, g) and 1 µM Cyclotraxin B (Ctx B, d, h). **C** Quantification of the total Gphn cluster density of EGFP positive somata, treated with DMSO control (Sham), PD98059, KN-62 or CtxB. Sham: 1.00 ± 0.04; PD98059 sham: 0.91 ± 0.04; KN-62 sham: 0.95 ± 0.04; Cyclotraxin B: 0.99 ± 0.04. **D** Quantification of mean cluster

size of total Gphn. Sham: 1.00 ± 0.04; PD98059: 0.90 ± 0.04; KN-62: 0.99 ± 0.04; Cyclotraxin B: 0.89 ± 0.04.**E** Quantification of extrasynaptic Gphn cluster density. Sham: 1.00 ± 0.04; PD98059: 0.88 ± 0.04; KN-62 sham: 0.95 ± 0.04; Cyclotraxin B: 1.05 ± 0.05. **F** Quantification of synaptic Gphn cluster density (colocalized Gphn + VGat marker). Sham: 1.00 ± 0.04; PD98059: 0.94 ± 0.05; KN-62: 0.97 ± 0.04; Cyclotraxin B: 0.92 ± 0.05. All treated values are normalized to the sham-treated group. Data represent the mean ± S.E.M. with n ≥ 113 somata obtained from four independent experiments. Statistical significance was assessed by Two-way ANOVA with Tukey's multiple comparisons test (only significant comparisons between sham and the respective chem iLTP group are shown, $p < 0.05$*). Detailed statistical data is stated in Table 37**.** Figure adapted from (193).

Table 37 Statistical data

Comparison	n	p
Figure 14		
TrkB Overexpression H(4) = 18.89, p = 0.0008		
CTR vs. WT	41 vs. 46	0.0113
CTR vs. SHC-	41 vs. 45	0.0009
CTR vs. PLC-	41 vs. 42	0.0086
CTR vs. KD	41 vs. 38	0.0252
WT vs. SHC-	46 vs. 45	> 0.9999
WT vs. PLC-	46 vs. 42	> 0.9999
WT vs. KD	46 vs. 38	> 0.9999
SHC- vs. PLC-	45 vs. 42	> 0.9999
SHC- vs. KD	45 vs. 38	> 0.9999
PLC- vs. KD	42 vs. 38	> 0.9999
Figure 15		
Cl. Csp3 H(3) = 2.317, p = 0.5093		
WT vs. SHC-	8 vs. 8	0.5076
WT vs. PLC-	8 vs. 8	> 0.9999
WT vs. KD	8 vs. 7	> 0.7986
Figure 16		
Gphn (total) H(3) = 20.76, p = 0.0001		
WT vs. SHC-	45 vs. 55	0.0091
WT vs. PLC-	45 vs. 54	> 0.9999
WT vs. KD	45 vs. 47	> 0.9999
Gphn (syn) H(3) = 25.98, p < 0.0001		
WT vs. SHC-	51 vs. 54	> 0.9999
WT vs. PLC-	51 vs. 53	0.0028
WT vs. KD	51 vs. 44	0.0054
Gphn (size) H(3) = 11.09, p = 0.0113		
WT vs. SHC-	49 vs. 60	0.0308
WT vs. PLC-	49 vs. 54	0.5553
WT vs. KD	49 vs. 43	0.0075
Figure 17		
$GABA_AR$ a2 (total) H(3) = 10.96, p = 0.0120		
WT vs. SHC-	80 vs. 86	0.3036
WT vs. PLC-	80 vs. 85	0.0032
WT vs. KD	80 vs. 89	0.6125
$GABA_AR$ a2/Gphn (total) H(3) = 2.29, p = 0.5153		
WT vs. SHC-	80 vs. 90	0.8989
WT vs. PLC-	80 vs. 90	0.7117
WT vs. KD	80 vs. 89	0.4752
Figure 18		
PSD95 (total) H(3) = 2.807, p = 0.4223		
WT vs. SHC-	51 vs. 52	> 0.9999
WT vs. PLC-	51 vs. 50	> 0.9999

WT vs. KD	51 vs. 43	> 0.9999
VGlut1 (total) H(3) = 1.263, p = 0.7380		
WT vs. SHC-	54 vs. 52	> 0.9999
WT vs. PLC-	54 vs. 48	0.9656
WT vs. KD	54 vs. 23	> 0.9999
PSD95 (syn) H(3) = 0.2936, p = 0.9612		
WT vs. SHC-	53 vs. 50	> 0.9999
WT vs. PLC-	53 vs. 47	> 0.9999
WT vs. KD	53 vs. 23	> 0.9999
PSD95 (extrasyn) H(3) = 2.187, p = 0.5345		
WT vs. SHC-	52 vs. 51	> 0.9999
WT vs. PLC-	52 vs. 50	0.7868
WT vs. KD	52 vs. 24	0.9619
Figure 20		
Event Frequency F(3, 74) = 4.683, p = 0.0047		
WT vs. SHC-	21 vs. 20	0.9118
WT vs. PLC-	21 vs. 17	0.0197
WT vs. KD	21 vs. 20	0.9092
AMP F(3, 75) = 2.710, p = 0.0510		
WT vs. SHC-	21 vs. 21	0.3045
WT vs. PLC-	21 vs. 17	0.0167
WT vs. KD	21 vs. 20	0.5414
AUC F(3, 74) = 4.683, p = 0.0144		
WT vs. SHC-	21 vs. 21	0.1078
WT vs. PLC-	21 vs. 17	0.0046
WT vs. KD	21 vs. 20	0.4129
FWHM F(3, 74) = 1.520, p = 0.2163		
WT vs. SHC-	21 vs. 20	0.3157
WT vs. PLC-	21 vs. 17	0.2416
WT vs. KD	21 vs. 20	0.9980
Figure 21		
pmTOR H(3) = 17.87, p = 0.0005		
WT vs. SHC-	90 vs. 89	0.0004
WT vs. PLC-	90 vs. 90	0.0623
WT vs. KD	90 vs. 90	0.0014
pS6K H(3) = 20.67, p = 0.0001		
WT vs. SHC-	86 vs. 89	0.0366
WT vs. PLC-	86 vs. 90	0.0732
WT vs. KD	86 vs. 89	<0.0001
Figure 22		
pCaMKII (Thr286) H(3) = 14.00, p = 0.0029		
WT vs. SHC-	81 vs. 81	0.3887
WT vs. PLC-	81 vs. 79	0.0018
WT vs. KD	81 vs. 80	0.0133
CaMKII H(3) = 9.714, p = 0.0212		

WT vs. SHC-	79 vs. 80	> 0.9999
WT vs. PLC-	79 vs. 79	0.2478
WT vs. KD	79 vs. 80	0.0122
Figure 23		
Gphn (total)		
sham vs. chem iLTP	89 vs. 90	0.0111
Gphn (size)		
sham vs. chem iLTP	87 vs. 87	0.0008
Gphn (extrasyn)		
sham vs. chem iLTP	89 vs. 89	0.0985
Gphn (syn)		
sham vs. chem iLTP	89 vs. 90	0.0060
VGat (total)		
sham vs. chem iLTP	89 vs. 89	0.2663
Figure 24		
Gphn (total) F(1, 696) = 3.363, p = 0.0671		
WT sham vs. chem iLTP	89 vs. 90	0.0273
SHC- sham vs. chem iLTP	80 vs. 90	0.4882
PLC- sham vs. chem iLTP	87 vs. 89	0.0815
KD sham vs. chem iLTP	90 vs. 89	0.3261
Gphn (size) F(1, 680) = 5.526, p = 0.0190		
WT sham vs. chem iLTP	87 vs. 86	0.0070
SHC- sham vs. chem iLTP	78 vs. 88	0.3056
PLC- sham vs. chem iLTP	84 vs. 88	0.0006
KD sham vs. chem iLTP	87 vs. 90	0.7056
Gphn (syn) F(1, 697) = 0.06560, p = 0.7979		
WT sham vs. chem iLTP	89 vs. 90	0.0016
SHC- sham vs. chem iLTP	80 vs. 90	0.3406
PLC- sham vs. chem iLTP	87 vs. 89	0.6974
KD sham vs. chem iLTP	90 vs. 90	0.0397
Gphn (extrasy) F(1, 680) = 15.97, p < 0.0001		
WT sham vs. chem iLTP	89 vs. 89	0.5985
SHC- sham vs. chem iLTP	78 vs. 90	0.0004
PLC- sham vs. chem iLTP	87 vs. 89	0.0022
KD sham vs. chem iLTP	90 vs. 89	0.4188
VGat (total) F(1, 680) = 2.126, p = 0.1453		
WT sham vs. chem iLTP	87 vs. 86	0.3746
SHC- sham vs. chem iLTP	78 vs. 88	0.1550
PLC- sham vs. chem iLTP	84 vs. 88	0.9859
KD sham vs. chem iLTP	87 vs. 90	0.0191
Figure 25		
Gphn (total) F(1, 937) = 4.279, p = 0.0389		
DMSO sham vs. chem iLTP	119 vs. 115	0.0269
PD98059 sham vs. chem iLTP	119 vs. 119	0.3177
KN-62 sham vs. chem iLTP	119 vs. 118	0.5711

Cyclotraxin B sham vs. chem iLTP	119 vs. 118	0.7281
Gphn (size) F(1, 937) = 1.159, p = 0.2821		
DMSO sham vs. chem iLTP	117 vs. 113	0.0281
PD98059 sham vs. chem iLTP	114 vs. 115	0.1474
KN-62 sham vs. chem iLTP	116 vs. 118	0.7476
Cyclotraxin B sham vs. chem iLTP	116 vs. 117	0.2319
Gphn (extrasyn) F(1, 935) = 2.222, p = 0.1364		
DMSO sham vs. chem iLTP	119 vs. 114	0.0814
PD98059 sham vs. chem iLTP	119 vs. 118	0.3595
KN-62 sham vs. chem iLTP	118 vs. 118	0.7704
Cyclotraxin B sham vs. chem iLTP	119 vs. 118	0.9893
Gphn (syn) F(1, 936) = 7.262, p = 0.0072		
DMSO sham vs. chem iLTP	118 vs. 116	0.0058
PD98059 sham vs. chem iLTP	119 vs. 119	0.3515
KN-62 sham vs. chem iLTP	118 vs. 118	0.5615
Cyclotraxin B sham vs. chem iLTP	118 vs. 118	0.2711
Supplementary Figure 13		
Gphn (total) H(3) = 3.101, p = 0.3763		
Sham vs. PD98059	119 vs. 119	0.3137
Sham vs. KN-62	119 vs. 118	>0.9999
Sham vs. Cyclotraxin B	119 vs. 119	>0.9999
Gphn (size) H(3) = 10.72, p = 0.0133		
Sham vs. PD98059	117 vs. 114	0.0434
Sham vs. KN-62	117 vs. 116	>0.9999
Sham vs. Cyclotraxin B	117 vs. 116	0.0209
Gphn (extrasyn) H(3) = 7.565, p = 0.0559		
Sham vs. PD98059	119 vs. 119	0.1663
Sham vs. KN-62	119 vs. 119	>0.9999
Sham vs. Cyclotraxin B	119 vs. 118	>0.9999
Gphn (syn) H(3) = 2.179, p = 0.5360		
Sham vs. PD98059	118 vs. 119	0.6373
Sham vs. KN-62	118 vs. 118	>0.9999
Sham vs. Cyclotraxin B	118 vs. 118	0.5748

8. Statement of Contributions

For several experiments presented in this thesis, I was pleased to receive some support from colleagues and students. Their contributions are outlined below:

Generation of TrkB mutants:

Framework of the experiment: To generate TrkB mutants deficient in signaling induction the corresponding rat TrkB cDNA was mutated via site-directed mutagenesis.

Names and shares of colleagues: Dr. Martin Kriebel (Department of Molecular & Neurobiology, NMI, Reutlingen) performed preliminary literature research and obtained the plasmid pEGFP-N1-TrkB (pEGFP-N1-TrkB was a gift from Rosalind Segal (Addgene plasmid # 32500 ; http://n2t.net/addgene:32500 ; RRID:Addgene_32500) which was used for the generation of the TrkB mutants.

Own contribution: Based on this plasmid, I performed the initial propagation, identification of sites of interest, mutagenesis and characterization of the TrkB mutants.

Analysis of Apoptosis Induction:

Framework of the experiment: To assess potential apoptosis induction through TrkB signaling modulation, transduced primary neurons were analyzed for the expression of cleaved caspase 3 as a indicator of apoptosis.

Names and shares of colleagues: Elisabeth Brand (Lab rotation Master of Cellular & Molecular Neuroscience, GTC, Tübingen) assisted with the cultivation, staining, and imaging of TrkB mutant-transduced primary neurons for two out of three experimental replicates.

Own contribution: I prepared all neuronal cultures, performed the cultivation, staining and imaging for the third replicate, and analyzed all replicates for Cl.Csp3-positive neurons.

9. Statement of Publication

During this study, it was possible to publish parts of this work in the following article, which is distributed under the terms of the Creative Commons Attribution License (CC BY):

Wüstner LS, Beuter S, Kriebel M, Volkmer H; Dissection of signaling pathways regulating TrkB-dependent gephyrin clustering. *Front. Mol. Neurosci., doi: 10.3389/fnmol.2024.1480820;* PMID: 39534513

This article includes Data sets from the following Figures:

Experiment	Chapter	Figure/Table Dissertation	Figure/Table Publication
Site-directed mutagenesis induced nucleotide exchanges in the rat *Ntrk2* (TrkB) coding sequence.	4.1.1.	Figure 6	Figure S2
Mutation of the rat TrkB phosphorylation and ATP binding sites reduced site-specific signaling pathway induction	4.1.2.	Figure 8; Figure 9	Figure S2
Generation of Lentiviral Transfer and Expression Vectors	4.1.3., 4.2.1.	Figure 11; Figure 12; Figure 13	Figure S3
Expression of TrkB variants in primary hippocampal neurons	4.2.1., 4.2.2.	Figure 14, Figure 15, Supp. Figure 7	Figure S4
Quantification of inhibitory synaptic markers	4.3.1.	Figure 16, Supp. Figure 8	Figure 2, Figure S5
Quantification of excitatory synaptic markers	4.3.3.	Figure 18	Figure S6
Calcium imaging of TrkB modulated neurons	4.4.	Figure 20	Figure 3
Analysis of CaMKII activation	4.5.2.	Figure 22	Figure 2,
TrkB mutant expression during chem iLTP	4.7.2.	Figure 24, Supp. Figure 12	Figure 4, Figure S8
Inhibition of kinases during chem iLTP	4.7.3.	Figure 25, Supp. Figure 13	Figure 4, Figure S8, Figure S9

Mutagenesis Oligonucelotides	3.1.11.	Table 23	Supplementary Table 1
Summaries of results during basal conditions and chem iLTP	4.6., 4.8.	Table 35 & 36	Table 1
Statistical Data	7	Table 37	Supplementary Table 3

10. Acknowledgement

Am Ende meiner Dissertation möchte ich die Gelegenheit nutzen, den Menschen zu danken, die mich auf diesem Weg unterstützt haben. Ohne ihre Hilfe, Inspiration und Begleitung wäre diese Arbeit nicht möglich gewesen.

Mein besonderer Dank gilt Prof. Hansjürgen Volkmer, der mir 2021 die Möglichkeit gegeben hat, Teil seiner Arbeitsgruppe zu werden, mich wissenschaftlich weiterzuentwickeln und mich stets mit seinen Ideen und Ratschlägen begleitet hat. Ich danke dir für die zahlreichen und ergiebigen Diskussionen, dein stets offenes Ohr und die Möglichkeiten, die du mir während meiner Zeit am NMI geboten hast.

Weiter möchte ich mich bei Prof. Andrea Burgalossi und Prof. Jan Benda bedanken, welche mich beide seit Beginn an stets begleitet haben und mich mit ihrem wertvollen Rat in meiner Doktorarbeit unterstützt haben.

Am meisten dankbar bin ich aber für die vielen, großartigen Menschen, die ich während meiner Zeit am NMI kennenlernen durfte. Besonders danke ich Dr. Martin Kriebel, der mich vom ersten Tag bei meiner Arbeit unterstützt und mit Rat und Tat zur Seite gestanden hat. Danke für die vielen positiven Worte, das stets offene Ohr und die vielen Dinge die ich von dir lernen durfte. Danke an Sabrina, Johanna, Sophia, Verena und Roswitha und alle weiteren tollen Kolleg:innen, die sich jeden Mittag im dritten Stock versammelt haben. Eure täglichen Späße, die aufmunternden Worte, die helfenden Hände und die zahlreichen Gespräche haben meine Zeit am NMI unvergesslich gemacht. Ich bin froh um die Freundschaften, die dabei entstanden sind und bin mir sicher, dass wir uns im Leben weiterhin begegnen werden.

Aber auch außerhalb des Instituts habe ich unendlich viel Unterstützung erhalten. Ich bin ewig dankbar für meine Freunde und meiner Familie, die mich in den letzten Jahren viel zu selten gesehen und mich trotzdem immer unterstützt haben. Danke, dass ihr mir die zahlreichen unbeantworteten Nachrichten und abgesagten Treffen immer verziehen habt. Euer bedingungsloser Rückhalt und die motivierenden Worte haben mich stets durchhalten lassen.

Mein tiefster Dank gilt meinem Partner Dennis. Danke, dass du das letzte Jahr mit mir durchgestanden hast. Die Selbstverständlichkeit, mit der du meine nächtlichen Analyse-Sessions und Schreib-Wochenenden mitgetragen hast und immer wusstest, wann es Zeit für eine Umarmung ist. Ich bin dir für immer dankbar für deine Liebe und deinen Support.

Zuletzt möchte ich mich noch meinem geliebten Großvater widmen: Opa, wie gerne hätte ich das noch mit dir zusammen erlebt - das hier ist für dich!